Dissertation

The ternary gyrase-DNA-quinolone complex: from molecular modelling to understanding quinolone action and resistance

Zur Erlangung des naturwissenschaftlichen Doktorgrades der Fakultät für Mathematik, Informatik und Naturwissenschaften der Universität Hamburg

vorgelegt von
Jörn-Benjamin Lenz
Hamburg, 2010

1. Gutachter:
Prof. Dr. Peter Heisig

2. Gutachter:
Prof. Dr. Andrew Torda

Institut für Pharmazie, Abt. Pharmazeutische Biologie und Mikrobiologie
ZBH - Zentrum für Bioinformatik, Abt. Biomolekulare Modellierung
Universität Hamburg, Bundesstrasse 45/43, 20146 Hamburg, Deutschland

Die vorliegende Arbeit wurde in der Zeit von Februar 2004 bis Juli 2009 unter der Leitung von Herrn Prof. Dr. P. Heisig und Herrn Prof. Dr. A. Torda in der Abteilung für Pharmazeutische Biologie und Mikrobiologie des Instituts für Pharmazie sowie in der Abteilung für Biomolekulare Modellierung des Zentrums für Bioinformatik der Fakultät für Mathematik, Informatik und Naturwissenschaften an der Universität Hamburg angefertigt.

1. Gutachter: Prof. Dr. P. Heisig

2. Gutachter: Prof. Dr. A. Torda

Tag der Disputation: 11. Februar 2011

Für Carolin

Contents

Abbreviations and notions

$\mathbf{r}_i$	vector of the x, y and z position of particle i
τ_P	pressure coupling constant [ns]
τ_T	temperature coupling constant [ns]
p_i	predicted activity of compound i
$PRESS$ value	predictive residual sum of squares
r_g	radius of gyration
$rmsd$	root man square deviation
SDR	standard deviation of the residuals
y_i	measured activity of compound i
3D	three-dimensional
gyrA	gene encoding the A-subunit of DNA gyrase
gyrB	gene encoding the B-subunit of DNA gyrase
Lk	linking number
parC	gene of the C subunit of topoisomerase IV
parE	gene of the E subunit of topoisomerase IV
S	sequence entropy calculated from BLAST alignment
topA	gene encoding topoisomerase I
topB	gene encoding topoisomerase III
Tw	twisting number
Wr	writhe
ADMET	adsorption, distribution, metabolism, excretion and toxicology
ATP	adenosine-5'-triphosphate
BLAST	basic local alignment search tool
CAP	catabolite activator protein
ccc	covalently closed circular
DNA	deoxyribonucleic acid
ds	double stranded

FIS	factor for inversion stimulation
fs	1 femtosecond = 10^{-15} seconds
GyrA	gyrase A subunit
GyrA59	59 kDa fragment of the N-terminal domain of GyrA
GyrB	gyrase B subunit
H-NS	histone-like nucleoid structuring protein
HTH	helix turn helix
HU	heat-unstable nucleoid protein
IHF	integration host factor
K	Kelvin
kDa	kilo Dalton
kJ	kilo Joule
LINCS	LINear Constraint Solver for molecular simulations
MD	molecular dynamics
nm	nanometer = 10^{-9} meter
NPT	isobaric, isothermal ensemble: constant number of particles N, constant pressure P, constant temperature T
NTD	N-terminal domain
ps	1 picosecond = 10^{-12} seconds
QRDR	quinolone resistance determining region
QSAR	quantitative structure-activity relationship
res.	residues
SAXS	small angle X-ray scattering
ss	single stranded
topoI	topoisomerase I
topoIII	topoisomerase III
topoIV	topoisomerase IV
Toprim domain	topoisomerase-primase domain
WHO	World Health Organization

Chapter 1

Introduction

Infectious diseases have always endangered human health and were the most common reason for human deaths at the beginning of the 20^{th} century. One third of these was due bacterial infections [1]. Fortunately, the introduction of antibiotic agents brought about a breakthrough in their treatment. Their history began in the early 20^{th} century with the introduction of Salvarsan®. However, it was the discovery of the sulfonamide antibacterials that denoted a real milestone as they were the only effective antibacterial drugs before penicillins became available. Since their discovery by Fleming in the 1940s, different groups of antibiotics with varying mechanisms of action have been developed (figs. 1.1 and table 1.1) [2, 3]. The fully synthetic group of the small-molecular quinolone-antibacterials was introduced by Lesher and coworkers in 1962 [4] (section 1.3.1). By the end of the 1960's, a variety of antibiotic drugs were developed and introduced. They offered the chance to efficiently combat bacteria. From there on however, only iterative improvements were reached by chemical or biotechnical modifications of existing drugs. This lead to drugs with improved pharmacokinetic and pharmacodynamic properties such as the fluoroquinolones that were launched in 1985. Thus, it took almost 40 years until the antibacterial innovation gap was closed by the introduction of the new class of

oxazolidinones [5, 6] in 1999, followed by the ketolides in 2000 and the glycylcyclines in 2007 [7]. However, the first real innovation since then was the introduction of the lipopeptide-antibiotic Daptomycine (USA 2003 and EU 2006) [8].

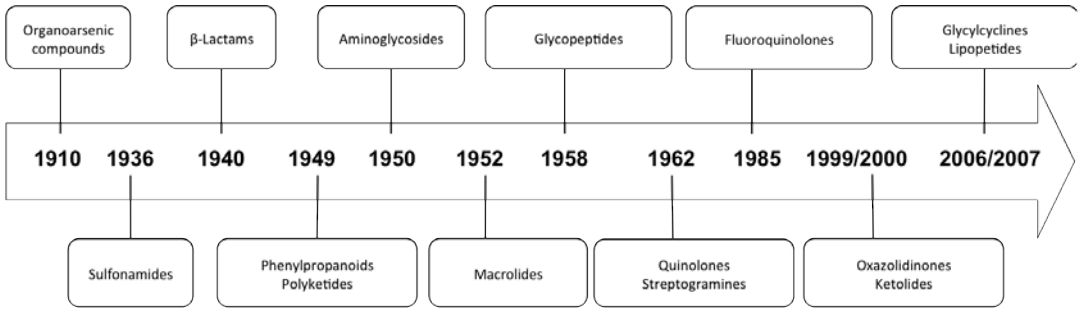

Figure 1.1: *Introduction of new agents for therapy of bacterial infections (modified after [3])*

antibiotic classes	cellular target of antibiotic drug
β-lactams, glycopeptides, cycloserine, bacitracin, fosfomycin	synthesis of bacterial cell wall
Daptomycin, polymyxins	integrity of bacterial cell membrane
Sulfonamides, trimethoprim	synthesis of nucleotides
Quinolones, nitrofurans, nitroimidazols	replication of DNA
Rifamycins	synthesis of RNA
Aminoglycosides, phenylpropanoids, fusidic acid, ketolides, macrolides, oxazolidinones, streptogramins, tetracyclines, mupirocin	synthesis of proteins

Table 1.1: *Antibiotic classes and their cellular targets (modified after [9])*

1.1 Bacterial Resistance

"[...] we essentially defeated infectious diseases and could close the book on them"

(William H. Steward, officer of the U.S. health department, 1969)

This quote nicely sums up the hopes that were once stirred by the development and the success of antiinfective drugs. However, despite modern antibiotics, infectious diseases are still one of the most urgent health-problems and are responsible for nearly one third of human deaths worldwide (WHO report 2008). One reason is the rapid emergence of bacterial resistance. This is well illustrated by the example of penicillinase producing isolates of *Staphylococcus aureus* that were found in the very same year as penicillins were introduced to the market. These enzymes are capable of hydrolyzing the β-lactam moiety of penicillins, leading to their inactivation [10]. As with the penicillins, such examples can be found for every class of antibiotic drugs such as quinolones [11–15].

One way to classify resistance is its form. An intrinsic (primary, natural) resistance is a stable genetic characteristic that affects all members of a bacterial species which naturally remain unaffected by a certain class of antibiotic drugs. Secondary or extrinsic resistance refers to mutations that can occur randomly or by the transfer of extrachromosomal elements via transformation, transduction or transfection.

Another classification scheme is based on the underlying mechanism by which resistance to antibiotic drugs can occur [16, 17]. The basic types are (1) alteration of the target structure via mutations and thus loss of affinity, (2) reduced access to the target structure due to increased efflux or decreased influx and (3) inactivation of the therapeutic agent by modifying enzymes. Important mechanisms of resistance to classes of antibiotic drugs are summarized in table 1.2.

The federal DART (Deutsche Antibiotika Resistenzstrategie) campaign [18] emphasizes the fact that bacterial resistance is a current problem. Since resistance is increasing and "major drug companies are pulling out of antibiotic development" [19], there is the urgent need to improve existing drugs or even better, find new antibiotic

drugs with novel chemical scaffolds and mechanisms of action.

class	mechanism of resistance
β-lactam antibiotics	(1, 2, 3)
Aminoglycosides (gentamicin)	(1, 2, 3)
Phenylpropanoids (chloramphenicol)	(1, 2, 3)
Polyketides (tetracyclin)	(1, 2, 3)
Quinolones (nalidixic acid, ciprofloxacin)	(1, 2, 3)
Macrolides (erythromycin)	(1, 2, 3)
Sulfonamides	(1, 2)

Table 1.2: *Classes of antibiotic drugs (and corresponding examples) and their underlying mechanism of resistance: (1) Alteration of the target structure due to mutations, (2) reduced access due to decreased permeability or increased efflux and (3) inactivation by modifying enzymes; modified after [2]*

1.1.1 Finding new antibacterial drugs

In the past, drug discovery often benefited from serendipity and a mixture of wrong working hypotheses and rational drug design [20]. These days, improved techniques and strategies like combinatorial chemistry allow the synthesis of a large number of compounds that may contain potential lead structures. However, picking those leads from the large number of structures is difficult. Hence, efficient techniques have to be used to have a reasonable chance to find a new drug. For this purpose, automated testing methods like high-throughput- or NMR-screening have to be applied [20, 21].
In principle, the development of new drugs is always a very time-consuming and expensive process which can generally be summarized in a five-step scheme. It is also applicable to the development of new antibacterial agents [6].
In this scheme, the first step is the identification of a new target by approaches like genomics and proteomics. In a second step, the target has to be checked by experiments like knock-out bacteria or structural biology. Subsequently, new lead structures that are able to modulate the activity of the target have to be identified and optimized. Finally, the drug candidate is tested in preclinical and clinical stages for its efficiency and ADMET-behavior.
Alternative strategies would be to search for new lead candidates that target known structures or to modify existing drugs in order to bypass resistances or to improve their pharmacokinetic parameters [22]. The modification of known drugs by chemical or biotechnological techniques was the preferred route in the lean period of antibiotic drug development between 1962 and 2000 (fig. 1.1 and section 1). This approach can be improved profoundly if high-resolution 3D structures of the target-ligand complexes are known.
For both concepts, the quinolones and their primary target in Gram-negatives, the DNA-gyrase in complex with DNA, is an instructive example.

1.2 DNA and its topology in the bacterial cell

An *Escherichia coli* cell is roughly cylindrical and typically has a diameter of about 10^{-6} m and a length of approximately $2 \cdot 10^{-6}$ m [23]. However, if stretched out, the roughly $4 \cdot 10^{6}$ basepairs (bp) of the circular chromosome of *E. coli* would make up a length of approximately $1.4 \cdot 10^{-3}$ m which is significantly longer than the bacterial cell. Hence, the DNA has to be condensed by nearly three orders of magnitude in order to fit into the cell. Nevertheless, proteins involved in cellular processes like transcription, cell division and recombination still have to be able to access the DNA.

The chromosome of *E. coli* adopts a right-handed double stranded (ds) helix whose two DNA strands are intertwined around the helical axis. In its B-conformation, a full helical turn occurs every 10.4 bp [24–26]. The linking number Lk of such DNA molecules defines how often the two strands are intertwined. For relaxed DNA with N basepairs, Lk can be determined by eq. 1.1 and is usually assigned the symbol Lk^0. In this state, it equals the number of helical turns of the two strands around each other, known as the twisting number Tw.

$$Lk^0 = \frac{N}{10.4} \tag{1.1}$$

If the number of basepairs needed to describe a full helical turn deviates from the ideal B-geometry, torsional stress is induced in the covalently closed circular (ccc) DNA rings. Since Lk is invariant and cannot be changed without introducing a break in one or both strands of the DNA, this stress is compensated by a coiling of the helical axis, known as supercoiling [27]. This writhe Wr characterizes the number of times the helix axis crosses over itself. The linking number Lk can thus be expressed as the sum of Tw and Wr (eq. 1.2) [28, 29].

$$Lk = Tw + Wr \tag{1.2}$$

If the number of twists Tw is increased, a negative writhe value Wr and thus a negative supercoiling or underwinding of the ccc-double stranded DNA ring results

(fig. 1.2). If the number of twists Tw is decreased, Wr becomes positive and the DNA ring is overwound or positively supercoiled. With respect to relaxed DNA rings, a positive supercoiling implies that $Lk > Lk^0$. If DNA is negatively supercoiled or underwound, the linking number Lk is less than Lk^0, i.e. $Lk < Lk^0$.

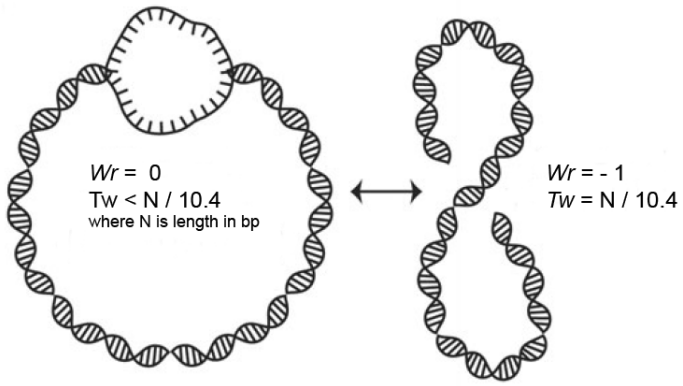

Figure 1.2: *Introduction of negative supercoils into ccc-dsDNA rings: Removing a few turns from a relaxed ccc-dsDNA ring with $Lk^0 = Tw$ results in $Tw < Lk^0$ and $Wr = 0$ (left) while the resulting torsional stress is compensated by the introduction of a negative supercoil with Wr = -1 (right); adapted from [30]*

Both types of supercoiling are equally effective in condensing the DNA for fitting it into the bacterial cell. But for naturally occurring DNA, there is a strong preference for the negatively supercoiled state [31–33]. Unwinding of DNA by the introduction of negative supercoils provides energy needed for cellular processes that require a transient separation of the DNA strands like transcription, replication and recombination [30, 34–36]. For the semi-conservative replication of dsDNA to take place, the strands of the DNA are temporarily separated by the helicase. However, since the ends of the DNA of bacteria are usually not allowed to freely rotate relative to each other, strand separation causes overwinding of the DNA ahead of the replisome (fig. 1.3) [30, 35, 37]. Furthermore, replication results in catenated daughter chromosomes. The organism must be able to decatenate the chromosomes.

The transcription of bacterial DNA leads to a similar alteration of local DNA topologies, but compared to the process of replication, transcription does not require a steady separation of the strands. While the RNA-polymerase is active, the DNA strands are pulled apart. Hence, oppositely supercoiled domains are generated ahead of the transcription enzymes complex (positive supercoils) and behind it (negative supercoils) as schematically depicted in fig. 1.3 [30, 35, 38, 39]. In order for the enzymatic complexes of transcription and replication to proceed, positive supercoils ahead of them have to be compensated.

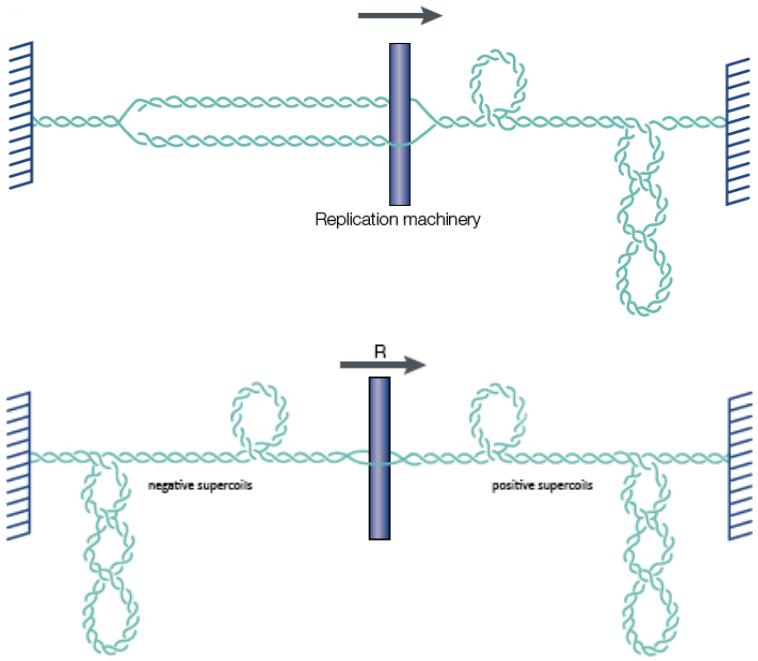

Figure 1.3: *Schematic representation of replication and transcription: Introduction of positive supercoils into DNA by the replication machinery (top); Introduction of positive supercoils into DNA ahead of the transcription machinery R (including the RNA-polymerase) and negative supercoils behind it (bottom); taken from and modified after [39]*

But not only the ability of RNA-polymerase to synthesize RNA is influenced by the topology of DNA. In fact, local topological properties of the DNA influence the

transcriptional efficiency by altering the ability of RNA-polymerase to bind to the –10 and –35 motifs of the promotor regions [40–42].

In general, the topological state of DNA in the cell has to be well balanced and precisely regulated [35, 36, 43]. According to eq. 1.2, the change of Lk which is necessary to remove or generate supercoils or the decatenation of daughter chromosomes, requires transient DNA strand breakages. This is accomplished by the protein class of topoisomerases (section 1.2.1).
However, the topology of DNA is also influenced by histone-like proteins [44, 45]. The most common one is the heat-unstable nucleoid protein HU [46–49]. Others are the integration host factor IHF, the factor for inversion stimulation FIS and the histone-like nucleoid structuring protein H-NS. Histone-like proteins are able to bind DNA, to wrap around or to bend it. These proteins can be sequence specific and thus, alter the topology of defined DNA regions.

1.2.1 Classification of Topoisomerases

Topoisomerases play essential roles for all organisms since they control and maintain the topological state of the DNA in the cell. They change the linking number Lk of DNA by passing one strand of DNA through the other [30, 35, 50, 51]. Depending on their mode of action, they are classified into type I and type II topoisomerases [39, 52]. Type I enzymes introduce temporary single strand breakages into the double-stranded DNA. As opposed to this, type II topoisomerases transiently break both strands of dsDNA simultaneously in an ATP dependent manner [35, 36, 53]. In general the enzymes achieve this by transesterifications. First, a phosphorus of the DNA is attacked by a tyrosyl oxygen of the enzyme. The result is a covalent phosphotyrosine link and a free hydroxyl group of the DNA [54]. This reaction is inverted by the hydroxyl group attacking the phosphotyrosine and hence, rejoining the DNA.
Based on similarities according to their structure and mode of action, topoisomerases are further divided into the subtypes IA, IB, IIA and IIB [40, 52]. Enzymes of

the subfamilies IA and II establish a covalent link between a tyrosine residue and the 5'-phosphoryl of the DNA, whereas members of the subfamily IB link to the 3'-phosphoryl group of DNA (fig. 1.4). The topoisomerases that are known to exist in *E. coli* either belong to the subfamilies IA (topoisomerase I and III) or IIA (topoisomerases IV and II) [30, 39, 52, 55]. They carry out both overlapping and specific functions to control the topological state of the DNA.

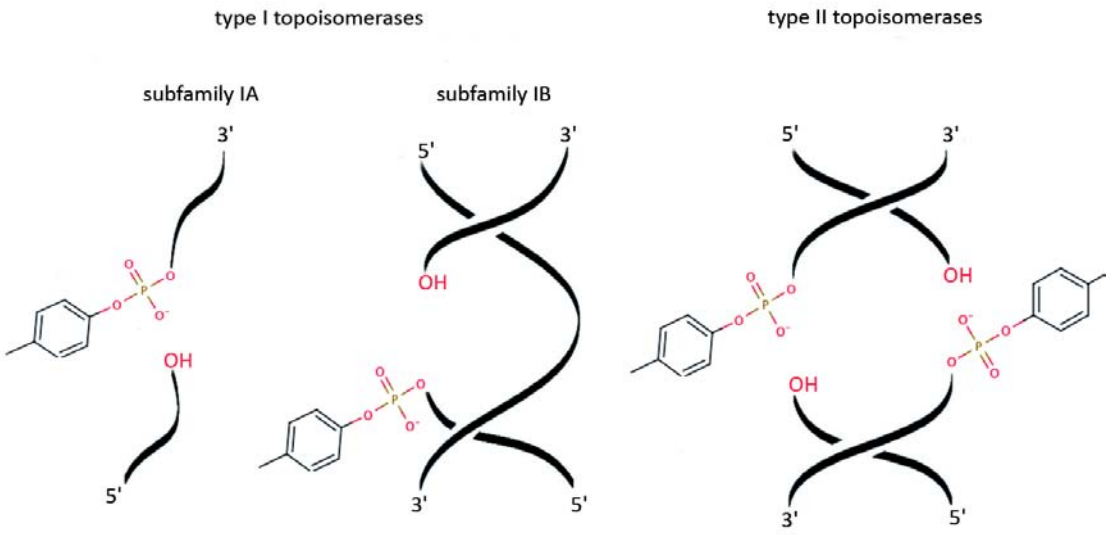

Figure 1.4: *Types of topoisomerases and the schematic depiction of their mode of action*

1.2.1.1 Topoisomerase I

The monomeric topoisomerase I (topoI) is encoded by the *topA* gene. Its main function is the control of the global degree of supercoiling by relaxation of negatively supercoiled DNA that occurs during the transcription process (fig. 1.3) [56–59]. TopoI preferentially binds to single stranded (ss) DNA that is transiently cleaved. If the DNA's degree of negative supercoiling is high enough, topoI is also able to generate a short stretch of ssDNA by unpairing dsDNA. But the efficiency of the enzyme significantly decreases as the DNA becomes less negatively supercoiled [35, 39]. Consequently, topoI is not able to completely relax DNA (fig. 1.5). Mutations in

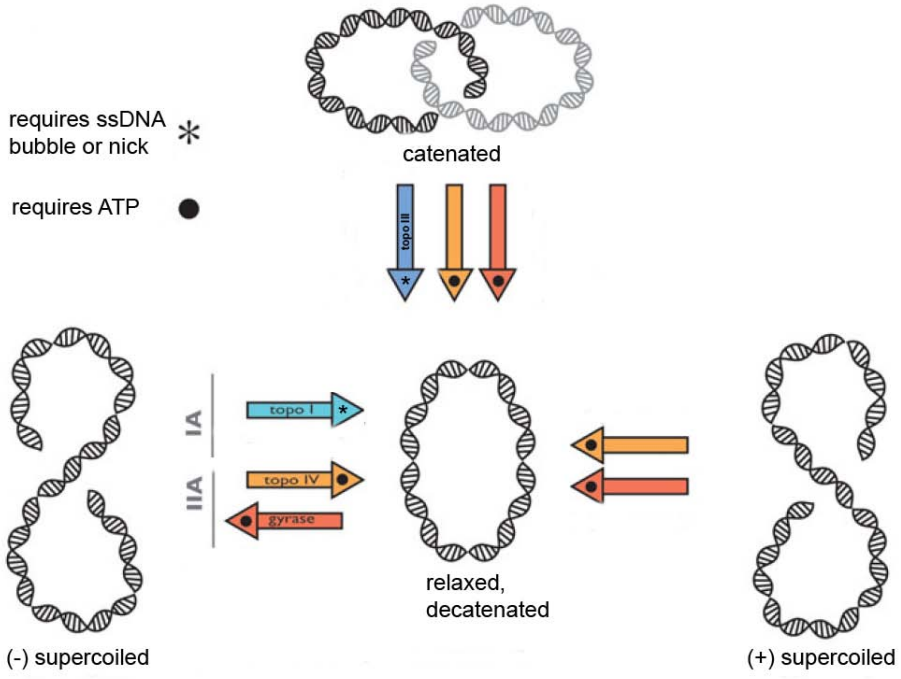

Figure 1.5: *Main roles of the four topoisomerases in E. coli: topoI (cyan), gyrase (red), topoIII (blue) and topoIV (orange); taken from and modified after [30]*

topA that lead to either a reduction or complete loss of topoI activity cause excessive negative supercoiling. Nevertheless, such effects can be compensated by increased levels of topoisomerase IV (section 1.2.1.4) or additional mutations in DNA gyrase (section 1.2.1.2) [60–62].

1.2.1.2 Topoisomerase II - DNA gyrase

DNA gyrase, the bacterial topoisomerase II, is build from two subunits A and B. These are encoded by the genes *gyrA* and *gyrB*, respectively. The active holoenzyme is composed of two GyrA- and two GyrB-subunits that form an A_2B_2 heterotetramer. From biochemical, genetic and biophysical approaches like X-ray crystallography or small angle X-ray scattering data (SAXS), structures and their spatial orientation were only partly available when the current work started (fig. 1.6).

The 97 kDa A subunit is composed of a 59 kDa (GyrA59) N-terminal domain (NTD) and a 38 kDa C-terminal domain (GyrA-CTD) and contains the functional parts that are involved in DNA binding. The 3D molecular structure of the GyrA59 fragment was solved by X-ray crystallography and consists of residues 30–522 (PDB ID: 1ab4) [63]. It contains a catabolite-activator-protein (CAP) like domain which includes the known DNA binding helix-turn-helix (HTH) motif [63–65]. The CAP-like structure element contains the active site tyrosine residues (Tyr^{122}). These are crucial for the breakage and religation of the DNA [54, 63, 66].
The structure of GyrA-CTD adopts a spiral circular-shaped β-pinwheel fold that plays an important role in DNA wrapping (fig. 1.6 (res. 535–841, PDB ID: 1zi0)) [67–69]. It is assumed to contribute to the unique ability of gyrase amongst the topoisomerases to introduce negative supercoils into positively supercoiled and relaxed DNA (fig. 1.5) [68, 69]. Although the spatial orientation of GyrA59 and GyrA-CTD has been proposed on the basis of SAXS, a high resolution structural model of the complete GyrA subunit is still missing [67].

The B-subunits amount to 90 kDa each and are responsible for ATP binding, its hydrolysis and support DNA binding [70, 71]. As schematically depicted in fig. 1.6, *E. coli* GyrB consists of three domains of which the 43 kDa NTD harbors the ATPase activity (res. 2–392, PDB ID: 1ei1) [72, 73]. The 47 kDa CTD of GyrB consists of a Toprim and a tail domain and contributes to the binding of DNA via interaction with the GyrA subunit [74]. The Toprim domain (topoisomerase-primase) encompasses the residues 393–533. It carries the conserved GyrB motifs EGDSA (res. 424–428), PLKGK (res. 445–449) as well as DxDxD (res. 498–502). These patterns appear to be conserved in type IA and IIA topoisomerases and are known to form the Mg^{2+} binding site which plays a role in DNA cleavage and religation [75–80]. The DNA binding Rosmann fold that is found within the Toprim domain contains a known nucleotide binding group [81, 82]. It is also known that the tail domain (res. 534–804) makes an essential contribution to gyrase's ability to bind DNA [71, 79, 80].
Since the current work was done, homologous topoIV $ParC_2ParE_2$ assemblies (section 1.2.1.4) were published for *Streptococcus pneumoniae* and *Acinetobacter baumannii*. These substantially contributed to the structural and mechanistic understanding of

bacterial type II topoisomerases. However, the exact arrangement of the complete $GyrA_2$-$GyrB_2$ complex remains unclear.

The currently accepted mode of gyrase action was proposed as an ATP dependent multistep model [67, 71, 83] (fig.1.7): After the holoenzyme is formed from its components (fig. 1.7-1), the T (transfer) segment is presented over the G (gate) segment (fig. 1.7-2). With the binding of two ATP molecules, the B-subunits dimerize and capture the T-segment. The GyrA dimer transiently introduces a double strand breakage into the G-segment (fig. 1.7-3) by an esterification between the Tyr^{122}-OH of GyrA59 and a 5'-phosphate of the DNA. The cleavage takes place at preferred cleavage sites of the DNA (5'–↓GRYC–3', with R=purine, Y=pyrimidine and ↓ indicating the cleavage site [84–86]). Hydrolysis of one ATP molecule causes the T-segment to be transported through the resulting gap of the G-segment (fig. 1.7-4). Afterwards, the DNA break in the G-segment is resealed again and the T-segment is released. The initial conformation of the enzyme is restored by hydrolysis of the second ATP molecule (fig. 1.7-5). Thus, in the presence of ATP, the linking number *Lk* is reduced by two. As a result, gyrase converts a low energy state relaxed DNA into a negative supercoiled DNA topology with a high energy. This energy facilitates transcription, recombination and DNA-replication (section 1.2). However, in the absence of ATP, gyrase supports the other topoisomerases by relaxing negatively supercoiled DNA [87, 88] (section 1.2.1).
It was recently shown that the G-segment is bent by about 75° at each site of the dimeric enzyme during the catalytic cycle of topoisomerase II in *S. pneumoniae* and *A. baumannii* as well as in the eukaryotic organism *S.cerevisiae* resulting in an overall bend of 150° [76–80, 89–91]. Moreover, the recent X-ray analyses showed that the DNA binding and cleavage process is supported by Mg^{2+} ions which are placed between the Toprim domain and the scissile phosphate [78–80]. The recent findings from topoIV also contribute to the understanding of gyrase since both enzymes share a high level of sequence similarity (section 1.2.1.4) [60, 92–94].

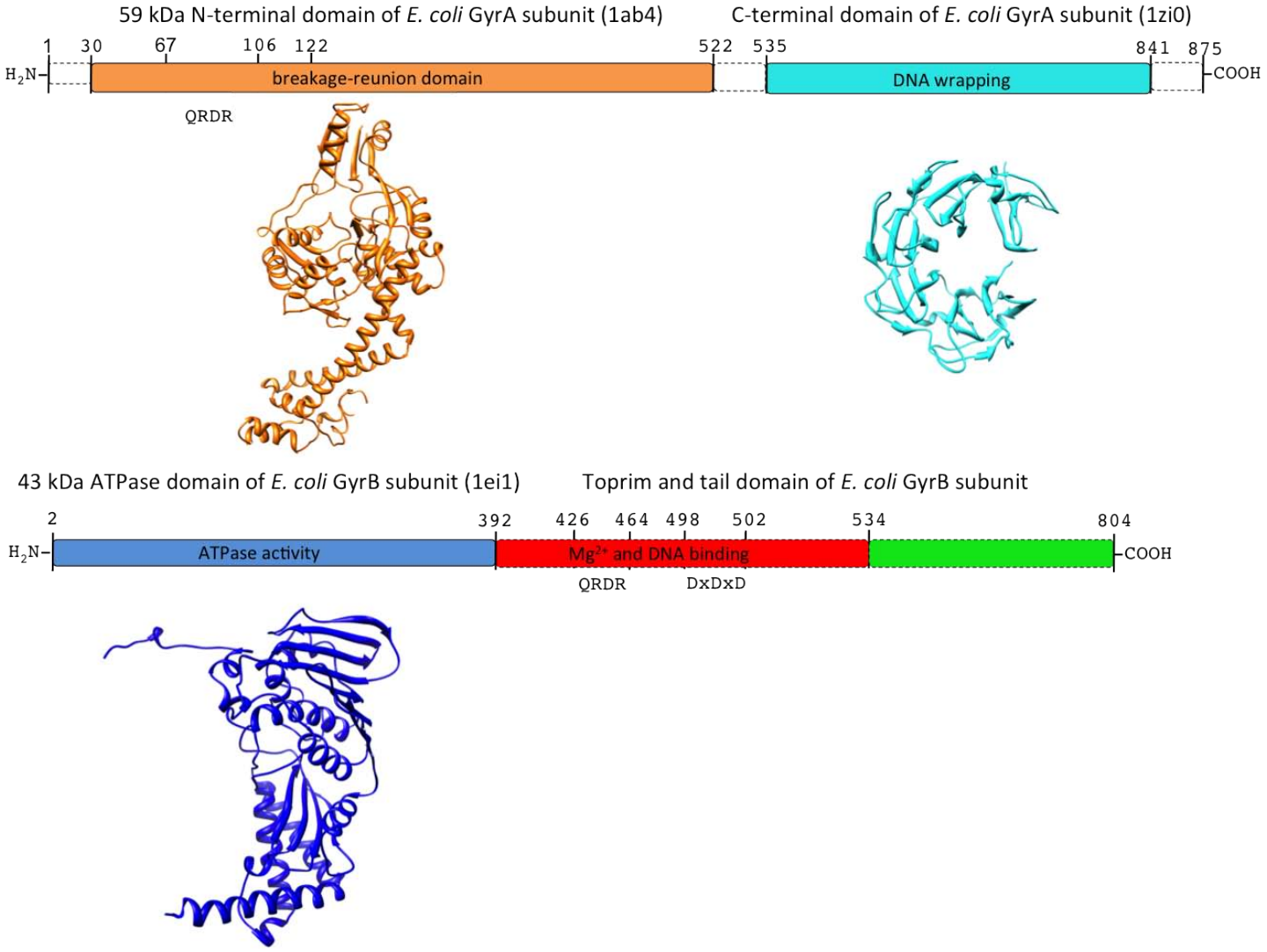

Figure 1.6: *Domain organization and availability of structural information for E. coli DNA gyrase: GyrA59 in orange, GyrA-CTD in cyan, GyrB43 in blue, Toprim domain in red and tail domain in green [82]. The dashed lines indicate missing structures. Details are given in the text.*

1.2.1.3 Topoisomerase III

The second type IA topoisomerase in *E. coli* is topoisomerase III (topoIII)[95]. The enzyme is encoded by the *topB* gene. Like topoI, it is a monomeric protein that needs a stretch of ssDNA and is unable to unwind positively supercoiled DNA [96]. However, the enzyme needs DNA with a negative superhelicity several times higher than normal (hypernegatively supercoiled DNA) [52, 97]. TopoIII also has a potent decatenase activity which is used by the cell to remove precatenanes behind the replication fork [97–100]. Although the enzyme is not essential for the cell, it is known that the lack of a functional topoIII is accompanied by an increased level of spontaneous deletions of chromosomal DNA [101].

1.2.1.4 Topoisomerase IV

Topoisomerase IV (topoIV) is the second type IIA topoisomerase in *E. coli*. The heterotetrameric enzyme is encoded by the genes *parC* and *parE* and consists of two C as well as two E subunits (C_2E_2) [60, 102–105]. The active site tyrosines are located in the C-subunits. The E-subunit is responsible for the enzyme's ATPase activity.

The main function of topoIV is the segregation of catenated DNA rings that result from replication or recombination *in-vivo* [60, 102, 106]. Aside from this, topoIV relaxes supercoiled DNA with a clear preference for positive supercoils which helps the replication fork to proceed [107]. However, although significantly slower than topoI, topoIV is still able to relax negatively supercoiled DNA. Remarkably, its relaxation activity is independent of the degree of negative supercoiling and DNA can be relaxed almost entirely (fig. 1.5) [94]. Besides its role in relaxation and decatenation, the enzyme is able to disentangle DNA knots *in-vivo* [108]. Since topoIV is essential for the bacterial cell, any mutation leading to inactivity of this topoisomerase is lethal [94, 109].

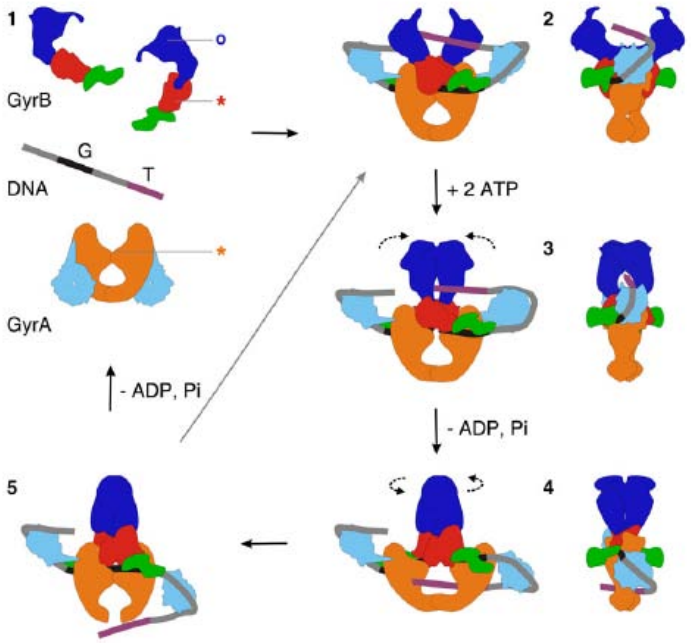

Figure 1.7: *Schematic mechanism of DNA-gyrase catalysis. The right column shows side views for steps 2-4. Stars indicate the active site residues for DNA cleavage and the circle the ATP-binding pocket in GyrB. GyrA59 in orange, GyrA-CTD in cyan, GyrB43 in blue, Toprim domain in red and tail domain in green [82]. The G-segment is shown in black, the T-segment in purple. Details are given in the text (taken from [71])*

1.2.2 Regulation of DNA supercoiling degree

A specific degree of DNA supercoiling in the cell is required for different crucial cellular processes. Uncontrolled topoisomerase actions in an organism would thus have vicious effects (section 1.2). For this reason, the activities of the topoisomerases have to be strictly regulated.
Especially due to the preference for naturally occurring DNA to adopt negative supercoils, a homeostatic regulation mechanism exists in *E. coli* to control supercoiling [32, 33, 110, 111]. This regulation is achieved by the antagonistic effects of topoisomerase I and gyrase as depicted in fig. 1.5 (sections 1.2.1.1 and 1.2.1.2). The differing specificities of the topoisomerases for varying degrees of DNA supercoiling also contribute to the homeostatic control: TopoI shows a high affinity to negatively supercoiled DNA, whereas it was shown that the affinity of topoIV is increased for positively supercoiled substrate DNA [35, 39, 107]. In addition, the degree of supercoiling influences the transcription of the topoisomerase encoding genes. Hereby, a relaxation of DNA augments the expression of DNA gyrase [110, 112]. However, the transcription of the topoI encoding *topA* gene is intensified if the rate of negatively supercoiled DNA is raised. This is additionally regulated by promotors that function as sensors for the degree of supercoiling [110, 112–114].

Furthermore, a variety of endogenous proteins also contribute to fine-tune the topoisomerase activity in bacterial cells. In this context YacG, GyrI or MurI are known to be potent inhibitors of DNA gyrase [115–122]. Aside from these intracellular activities, a variety of other factors like temperature, osmolarity, oxygen content or the different growth periods have an impact on the degree of supercoiling in the cell [123–127].

1.3 Inhibition of topoisomerases

Inhibition of fundamental cellular activities like cell-division, recombination or transcription in microorganisms is an interesting approach in the treatment of bacterial infections. Due to the pivotal contribution in such processes, topoisomerases were exploited as attractive molecular structures with a high therapeutic potential [128, 129]. Although topoI inhibitors have been found [130], clinically relevant inhibitors focus on gyrase and topoIV.

The aminocoumarin-type compounds novobiocin, clorobiocin and coumermycin A_1 target the ATP binding pocket of the GyrB and ParE subunits of gyrase and topoIV, respectively. This way, they inhibit gyrase to carry out negative supercoiling and prevent topoIV from decatenation [131–135]. Aminocoumarin-type compounds are of less importance due to their toxicity and solubility. Thus, they are not in clinical use [136–138]. Far more important inhibitors of bacterial topoisomerases are the quinolones [87, 88] (section 1.3.1).

1.3.1 Quinolones

In 1962, Lesher and coworkers first described the fully synthetic family of quinolones [4]. Nalidixic acid, a 1,4-dihydro-4-oxo-1,8-naphtyridine-3-carboxylic-acid, is the prototypical compound of this group (fig. 1.8(a)), but only shows a narrow antibacterial spectrum and low bioavailability. Substitution of the methyl-group at C7 by a piperazinyl-moiety lead to its successor, pipemidic acid (1.8(b)). Pipemidic acid showed slightly better pharmakokinetic properties and was used for the treatment of infections of the urinary tract. Together with flumequin, a C6-fluoro substituted 1,4-dihydro-4-oxo-3-quinoline-carboxylic-acid (fig. 1.8(c)), these structures belong to the first generation of quinolones. The breakthrough was made by the introduction of the second generation of quinolones that combined the fluoro-substituent at C6 and the saturated nitrogen-containing heterocycle at C7. The first representative of this generation was norfloxacin, a 1-ethyl-6-fluoro-4-oxo-7-piperazin-1-yl-1H-quinoline-

3-carboxylic acid. Norfloxacin and its derivatives ciprofloxacin and ofloxacin (fig. 1.8(d-f)) show a broad spectrum of activity and good pharmakokinetic properties. Further modifications of the quinolone-skeleton lead to drugs of the 3^{rd} (e.g. levofloxacin) and 4^{th} (e.g. moxifloxacin) generation that show even broader and different spectra of activity and pharmakokinetic characteristics [139, 140].

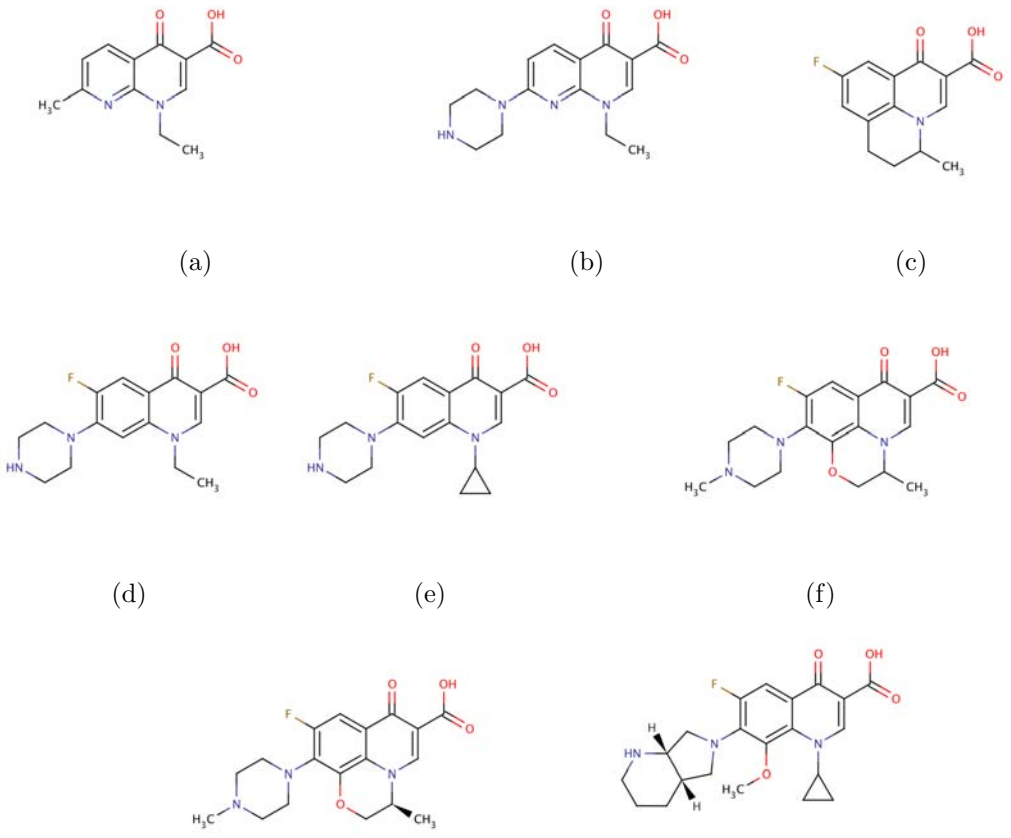

(a) (b) (c)

(d) (e) (f)

(g) (h)

Figure 1.8: *2D-structures of (a) nalidixic acid, (b) pipemidic acid, (c) flumequin, (d) norfloxacin, (e) ciprofloxacin, (f) ofloxacin, (g) levofloxacin, (h) moxifloxacin*

1.3.1.1 Mechanism of action

Quinolones are popular antibiotics which have been in use for more than four decades and remain the drugs of choice for some applications (table 1.3). They do, of course, inhibit the eukaryotic enzymes, but two to three orders of magnitude more weakly. In the context of cancer therapy, the mammalian enzyme is used as a target, but with a different class of drugs like podophyllotoxins (etoposide) [51, 141–143]. Most interestingly, the eukaryotic enzyme appears not to be too different from the bacterial, since a small set of mutations render the eukaryotic enzyme more susceptible to quinolones [144].

group	indication	spectrum	example drug
I	infections of the urinary tract prostatitis gonorrhea bacterial enteritis	gram-negative	norfloxacin
II	urinary tract infections infections of skin and bone respiratory tract infections	group I staphylococci pneumococci enterococci streptococci	ofloxacin ciprofloxacin
III	respiratory tract infections skin and bone infections gonorrhea cervicitis urethritis	group II chlamydia mycoplasma	levofloxacin
IV	respiratory tract infections skin and bone infections abdominal infections systemic infections sepsis, meningitis	group III gram-positives atypical bacteria	moxifloxacin

Table 1.3: *Groups of quinolones listed with their indication, spectra and example drugs (modified after [139, 140]).*

Quinolones exert their antibiotic effect by the formation of a ternary complex in which they bind to the cleaved protein-DNA complexes (cleaved complexes) non-covalently. This way, the drugs stabilise the cleaved complexes, prevent the religation

of the cleaved DNA, and generate DNA-lesions [11, 12, 145, 146]. Since quinolone binding is reversible it needs inhibitory drug concentrations to stabilise double strand breakages in DNA. The cleavage complex is a barrier for replicative enzymes (section 1.2). Consequently, this leads to an impaired DNA replication, recombination, transcription, and thus impedes bacterial growth [147–149]. The strand breakages activate the SOS regulon consisting of more than 30 genes involved in recombination and DNA repair [150]. This leads to decreased cell division while the production of enzymes necessary for DNA repair is increased. The induction of the SOS response needs the action of the RecBCD enzyme complex which plays an important role in the recognition of DNA strand breaks [145, 151]. Due to its 3' $\rightarrow$ 5' exonuclease activity, RecBCD generates a single stranded DNA segment. This segment is then bound to the SOS-regulatory protein RecA [152], an important factor in homologous recombination, and induces the autoproteolytic activity of LexA. Since LexA is a known repressor of SOS genes this results in a derepression of the SOS response [153]. Once the DNA damage is repaired, the RecA concentration is lowered again, leading to a rise of LexA levels and the repression of SOS genes [154]. Due to inhibitory concentrations of quinolones, the DNA break repair mechanism is constitutively induced and bacterial growth is blocked. Additionally, since SOS mechanisms are prone to errors, potentially deleterious mutations in the bacterial DNA can accumulate and promote bacterial cell death.

There is recent experimental evidence that the major contribution to the bactericidal effect of quinolones is from excessive chromosome fragmentation [148, 155, 156]. In *E. coli*, the quinolone-associated rapid cell death occurs by two pathways. The first one requires active protein synthesis and is accompanied by increased concentrations of toxic hydroxyl radicals. The second pathway is independent of protein synthesis and does not require reactive oxygen species for killing the cells. However, quinolone binding might result in a dissociation of gyrase subunits [148, 157–159].

It was shown that the bactericidal effects of quinolones differ significantly in the presence of the protein-synthesis inhibitor chloramphenicol. In this context it was found that ciprofloxacin was able to exert its lethal effect in the presence of chloramphenicol while norfloxacin was not. These drugs only differ by their N1-substitutions

as shown in fig. 1.8. Furthermore, it was recently shown that the action of quinolones is improved by N1-cyclopropylic and C8-methoxy substituents if protein-synthesis is blocked. Another influence is the substituent at C7 [156].

1.3.1.2 Resistance

Quinolones are losing their antibacterial effectiveness due to quickly emerging bacterial resistance. The intracellular quinolone concentration and the affinity to its target structure determine the susceptibility of a bacterial cell. As with all antiinfective drugs resistance against quinolones can be due to the following mechanisms (section 1.1) [160–162]: The effectiveness of quinolones can be lowered by a decreased influx of the therapeutics into the cells. In Gram-negative bacteria, drugs have to penetrate the cytoplasmic membrane, the cell wall and the outer membrane. While rather lipophilic quinolones are able to diffuse into the cells through the lipopolysaccharides and porins, hydrophilic drugs mainly have to penetrate through porins. The decreased influx of quinolones is mainly based on a reduced expression of porins. Porins are transmembrane-channels build from outer membrane proteins. They can be specific and non-specific [163]. The decreased expression of the non-specific outer membrane protein F (OmpF) is of particular interest for the development of resistance in *E. coli*. Its expression has to be strictly regulated in order for the cells to be able to adapt changing environmental conditions [164–168]. Such regulation can be carried out by the OmpR regulator and the post-transcriptional antisense-RNA *micF* [169]. The translation of *ompF* is blocked by the assembly of a dsRNA which is composed of *micF*-RNA and the *ompF*-mRNA. The expression of *micF* is regulated by the activator MarA and its repressor MarR. Mutations that lead to a loss of MarR activity result in a constitutive expression of MarA. Thus, *micF* is permanently available for the formation of *micF*-RNA / *ompF*-mRNA complexes. Hence, the translation of *ompF*-mRNA is inhibited. As a result, the outer membrane lacks OmpF porins. This is accompanied with a decreased influx of quinolones and other antibacterial agents [170–172]. In addition to a decreased influx, quinolone resistance is also mediated by increased levels of multi-drug efflux pumps. Of these,

the AcrAB/TolC efflux pump is believed to play a major role with respect to the development of clinical resistance against fluoroquinolones in *E. coli* [173–178]. This pump is directly regulated by MarA and MarR [179–181].

Aside from the quinolone-modifying and plasmid-borne gene *aac(6')-Ib-cr* that may contribute to a decreased susceptibility by metabolising quinolones [182], the products of the five known *qnr* gene family members (QnrA, QnrB, QnrC, QnrD and QnrS) protect gyrase and topoisomerase IV against the therapeutics and were found in different *Enterobacteriaceae* [183–187].
The protection of gyrase and topoisomerase IV by Qnr proteins as well as the enzymatic inactivation of the drugs only results in a moderate decrease of susceptibility against fluoroquinolones. But since they may allow bacteria to survive longer under the influence of fluoroquinolones, such Qnr proteins may promote the development of mutants that carry mutations of the quinolones' target structure. This way, the bacteria may acquire reduced susceptibilities against fluoroquinolones. Moreover, Qnr is usually located on a multi-resistance plasmid which may also mediate resistances against further antibiotic agents like chloramphenicol, streptomycin, β-lactams, sulfonamides and trimethoprim. Hence, the development of multi-resistant bacteria is a serious threat that was already shown *in-vitro* [188].

Finally, and believed to be most relevant, is the acquisition of mutations in the genes encoding gyrase (*gyrA* and *gyrB*) and topoisomerase IV (*parC* and *parE*). Such mutations can lead to structural modifications of the target and thus affect the binding affinity. They have been mapped to a region known as the quinolone resistance determining region (QRDR) of gyrase subunits A (residues 67–106) [189–191] and B (residues 426–464) [192] (section 1.2.1.2). In quinolone-resistant bacteria, mutations are most often found in the *gyrA* and *parC* genes and less often in *gyrB* and *parE*. But amino acid exchanges within the QRDR often occur at Ser^{83} and Asp^{87} of GyrA and positions 80 and 84 of ParC (numbering refers to *E. coli*). Aside from these, *E. coli* GyrA residues Gly^{81}, Asp^{82} as well as GyrB residues Asp^{426}, Lys^{447} and Ser^{464} are also important since they are further positions of resistance mutations [160, 190, 192–197]. While single mutations are sufficient to confer resistance to older quinolones like nalidixic acid, resistance to fluoroquinolones requires multiple amino

acid substitutions, like the GyrA Ser^{83} / Asp^{87} or Gly^{81} / Asp^{82} double mutations [198–200].

Whether a mutation leads to resistance or not depends on which enzyme is the primary target in a given bacterial species. Generally, gyrase is the primary target in Gram-negative bacteria, whereas topoIV is primarily targeted by quinolones in Gram-positives. This was shown by *in-vitro* selection experiments. Mutations in topoisomerase IV were not found until the second or third selection step [194, 198, 199]. In *S. pneumoniae*, the primary target depends on the specific drug [201–203].

The presence of quinolones and mutations in gyrase / topoIV can affect the balance of the DNA supercoiling degree in the cell (section 1.2) [131, 204, 205]. Mutations in the target structure might decrease the effect of quinolones on the cell. In the presence of quinolones this confers an evolutionary advantage. But there might be a tradeoff with bacterial fitness. This may be exhibited by a loss of enzymatic activity (section 1.2) and the resulting change in gene expression may also affect genes important for bacterial virulence [41, 123, 198, 206].

1.4 Aims of this work

Understanding the drug-enzyme-DNA interactions in molecular terms is the basis for the development of new chemical leads or the optimization of quinolone-derivatives which are refractory to resistance. In order to obtain a detailed understanding of the interaction between quinolones and the gyrase-DNA complex, it is crucial to have a structural model. However, there were no structures from experimental approaches like X-ray crystallography, NMR-spectroscopy or cryoelectron-microscopy to explain the exact mode of inhibition. Biochemical data indicates that distinct residues in GyrA, in particular Ser^{83} and Asp^{87}, are important for the interaction with fluoroquinolones [190, 207] (sections 1.2.1.2 and 1.3.1). The goal of this project was therefore to build a model of the protein-DNA complex which reconciles existing biochemical knowledge such as resistance mutations and partial structures. This model should have predictive power for previously unknown residues involved in the reaction mechanism, quinolone binding, and the development of resistance.

After the completion of this model, crystal structures of homologous topoIV-DNA-quinolone complexes were released and a comparison with the theoretical models could be carried out. In order to explain the effects of quinolones, homology modelling, conservation analyses and a CoMSIA model will be used. Some novel mutations from mutant selection and inhibition measurements that were not previously described will be discussed in the light of the homology model. The prospect of this work is to develop a rational basis for the design of new inhibitors of DNA-gyrase, a concept that already has successfully been applied for the development of beta-lactamase inhibitors.

Chapter 2

Theoretical background information

This chapter gives a general introduction to computational methods used in order to facilitate the understanding of the applied techniques.

2.1 Molecular docking

The general aim of molecular docking is to find transformations of a molecule A (ligand) with respect to a second molecule B (target) that assembles the two to the complex AB. The underlying concept is also referred to as the 'lock-and-key' principle [208]: A and B are only able to interact, if they possess complementary surface patches. In order to match, these patches must arrange in the right configuration. This can be compared to a molecular puzzle in which parts of the molecules have to be matched (fig. 2.1). This is important for the formation of hydrogen-bonds, salt-bridges, hydrophobic and electrostatic interactions as well van der Waals forces.

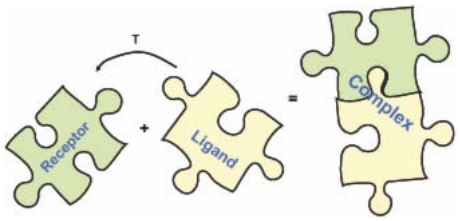

Figure 2.1: *Given the structures of the ligand and its target, find a transformation* T *which yields the complex.*

2.1.1 Protein-DNA docking and docking of small molecular ligands

One approach to the docking of macromolecules begins by simplifying the surface representation to just convex, concave and flat patches which can be fitted to another rather swiftly (fig. 2.2). Removing atomic detail is a necessary approximation for problems such as DNA-protein docking.

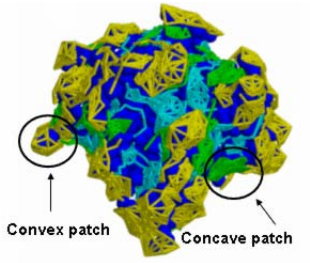

Figure 2.2: *Reduced representation of a molecular surface: Concave patches (green) match to convex patches (yellow) and vice versa. Flat patches (light-blue) match every other patch (taken from and modified after [209]).*

In contrast, one usually works with atomic detail when trying to place smaller ligands into proteins. Of the many available methods, the approach in this work begins by calculating 3D grids to find potential binding sites for the ligands in the target protein. The calculation of the grid and docking of ligands into such grids are usually

separated. Probe atoms that represent the atom types of the ligand are placed at each grid point. Next, the interactions between probe atoms and the target site are evaluated and stored. Afterwards, the docking procedure places a ligand into the set of grids.
This can be done by applying a genetic algorithm: For each ligand, an initial population of candidate dockings is calculated. In this context, a docking is described by its individual state variables: conformation, orientation and translation relative to the target molecule. Each state variable corresponds to a gene whereas the 3D coordinates of an individual ligand describe its phenotype. Furthermore, the fitness of a docking, i.e. the total interaction energy with its molecular target is computed based on the precalculated grids. Thus, as in genetics, an individual is characterized by its genotype, phenotype and fitness. New dockings are generated by a mixture of mutations and recombinations of the state variables. Whether a new individual docking survives or not is based on its fitness. This way, the genetic algorithm evolves new ligand poses that are more and more likely to represent favorable binding interactions.

2.2 Molecular dynamics simulations

Even if molecules are usually represented as static structures, they are in fact dynamic and can adopt a variety of conformations. Molecular dynamics (MD) simulations are the natural method for generating and sampling these conformations.
In MD simulations, a sequence of molecular conformations is computed as a function of time. This is done by the integration of Newton's equations of motion [210–215].
Newton's second relates the force $\mathbf{F}_i$ acting on a particle i ($i = 1..N$, with N being the number of particles in the system) to its mass m_i and the resulting acceleration $\mathbf{a}_i$ as shown in the next line (eq. 2.1).

$$\mathbf{F}_i = m_i \mathbf{a}_i \quad \Longleftrightarrow \quad \mathbf{a}_i = \frac{\mathbf{F}_i}{m_i} \tag{2.1}$$

The acceleration $\mathbf{a}_i$ is defined as the first derivative of the velocity $\mathbf{v}_i$ with respect to

time t, i.e. the change of velocity $d\mathbf{v}_i$ with respect to the change of time dt (eq. 2.2). The velocity $\mathbf{v}_i$ is the first derivative of the particles' position $\mathbf{r}_i$ with respect to time t (eq. 2.3). Thus, the acceleration $\mathbf{a}_i$ is the second derivative of the positions $\mathbf{r}_i$ with respect to time t as given in eq. 2.4.

$$\mathbf{a}_i = \frac{d\mathbf{v}_i}{dt} \tag{2.2}$$

$$\mathbf{v}_i = \frac{d\mathbf{r}_i}{dt} \tag{2.3}$$

$$\mathbf{a}_i = \frac{d^2\mathbf{r}_i}{dt^2} \tag{2.4}$$

Substituting the acceleration term in eq. 2.1 by eq. 2.2 yields eq. 2.5. Afterwards, eq. 2.6 results from the replacement of the velocity $\mathbf{v}_i$ in eq. 2.5 by eq. 2.3.

$$\frac{\mathbf{F}_i}{m_i} = \frac{d\mathbf{v}_i}{dt} \tag{2.5}$$

$$\frac{\mathbf{F}_i}{m_i} = \frac{d^2\mathbf{r}_i}{dt^2} \tag{2.6}$$

The force $\mathbf{F}_i$ from eq. 2.6 that acts on an atom i can be calculated by taking the negative partial derivative of the energy V with respect to the change in the atom's position $\mathbf{r}_i$ (eq. 2.7). The energy V is calculated from a standard forcefield [210].

$$\mathbf{F}_i = -\frac{\partial V}{\partial \mathbf{r}_i} \tag{2.7}$$

If forces $\mathbf{F}_i$ and masses m_i are known, the positions $\mathbf{r}_i$ of each atom i of the system can be calculated along a series of time steps. These are usually in the order of femtoseconds. The result is a sequence of structural changes over time t, the trajectory.

At the beginning of a simulation, the particles of the system are given initial positions

$\mathbf{r}_i$ and velocities $\mathbf{v}_i$. Taking this information, the potential energy V is calculated. Afterwards, forces $\mathbf{F}_i$ between all pairs of atoms i are computed according to eq. 2.7. Thereafter, the movement of the particles is simulated by numerically solving Newton's equations of motion (eq. 2.6, fig. 2.3).

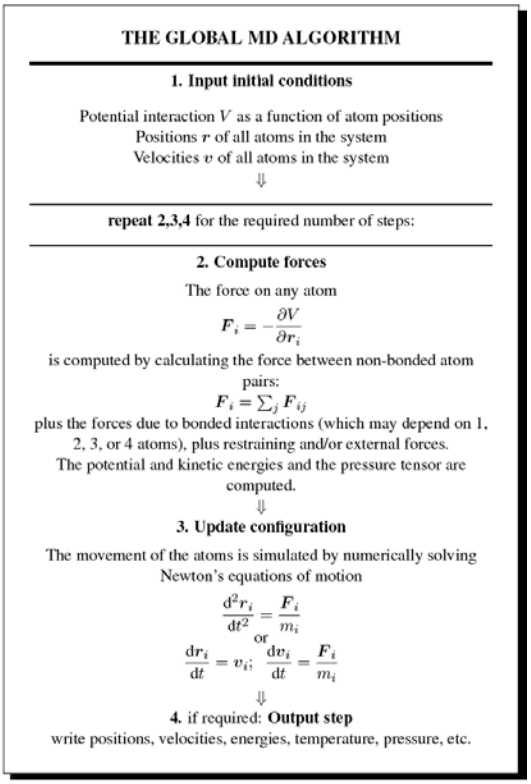

Figure 2.3: *The global MD algorithm (taken from [214])*

2.3 Quantum mechanical optimizations

Docking calculations and their scoring functions usually depend on the partial charges assigned to atoms. If ligands have unusual chemistry, with a mixture of aromatic and very electronegative groups, it is preferable to apply some kind of quantum chemical

method to estimate charges and geometries of the molecules.
Unlike most classical approaches, these methods do not regard electronic structure as fixed. One actually tries to estimate the probability functions which describe the location of the electrons. At the same time, one can optimize the positions of the atoms, so these methods allow one to optimize charges and geometry simultaneously. The methods differ in the approximations they use, which interactions between electrons are considered and the underlying representation (basis set) for the electrons.

2.4 Quantitative Structure Activity Relationships

The aim of QSAR (quantitative structure-activity relationship) analyses is to quantitatively correlate the chemical structure of ligands with their biological activity [20, 216–220] assuming that such activities can be expressed as functions of the structural properties. In QSAR the molecules under consideration have to share chemical similarity and the same mechanism of action as well as the same molecular target.
In contrast to the 2D QSAR approaches (Hansch-, Free-Wilson analysis) three-dimensional QSAR methods consider the 3D binding modes of ligands in their target. CoMSIA is one such approach and compares ligands with respect to local structural similarities. These common features are hopefully relevant for binding to the biologically relevant target.
In general, a CoMSIA analysis starts with the structural alignment of compounds from a training set and their placement into a three dimensional grid. At each grid point, the similarity of the compounds with a probe is determined. Afterwards, the derived data at the grid points is correlated with the biological activities. Based on compounds from the training set, a CoMSIA model is derived and validated. Finally, this model can be used to predict activities of compounds from a test set.

Parts of the validation procedure are the calculation of the $PRESS$ value (predictive residual sum of squares) and the cross-validated correlation coefficient q^2. $PRESS$ is calculated as the sum over the differences between the actual y_i and the predicted

activities p_i (eq. 2.8) [221, 222].

$$PRESS = \sum_{i=1}^{n} (y_i - p_i)^2 \tag{2.8}$$

The q^2 value is also referred to as the predictive r^2. It relates the $PRESS$ and the sum of squares SS, with $\overline{y}$ being the arithmetic mean of the actual activities (eqs. 2.9 and 2.10).

$$SS = \sum_{i=1}^{n} (y_i - \overline{y})^2 \tag{2.9}$$

$$q^2 = 1 - \frac{PRESS}{SS} \tag{2.10}$$

Chapter 3

Material

3.1 Software

A variety of different software tools was used in this work. Molecular dynamics simulations were carried out with GROMACS [213, 214]. Molecular modelling was done with UCSF Chimera and SYBYL [223–228]. PatchDock and AutoDock4 were used to approach the molecular docking problem for protein-DNA as well as for protein ligand complexes [209, 229–233]. The APBS plugin in PyMOL was used for the evaluation of electrostatic properties of proteins [234, 235] whereas SWISS-MODEL was used for homology modelling [236–238]. The pK_a calculator plug-in of MarvinSketch (version 5.1.03, ChemAxon 2008, http://www.chemaxon.com) was applied for the estimation of protonation states and net charges of compounds. Compound charges and geometries were optimized using Gaussian03 as well as the AM1 method within MOPAC (v6.0) [239, 240]. OMEGA2 (OpenEye Scientific Software, version 2.3.2) and ROCS were applied for the generation of compound conformers and their structural alignments [241, 242].
The application of these tools is mentioned in the following sections.

Chapter 4

Methods

A variety of computational methods, ranging from molecular docking to molecular dynamics (MD), quantum mechanical calculations, 3D-QSAR and conservation analyses were applied to work out a molecular model of the quinolones complexed with the covalent gyrase-DNA model.

4.1 Building the DNA

Due to the lack of structural information of the *E. coli* gyrase DNA complex, the first step was to build an appropriate DNA molecule. Since DNA approaches the gyrase in an uncleaved form, the initial 3D coordinates of a 21 bp dsDNA including the preferred cleavage sites 5'–↓GRYC–3' was modelled, where the first guanine was termed the +1 (G^{+1}) while the last cytosine was the +4 nucleotide position (C^{+4}). These were known from analyses of DNA sequence alignments [84–86]. The dsDNA was assumed to adopt its standard B-DNA geometry and was assembled using the SYBYL molecular modelling package [228].

4.2 Protein-DNA-docking using PatchDock

The 59 kDa N-terminal domain of the *E. coli* GyrA subunit served as the target structure (PDB ID: 1ab4), while the 21 bp dsDNA was used a the ligand (section 4.1). PatchDock was run using its default parameters but with an additional input list of amino acids that might be involved in interactions with the dsDNA [209, 229, 230, 243]. This way, the docking volume to be sampled was reduced and the potential DNA binding site in the target was defined. The residues were selected based on experimental findings as well as electrostatic surface characteristics of the protein and DNA [54, 63, 84–86, 191]. They are depicted in the structure model of the 59 kDa N-terminal domain of *E. coli* GyrA in fig. 4.1.

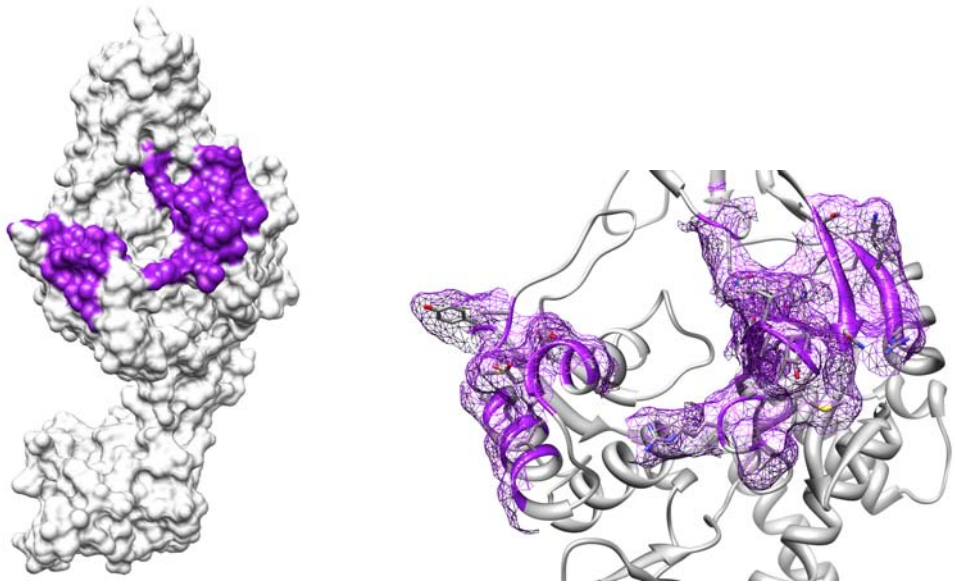

Figure 4.1: *PatchDock volume depicted as solid molecular surface (left) and mesh representation of zoomed GyrA59 (right). The docking volume was defined by the following residues (purple): Val^{30}, Arg^{32}, Ala^{33}, Ala^{67}, Val^{70}, Gly^{71}, Ile^{74}, Gly^{75}, Gly^{81}, Asp^{82}, Ala^{84}, Ser^{83}, Tyr^{86}, Ala^{119}, Met^{120}, Tyr^{122}, Ser^{172}, Gly^{173}, Ile^{174}, Ala^{175}, Val^{176}, Gly^{177}, Met^{178}, Ala^{179}, Thr^{180}, Asn^{181}, Arg^{237}, Gly^{238}, Lys^{239}, Val^{240}, Gln^{267}, Val^{268}, Ser^{329}, Phe^{330}, Gly^{331}, Ile^{332}, Asn^{333}*

4.3 Docking of quinolones using AutoDock4

Candidate conformations of quinolones bound to their target structures, the GyrA59-DNA complexes, were proposed using AutoDock4 [232, 233, 244–248]. Here, docking was carried out with a set of eleven quinolones (fig. 4.2). The grids were calculated with AutoGrid using a spacing of $3.75{\cdot}10^{-2}$ nm. They were defined to contain the potential binding pocket between Ser^{83} and Asp^{87} in the QRDR of GyrA as well as the four overhanging bases of the cleaved dsDNA. Sidechains of selected residues in the potential quinolone binding pockets were set to be flexible (section 5.3).
Docking was parameterized to terminate if either a maximum of $2.5{\cdot}10^{7}$ energy evaluations was reached or a maximum number of $2.7{\cdot}10^{4}$ generations was sampled. A population size of 300 individuals and a maximum number of 250 runs was used. Aside from this, the default settings were applied as listed in the example docking parameter file in appendix A.
For each compound 250 conformations were written out and clustered based on *rmsd* with a tolerance of 0.2 nm. This way, two quinolone conformations were clustered together if their *rmsd* was less then 0.2 nm.

4.4 Molecular dynamics simulations of protein-DNA-complexes using GROMACS

In this work, all MD simulations were carried out using GROMACS v3.3.1 with the AMBER03 forcefield ports [213, 250]. Each system was simulated in the isothermal-isobaric ensemble (NPT) at a pressure of 1 atm and temperatures as described below. Pressure P and temperature T were kept constant using the pressure and temperature coupling methods with pressure and temperature coupling constants τ_P and τ_T as given in appendix B [251]. Each simulation was performed in a rectangular box using periodic boundary conditions with about $7.5{\cdot}10^{4}$ molecules of TIP4P-water [252]. Cut-off radii for long range interactions were set to 1.4 nm for the Lennard-Jones potential and to 0.9 nm for Coulomb interactions with long-range terms treated with

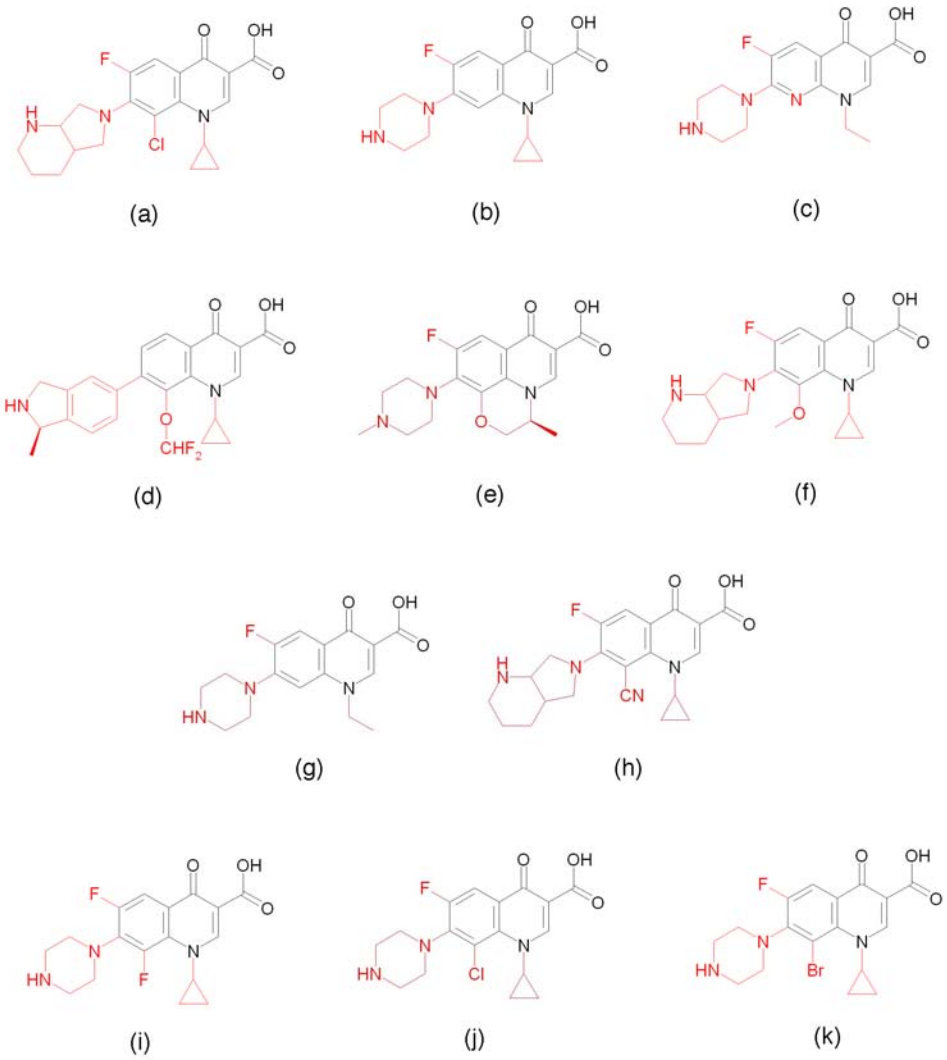

Figure 4.2: *Quinolones used for docking: (a) BAY-Y-3118, (b) ciprofloxacin, (c) enoxacin, (d) garenoxacin, (e) levofloxacin, (f) moxifloxacin, (g) norfloxacin, (h) pradofloxacin, (i) PD0117962, (j) PD0129603 and (k) PD0163449 [249]*

the Particle Mesh Ewald method [253, 254]. Bond-lengths were constrained with the LINCS algorithm [255]. Systems were neutralized by adding sodium counterions. A first set of MD calculations started after 400 steps of energy minimization to remove bad contacts using the steepest descent method. The simulations were gradually equilibrated by 200 ps MD at 100, 200 and 300 K. Subsequently, a 1500 ps MD simulation was started in order to find those complexes that could support the phosphotyrosine bond between Tyr^{122}-OH and the guanine phosphates at the 5'-end of the DNA. Each simulation was scanned to find the conformation with the smallest distance $d_{(Tyr_{122}-OH,\, guanine_{phosphate})}$ between the four guanine-phosphate residues that immediately follow the cleavage site and GyrA-Tyr^{122}-OH. If this was below the threshold of 0.8 nm, the conformation was used as a starting point for the next step, the intermediate set (fig. 4.3), where the covalent bond was introduced. Temperature, pressure and energies were checked as crude indicators of stability for each MD run. The covalent ester bond of DNA to protein was introduced by gradually increasing a harmonic distance restraint from the hydroxyl oxygen of Tyr^{122} to the guanine-phosphate of DNA and initially with harmonic position restraints on the solute atoms. At first, the reference distance was set to 0.66 nm with a force constant of 4393 $kJ\,mol^{-1}nm^{-2}$. Position restraining was then removed and a further 100 ps MD run at 300 K. Each system was then subjected to eight MD runs of 200 ps each, with the force constant for the distance restraint increased in steps to 43932 $kJ\,mol^{-1}nm^{-2}$ and the distance restraint lowered to 0.148 nm. Simultaneously, the Lennard-Jones parameters of the oxygen and guanine-phosphate atoms were changed so as to allow the atoms to reach bonding distance. Structures were subsequently subjected to the third set of MD runs to equilibrate with the new topology. Position restraining was used on all solute atoms with 400 steps of energy minimizing and 200 ps MD at 100 K, 200K then 300K. Position restraints were removed and 200 ps MD were run at 300K. This system was finally used for longer simulations of 2000 ps at 300K. In addition to the simulation parameters mentioned above, the compactness of the structures were roughly assessed by monitoring the fluctuations of the radii of gyration (r_g). The extent to which the molecular structures change over the course of simulation time was estimated using the root mean square deviation ($rmsd$) with respect to the

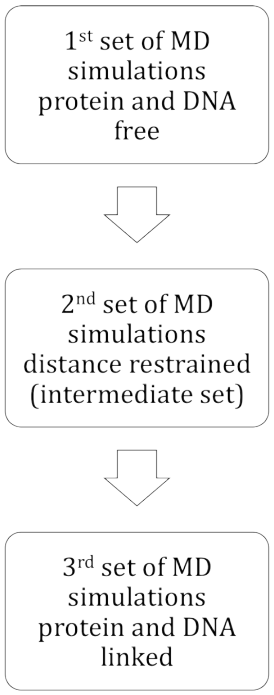

Figure 4.3: *MD simulations workflow*

starting structure [214]. Subsequently, remaining complexes were used for molecular docking of eleven quinolones.

4.5 Quantum mechanical optimization of quinolones

Partial charges for the quinolones in fig. 4.2 were estimated and geometries optimized using density functional theory with the B3LYP functional [256–259] and the split valence 3-21 G basis set as implemented in Gaussian03 [210, 239]. Calculations were performed assuming the dielectric constant and polarisability of water.

4.6 Homology Modelling of the C-terminus of GyrB

The coordinates for the *E. coli* GyrB subunit were carried over from the known homologue topoisomerase IV from *S. pneumoniae* based on an alignment of the sequences. This way, a homology model for the missing *E. coli* GyrB C-terminus was built (fig. 1.6). GyrB residues 406–543 (http://www.uniprot.org/uniprot/P0AES6) which were used as the query sequence, were subjected to SWISS-MODEL [236–238]. The crystal structure of *S. pneumoniae* topoisomerase IV (PDB ID 3k9f) served as the structural template [76, 77, 90, 93, 260]. The homology model is shown in section D of the appendix.

4.7 Mapping Protein conservation and Resistance Mutations

The evaluation of the degree of conservation of *E. coli* gyrase residues was carried out. For this purpose, a general entropy-like measure definition at each sequence position was used [261, 262].
BLAST searches against a non-redundant sequence database were used to find the 4000 closest sequence homologues [263]. This database consisted of the sequences from all non-redundant GenBank CDS translations, the Protein Data Bank , the SwissProt protein sequence database, the international protein sequence database PIR and the Protein Research Foundation PRF [264–266]. From each column of the sequence alignment, the probability p_j of each residue type j was extracted and the entropy S for the sequence position calculated from eq. 4.1, where the summation runs over the 20 amino acid types and the units are bits of information. Gaps were ignored rather than being treated as an additional residue type. This entropy-like measure runs from $S = 0$ for a completely conserved site to $S = log_2 20 \approx 4.3$ for a site which is totally unconserved. Searches were conducted based on the amino acid sequence of the 59 kDa N-terminal domain of the GyrA subunit of *E. coli* (PDB ID 1ab4) and residues 406–543 of *E. coli* GyrB (section 4.6).

$$S = -\sum_{i=1}^{20} p_j \; log_2 \; p_j \tag{4.1}$$

4.8 CoMSIA of quinolones

CoMSIA was carried out using the SYBYL molecular modelling package [226, 227]. The calculations were based on moxifloxacin and levofloxacin templates that were taken from crystal structures of *S. pneumoniae* topoIV (PDB IDs 3fof, 3k9f). All compounds and their corresponding cleavage activities were taken from an original set of 59 structures published by Domagala [267]. These were of diverse chemical nature and consisted of quinolines, pyrido[2,3-d]pyrimidines, 4-pyridones as well as 1,8-naphtyridines.

Of the 59 compounds with available cleavage activity values, 6 were reserved for testing, 49 were used for training of the CoMSIA model and four had to be rejected due to undefined stereochemistry or gyrase cleavage activity [87, 268]. The cleavage activities [mmol/L] of the training set spanned a range of approximately 2.6 log units. The test set covered an activity interval of about 2.0 log units. It was chosen by picking every sixth structure after sorting of all compounds by increasing cleavage activities.

Three-dimensional structures of the ligands under consideration were generated using the Dundee PRODRG2 server [269, 270]. Subsequently, their protonation states and resulting net charges were estimated at physiological pH using the pK_a calculator plug-in of MarvinSketch (version 5.1.03, ChemAxon 2008, http://www.chemaxon.com). Next, the semiemiprical AM1 method within MOPAC (v6.0) was used to calculate the partial atomic charges for each structure using the overall net charges [240]. The structures were subjected to energy minimization with a simplex method followed by a maximum of 10^4 Powell conjugate gradient steps with a convergence criterion of 0.005 kcal·(mol·Å)$^{-1}$ in the Tripos force field [210, 271].

Next, conformers for each structure of the training and the test set were generated using OMEGA2 (OpenEye Scientific Software, version 2.3.2). Then, conformers were

structurally aligned to the template quinolones using ROCS [241, 242] and the best alignment for each structure was chosen after manual inspection. Subsequently, the superimposed compound structures of the test- and training set were placed into a 3D lattice with a grid spacing of 0.2 nm. In order to calculate the similarity indices, different combinations of the five CoMSIA fields (electrostatic, hydrophobic, H-bond donor, H-bond acceptor, steric) were used with an attenuation factor of 0.3.
The overall CoMSIA procedure was executed for the bioactive template conformations of levofloxacin and moxifloxacin. Throughout the subsequent analyses of the CoMSIA, the contributions of the different fields were regarded as independent variables. Cleavage activities (as -lg [mmol/L]) were used as the dependent ones.
Initially, a partial least squares regression analysis (PLS) was carried out on different combinations of CoMSIA fields by applying the SAMPLS method to compounds of the training set [272–274]. $PRESS$ and q^2 values were calculated for each field composition. Based on the largest q^2 and lowest $PRESS$ value, the most appropriate combination of fields was chosen. Simultaneously, the optimal number of components for the CoMSIA that was associated with these values was derived.
Next, the models were subjected to cross-validation using a leave-one-out method. In order to optimize the models, column filtering with values ranging from 0 to 1.0 was applied and q^2 of the training set as well as $PRESS$ were calculated and used to assess the predictivity of the models. The non-validated models were created in the third step of the CoMSIA calculation. The conventional correlation coefficient r^2 and the standard deviation of the residuals (SDR) were computed according to the definitions in SYBYL. The F ratio (Fisher value) was determined from r^2 and the number of data points in the data set. These values were used to assess the statistical value of the final model. Furthermore, the SDR was used to determine which compounds could not be predicted well or had to be characterized as outliers if they had absolute residuals bigger than twice the SDR [275].
Finally, contour plots were generated and partially used for the subsequent interpretation of the CoMSIA for the DNA-gyrase model.

Chapter 5

Results

Computational methods were used to obtain a molecular understanding of the relation between quinolones, the gyrase-DNA complex and known resistance mutations. These will be presented in this chapter. First, the results of the protein DNA docking, followed by the molecular dynamics simulations will be shown. Subsequently, the outcomes of the molecular docking of quinolones into the gyrase-DNA complexes will be described. Next, the mapping of protein conservation and resistance mutations to the structure models will be shown. The section will close with the findings of the 3D-QSAR approaches.

5.1 Protein-DNA docking

A double stranded 21bp DNA was built in its standard B-configuration including a known preferred cleavage site 5'–↓GGCC–3' (fig. 5.1).

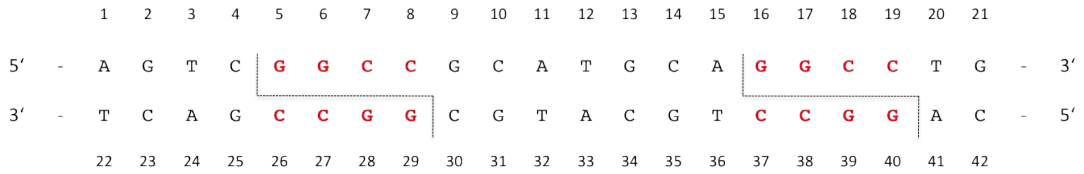

(a)

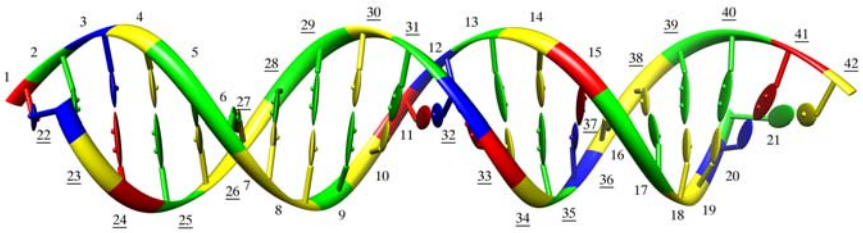

(b)

Figure 5.1: *(a) Numbered 21bp dsDNA showing the cleavage sites indicated by the dashed lines. (b) The same DNA in 3D with the nucleotides A in red, T in blue, C in yellow and G in green. Numbers of the anti sense strand are underlined for clarity reasons [223].*

Subsequently, the DNA was used for the protein-DNA docking as described in section 4.2. Hundreds of different conformations of this dsDNA with respect to the GyrA59 breakage-reunion domain of *E. coli* (PBD ID 1ab4) were sampled and manually assessed. The criterion for rejecting candidates was the distance between Tyr^{122} of GyrA and the DNA. This way, promising dockings that fit available experimental information could be generated by restricting the protein-DNA dockings to a relevant target area. If DNA was docked near the Tyr^{122} and also matched the defined docking volume, it was regarded as a plausible docking result. A docking result was rejected, if the DNA was placed near Tyr^{122} but did not match the proposed docking volume or vice versa. In this context, the distance between Tyr^{122} and the 5'-guanine phosphates of the modelled cleavage site 5'-↓GGCC-3' was important. As shown by the example in fig. 5.2, a high scored docking could not necessarily

be regarded as a plausible one. Thus, although all promising dockings were scored amongst the top 200 poses according to the geometric scoring of PatchDock [209], a manual assessment was required and allowed the reduction of complexes for molecular dynamics simulations to 24 (fig. 5.3).

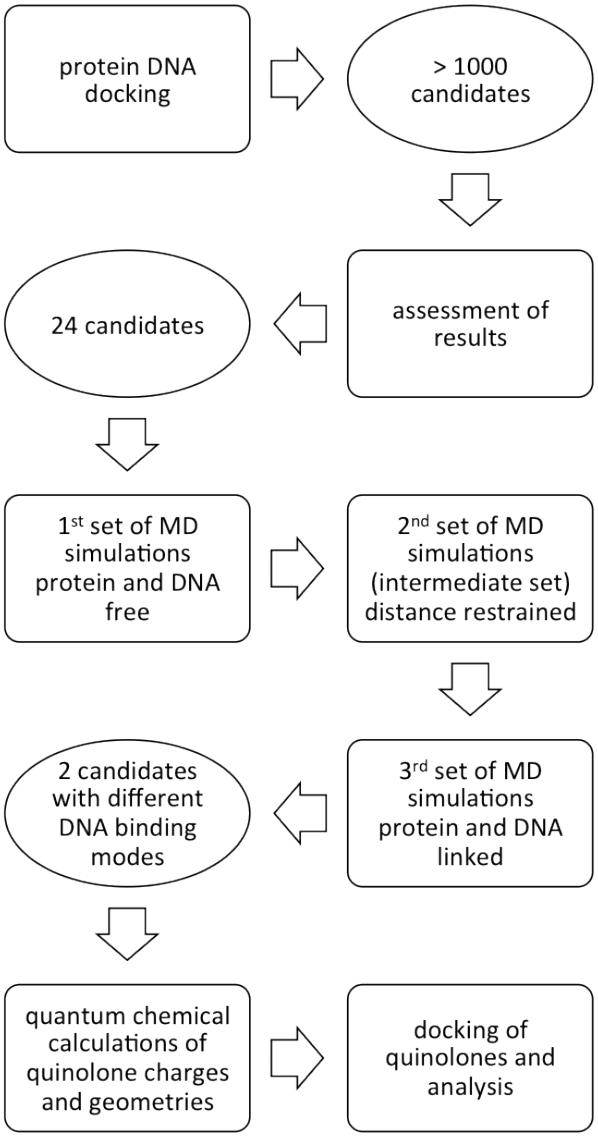

Figure 5.3: *Route to 3D model of quinolone-gyrase-DNA complexes*

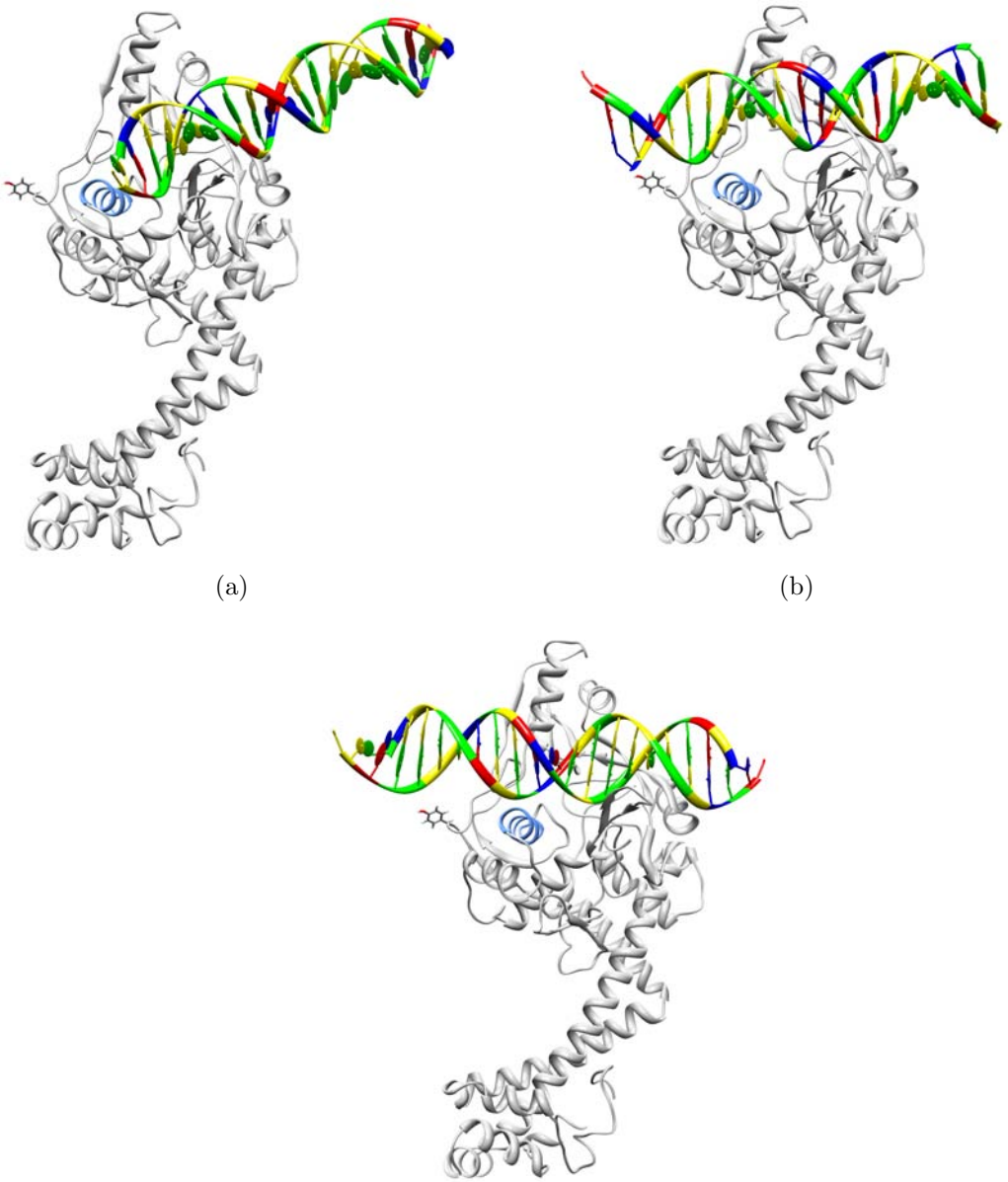

(a) (b)

(c)

Figure 5.2: *Results of protein-DNA docking with E. coli GyrA59 in grey, helix α_4 in lightblue, the DNA colored as in fig. 5.1 and Tyr^{122} sidechain shown. An example for a rejected docking (assigned rank 2) is shown in (a). Plausible dockings (ranks 20 and 166) are shown in (b) and (c), respectively.*

5.2 Molecular dynamics simulations of protein-DNA complexes

The aim of MD simulations was to find covalently linked protein DNA complexes that could be used for subsequent docking studies.
MD simulations were carried out on the 24 most promising DNA-GyrA59 complexes from the previous docking exercise. The first set of MD simulations on these complexes was carried out with the DNA and the protein not covalently linked (fig. 4.3).
Monitoring the distances between the four 5'-guanine phosphates and the GyrA59-Tyr^{122}-OH pairs for each complex model revealed five candidates with a distance less than the threshold of < 0.8 nm. Of these, three were rejected since they did not satisfy the cut-off between GyrA59-Tyr^{122}-OH and guanine phosphates 5 or 40 (nucleotide numbering according to fig. 5.1).
The remaining two complexes showed different DNA binding modes. For them, the variation of the distances under consideration are shown in figs. 5.4 and 5.5.
For complex 20, a minimum distance of 0.78 nm was found at 531 ps for the Tyr^{122}-OH and the 5'-guanine phosphate of nucleotide 5. For this complex, the α_4-helix of the HTH motif of GyrA59 with residues Ser^{83} and Asp^{87} pointed into the major groove of the DNA which was partly made up of the 5'–↓GGCC–3' motif.
The minimum distance of 0.3 nm for complex 166 was found at 799 ps. For this complex, the α_4-helix was directed into the minor groove of the dsDNA. The cleavage pattern was not part of this groove. The relevant conformations were extracted and subjected to the intermediate set of molecular dynamics simulations until bonding distance between the guanine 5'-phosphate and GyrA59-Tyr^{122}-OH was reached.
Finally, the resulting complexes were subjected to the third set of MD simulations with the protein and the cleaved DNA covalently linked (fig. 5.3). For both complexes, r_g and *rmsd* changes over time were tracked in order to obtain a rough estimation of the system's stability during the MD runs. The radii of gyration r_g for both complexes changed within a range of approximately 0.1 nm. This is shown in figs. 5.6 (a) and 5.7 (a). For complex 20, the *rmsd* with respect to the starting conformation

equilibrated to approximately 0.28 nm after 1000 ps simulation time (fig. 5.6 (b)). For complex 166, the *rmsd* started to level around 0.23 nm after roughly 900 ps of the simulation was run (fig. 5.7 (b)).

Regarding complex 20, the final MD run resulted in the α_4-helix being opposite to the +4 cytosine (C^{+4}) of the overhanging tetranucleotide (fig. 5.8 (a)). Inspecting amino acids that were found within a 0.5 nm sphere of any nucleic acid, yielded 37 residues. Of them, there were five arginines and one lysine. Three of the five arginines were found within a 0.5 nm sphere around the overhanging tetranucleotide opposed to the α_4-helix. The sidechain of the Arg^{121} appeared to be 0.35 nm away from the phosphate oxygens of the +1 guanine (G^{+1}), whereas the Arg^{266} guanidinium moiety was at the same distance to a phosphate oxygen of C^{+4}. Additionally, with a distance of 0.35 nm, the hydroxyl-hydrogens of Ser^{83} and Ser^{116} pointed towards negatively charged phosphate oxygens of C^{+3}. The distance between Arg^{91} and DNA was 0.44 nm. However, this residue established a salt-bridge with Asp^{87}.

An examination of complex 166 revealed that the aromatic plane of the adenine nucleotide 30 (numbering according to fig. 5.1) was no longer perpendicular to the helical axis. This distortion of the DNA allowed the adenine to form hydrogen-bonds with cytosine nucleotides 37 and 38 instead of thymine 36 (fig. 5.8(b)). There were also five arginines and one lysine among the 39 amino acids that were found within a 0.5 nm radius of any DNA of this complex. One of the arginines and the lysine differed from complex 20 but were not within the focussed set of residues which was compiled by narrowing down the selection of amino acids to those adjacent to the α_4-helix and the four overhanging DNA bases. It showed that Arg^{121} was involved in a salt-bridge with the phosphate-oxygens of G^{+1}. However, as opposed to complex 20, Arg^{91} on the one hand formed a salt-bridge with the phosphate oxygens of nucleotide 12 which were found to be 0.2 nm – 0.3 nm away. On the other hand it also established a salt-bridge with Asp^{87}. Once more, Ser^{83} and Ser^{116} appeared to be in contact with DNA. In Ser^{83}, the hydroxyl moiety acted as a donor in the H-bond that was formed with a phosphate oxygen of cytosine C14. In contrast to Ser^{83}, the sidechain of Ser^{116} served as an H-bond acceptor. This way, it was able to form an H-bond with the primary amine of the adenine nucleotide A15.

Both complexes were subsequently used as target structures for the docking of the eleven quinolones from fig. 4.2 as methodologically described in section 4.3. The results will be presented in section 5.3.

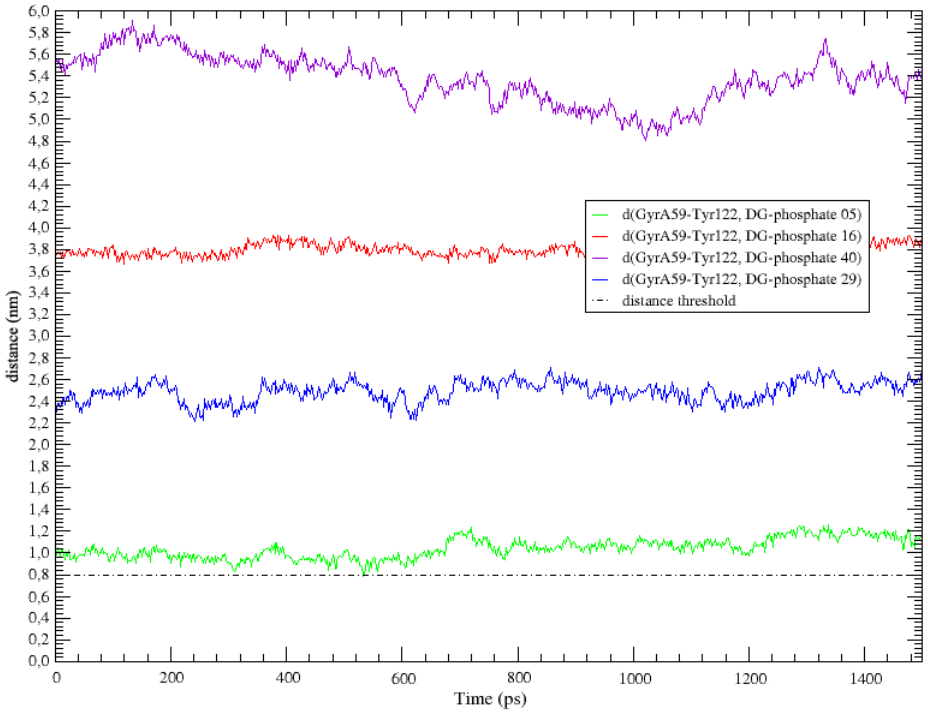

(a)

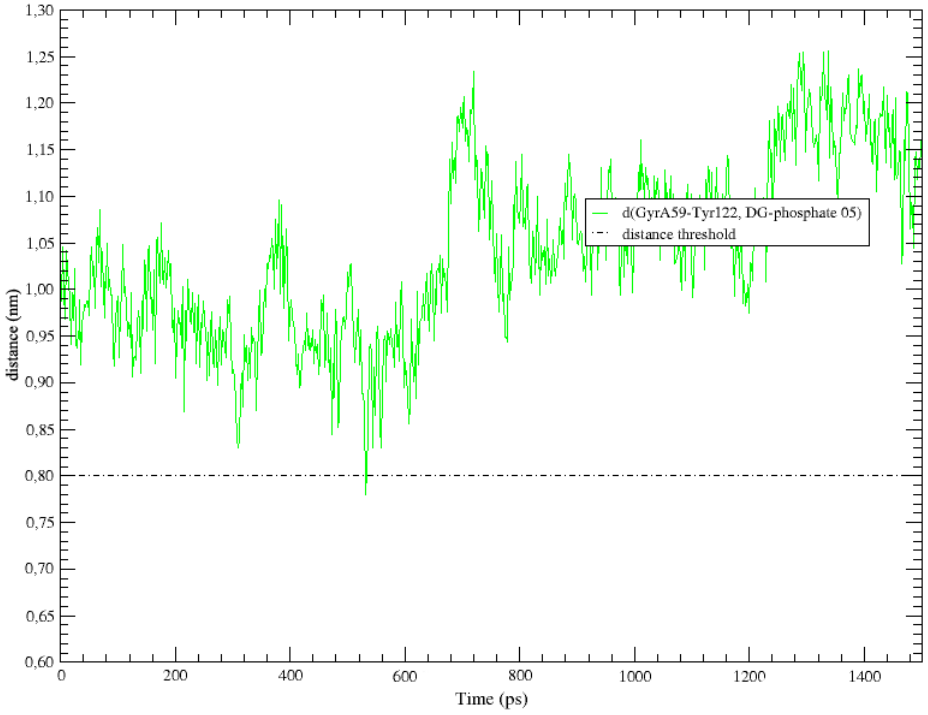

(b)

Figure 5.4: *(a) Changes of distances* $d_{(Tyr^{122}-OH,\, DG_{Px})}$ *over time in complex 20 and (b) focused on* $d_{(Tyr^{122}-OH,\, DG_P\, 05)}$

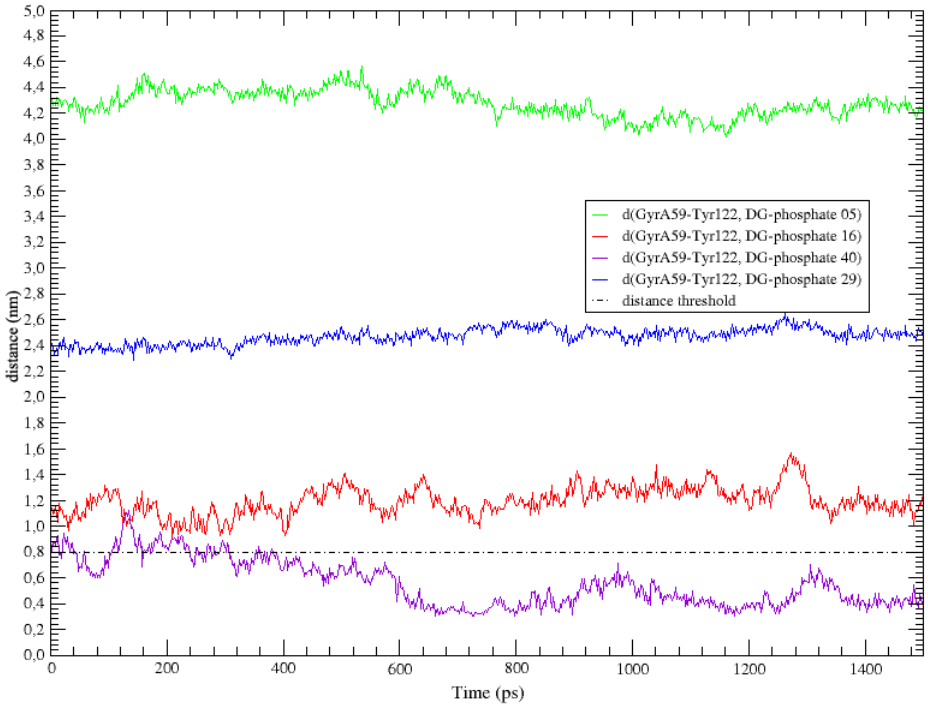

(a)

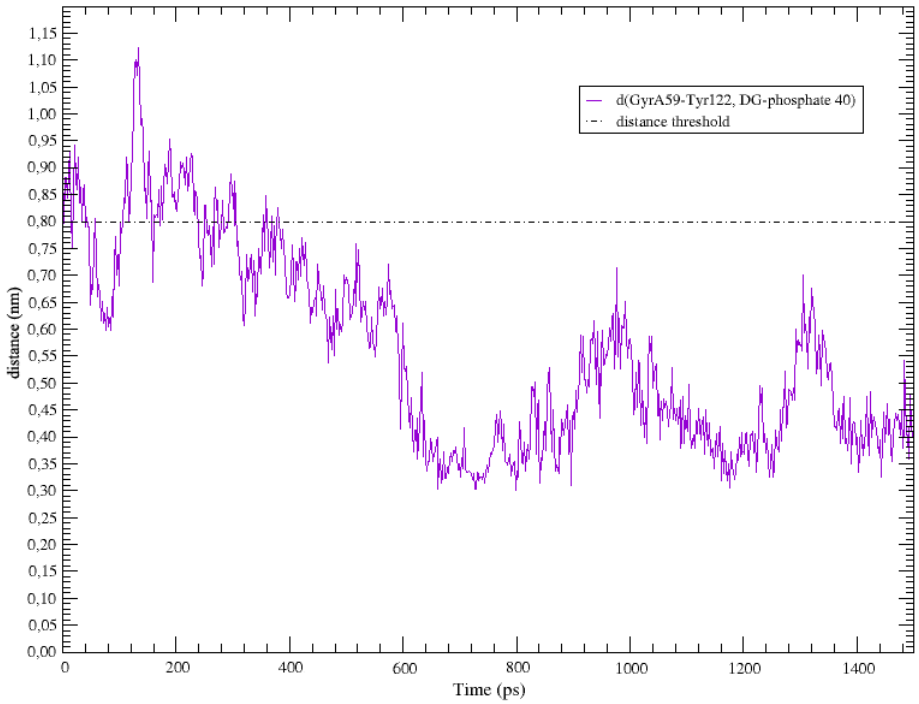

(b)

Figure 5.5: *Changes of distances* $d_{(Tyr^{122}-OH,\, DG_{Px})}$ *over time in complex 166 and (b) focused on* $d_{(Tyr^{122}-OH,\, DG_P\ 40)}$

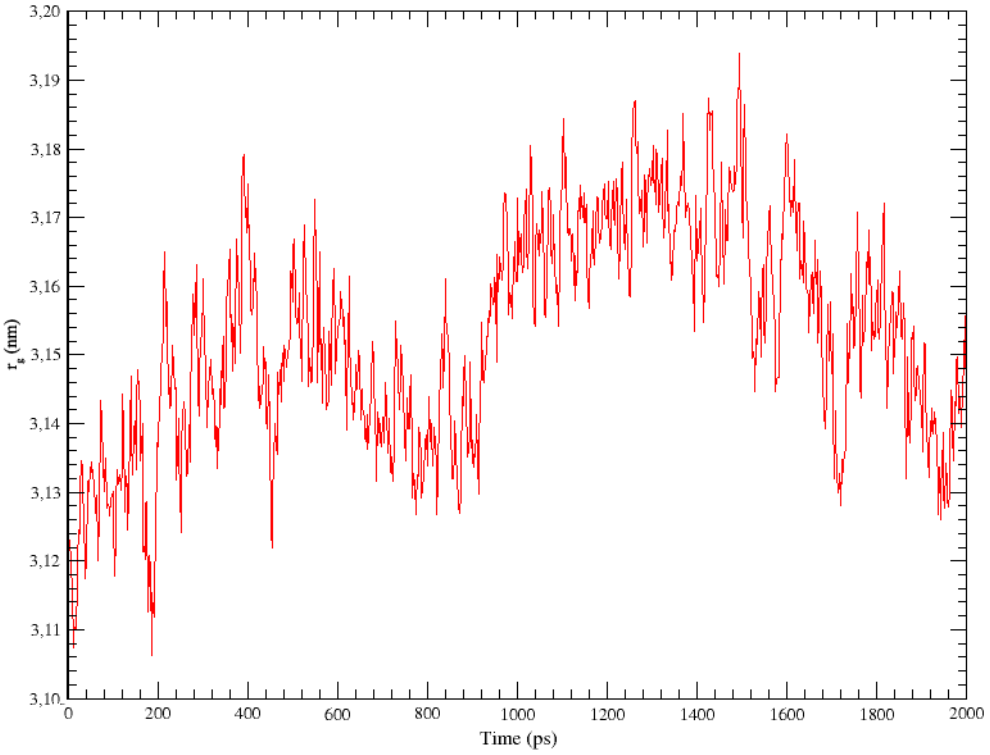

(a)

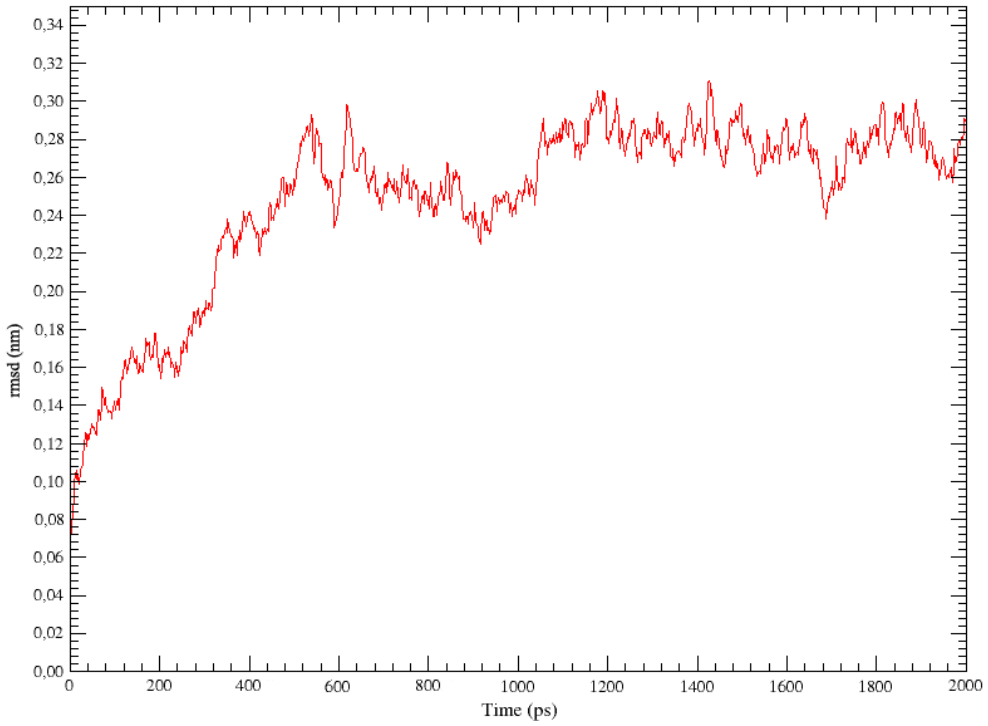

(b)

Figure 5.6: *Change in (a) radius of gyration r_g and (b) rmsd of complex 20 over simulation time*

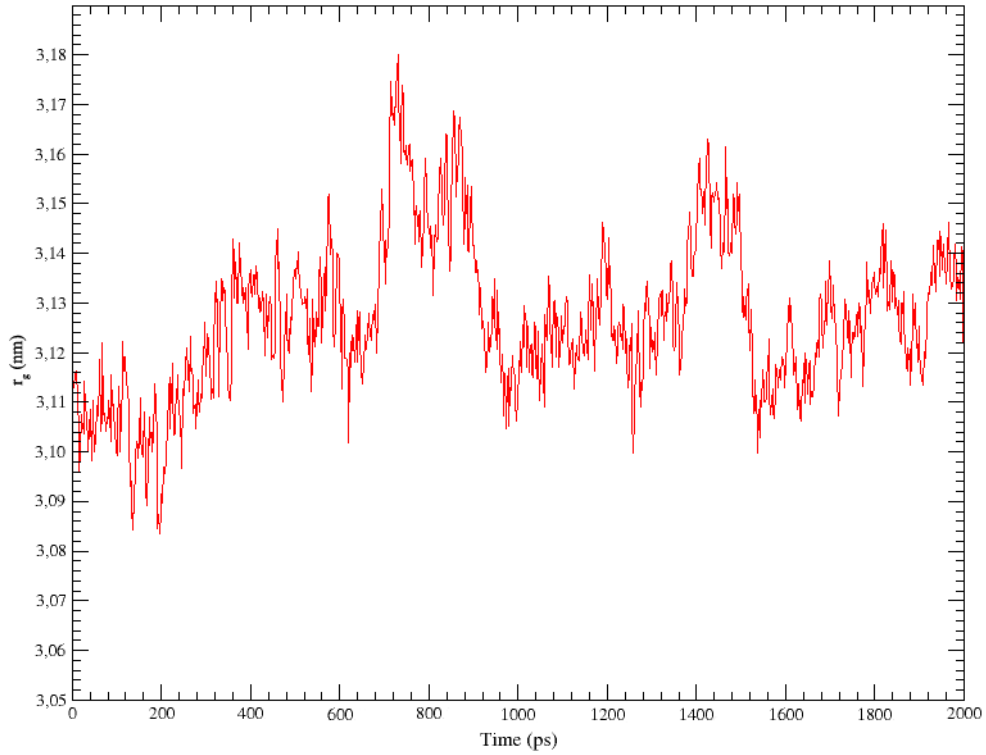

(a)

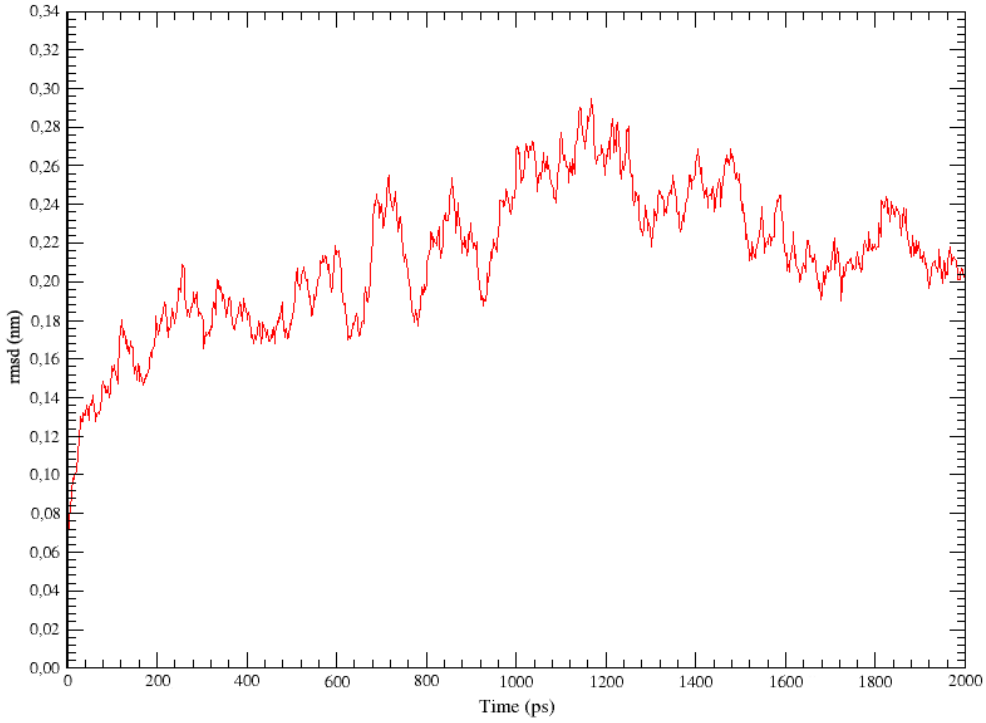

(b)

Figure 5.7: *Change in (a) radius of gyration r_g and (b) rmsd of complex 166 over simulation time*

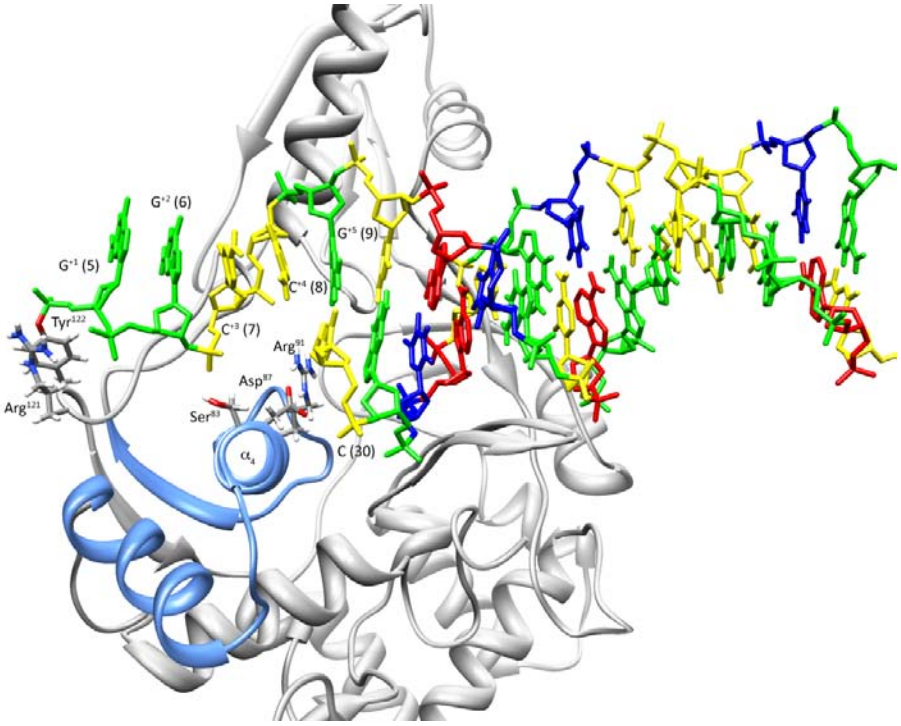

(a)

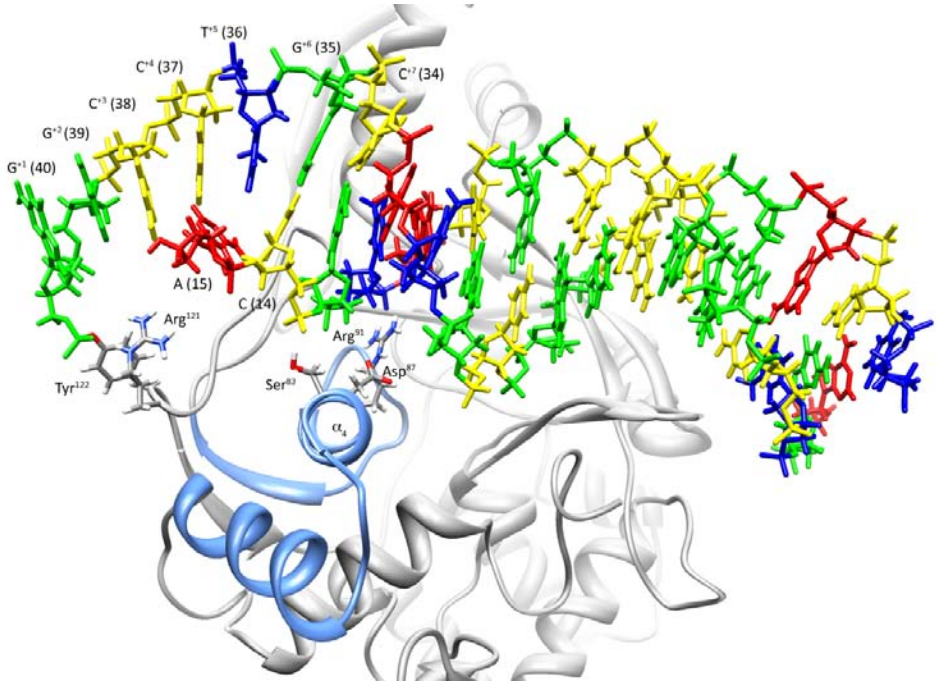

(b)

Figure 5.8: *DNA covalently linked to (a) complex 20 and (b) complex 166. The GyrA59 structures are shown in grey with the QRDRs in lightblue. Nucleotides are colored as in fig.5.1.*

5.3 Docking of quinolones

Molecular docking of eleven different quinolones from fig. 4.2 was carried out after their quantum chemical charge calculation and geometry optimization.
Given the experimental results, dockings were selected if they showed interaction with both, DNA and GyrA's α_4-helix [85, 276]. It has been suggested that quinolones must have aromatic ring interactions with nucleotide bases [85, 277–280]. Thus, representative poses from the different clusters, i.e. conformations with the lowest binding energy [kcal·mol^{-1}], were selected by this criterion after manual assessments. Furthermore, dockings were chosen if they allowed a Mg^{2+} or water dependent interaction with residues of the GyrA-α_4-helix or if they were placed into the minor groove of DNA [85, 281–284].
The default settings of UCSF Chimera were used to detect hydrogen-bonds between docked conformations and the target structures [223–225, 285]. Furthermore, the H-bond constraints were relaxed by adding a tolerance distance of 0.04 nm and a tolerance angle of 20° to the strict values [285, 286]. A detailed overview of detected H-bonds is given in section C of the appendix .

5.3.1 Docking into target complex 20

The docking into complex 20 was carried out using flexible sidechains in GyrA residues Ser^{83}, Asp^{87} and Arg^{91}. The results of the subsequent conformational clustering of docked drug poses is shown in fig. 5.9. Only for garenoxacin, the cluster containing the best scored docking was also the one that contained most dockings. The figure also shows that none of the top scored conformations was clustered as a singleton.
None of the sampled representative drug conformations from the best scored clusters reflected the aromatic ring stacking capability of the therapeutics. For lower ranked dockings however, possible interactions were detected for all quinolones but enoxacin. The interaction was found to take place between the aromatic drug skeletons and the juxtaposed cytosine (nucleotide 30 in fig. 5.1)) which was opposed to the +5 guanine (fig. 5.1). However, there was no clear evidence for the preference of a

certain conformation. The docking results could be further separated into the three sets A, B and C which differed by the orientations of the drugs' 3-carboxy-4-oxo moieties within the target site (fig. 5.10). Neither enoxacin nor pd0163449 were found to fit into one of these sets. In contrast, norfloxacin was the only compound which was found in all sets. For each such set, table 5.1 shows the associated drugs together with their corresponding binding energies, the rank of the cluster they were found in and the number of dockings within that cluster.

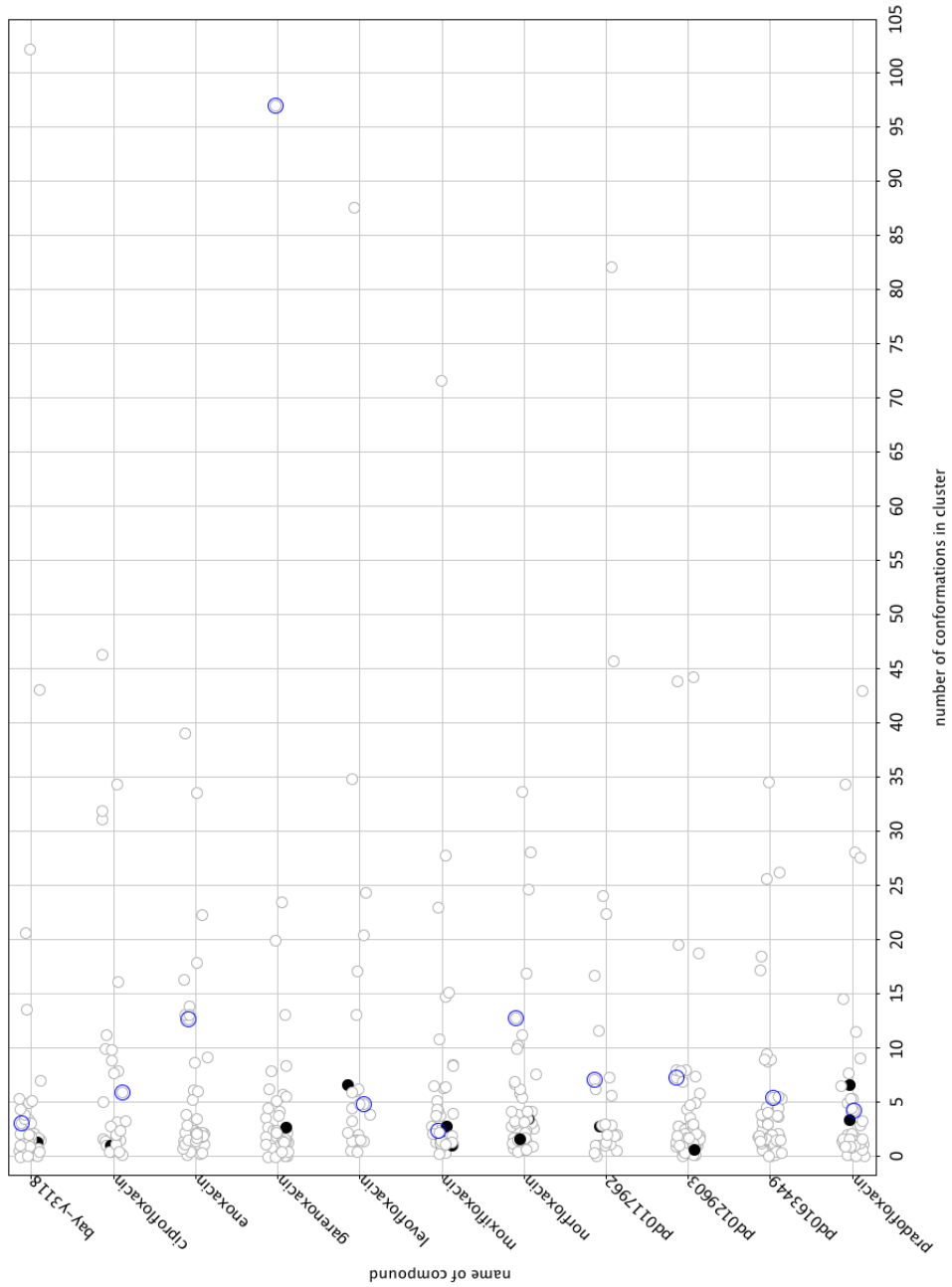

Figure 5.9: *Conformational clustering of docked drug poses for complex 20: A cluster (○) was encircled blue if it contained the pose with the lowest overall energy. A (●) indicated clusters with plausible and selected docking results from sets A–C. The number of conformations in each cluster is given for each quinolone.*

Set A was composed of five different compounds of which only the representative conformation of pradofloxacin was found amongst the top ten clusters containing six conformations. For moxifloxacin two plausible conformations were found of which one (A3), together with norfloxacin and pd0129603, was clustered as singletons. For all poses of this set, the 3-carboxy-4-oxo groups pointed into the direction of the +3 and +4 nucleotides with the N1-substituents directed into the opposite direction (fig. 5.10 (a)), i.e. away from the DNA. It was noteworthy that for all docked poses, the 3-carboxyl groups of the drugs were rotated out of the plane of the quinolone skeletons.
The estimated binding energies of the quinolones from this set did not differ from the lowest overall binding energy found for this drug by more than 3 kcal·mol^{-1} as indicated by the $\triangle E$ values (tab. 5.1). Thus, there was no significant difference between the energies of the poses given the expected error in the AutoDock4 scoring function [232]. All quinolones from this set were stabilized in the potential target site by hydrogen bonds. These were mainly formed between cytosines and the 3-carboxy and 4-oxo substituents, respectively. Aside from this, the positively charged C7-substituents of one moxifloxacin representative and pradofloxacin established hydrogen bonds with the Asp^{82} sidechain oxygens (tab. C.1). Additionally, all drugs were able of stacking interactions with the cytosine (nucleotide 30) opposed to the +5 guanine. Furthermore, the docking generated sidechain rotamers of Ser^{83}, Asp^{87} and Arg^{91} that not only allowed the formation of salt bridges between the negatively charged Asp^{87} and its positively charged counterpart Arg^{91}. Also a hydrogen bond was found between Ser^{83}-OH and the phosphate oxygens of C^{+3}. Interestingly, all compounds with a (1*S*, 6*S*)-2,8-diazabicyclo[4.3.0] non-8-yl substituent at C7 (bay-y3118, moxifloxacin and pradofloxacin) were found in this set.

Set B consisted of eight representative conformations (fig. 5.10 (b)). Of these, plausible poses for pd0129603 were found in two clusters. As shown in table 5.1, ciprofloxacin and both pd0129603 conformations were classified as singletons. Besides this, the estimated binding energies of all conformations were within the estimated error of the scoring function as already seen for set A. In contrast to set A, quinolones of this set appeared to be rotated around the y-axis by ∼180°. Hence, the quinolones'

N1- substituents were pointing towards the DNA bases, whereas the 4-oxo group was pointing into the opposite direction.
Drug conformations from set B were mainly stabilized by hydrogen bonds between their 3-carboxy-4-oxo moieties and DNA bases. The hydrogen bonding patterns were similar to the ones observed for set A (tab. C.1). The aromatic ring stacking of the therapeutics of this set was carried out with the juxtaposed cytosine which appeared to be opposed to the +5 guanine. Moreover, the formation of salt bridges between the Asp^{87} and Arg^{91} as well as hydrogen bonding between Ser^{83}-OH and the phosphate oxygens of C^{+3} was also observed for the drug orientations from the set under consideration. Remarkably, one of the plausible pd0129603 representatives (B7) was found in the lowest scored cluster for that compound. Apart from that, ciprofloxacin, levofloxacin and pd0117962 were only found in set B. Interestingly, an H-bond was formed between the morpholine-oxygen of one levofloxacin placement and the hydroxyl group of Ser^{83}.

Two compounds fit into set C, norfloxacin and garenoxacin (tab. 5.1). The latter one was only found in this set, while norfloxacin was the only drug which also fit into sets A and B. Although both representatives were found to carry out stacking with the juxtaposed cytosine nucleotide, the differences of the drug orientations compared to sets A and B were striking (fig. 5.10(c)). The drugs' C7-substituents pointed into the direction of a cavity which was built from the GyrA α_4-helix , C^{+3} and C^{+4}. Thus, the protonated (1*R*)-1-methyl-2,3-dihydro-1H-isoindole moiety of garenoxacin formed a salt-bridge with Asp^{87}. This way, Asp^{87} shielded the positive charges of garenoxacin's C7-group from Arg^{91}.
The smaller norfloxacin formed a hydrogen bond with the sugar of the DNA (tab. C.1). Remarkably, norfloxacin as a singleton, was found in the lowest ranked cluster. Moreover, it was the only representative conformation of all sets with a $\triangle E$ of 3.7 kcal·mol^{-1}.

no.	compound	cluster analysis			
		cluster rank$^{(*)}$	conf. in clust.	singletons found	energies in [kcal·mol^{-1}] actual / lowest$^{(\dagger)}$ / $\triangle E$
complex 20 set A					
(A1)	bay-y3118	14 / 37	2	18	–3.55 / –5.56 / 2.01
(A2)	moxifloxacin	25 / 39	2	16	–3.25 / –5.21 / 1.96
(A3)	moxifloxacin	26 / 39	1	16	–3.18 / –5.21 / 2.03
(A4)	norfloxacin	14 / 49	1	18	–3.38 / –5.46 / 2.08
(A5)	pd0129603	21 / 55	1	27	–3.02 / –4.79 / 1.77
(A6)	pradofloxacin	9 / 45	6	21	–4.03 / –6.32 / 2.29
complex 20 set B					
(B1)	ciprofloxacin	19 / 30	1	11	–3.31 / –5.54 / 2.23
(B2)	levofloxacin	10 / 24	7	4	–3.57 / –4.54 / 0.97
(B3)	moxifloxacin	17 / 39	2	16	–3.88 / –5.21 / 1.33
(B4)	norfoxacin	22 / 49	4	18	–2.95 / –5.46 / 2.51
(B5)	pd0117962	14 / 25	2	10	–3.08 / –5.31 / 2.23
(B6)	pd0129603	15 / 55	1	27	–3.12 / –4.79 / 1.67
(B7)	pd0129603	55 / 55	1	27	–1.86 / –4.79 / 2.93
(B8)	pradofloxacin	14 / 45	3	21	–3.59 / –6.32 / 2.73
complex 20 set C					
(C1)	garenoxacin	40 / 47	2	26	–2.75 / –5.14 / 2.39
(C2)	norfloxacin	49 / 49	1	18	–1.76 / –5.46 / 3.7

Table 5.1: *Results of quinolone docking into complex 20: Each row shows the compound contained in a cluster, listed with the rank of the cluster it was found in and the number of overall clusters found for the compound (*). The number of conformations in this cluster is given with its actual estimated binding energy, the lowest energy of all clusters (†) and their difference $\triangle E$.*

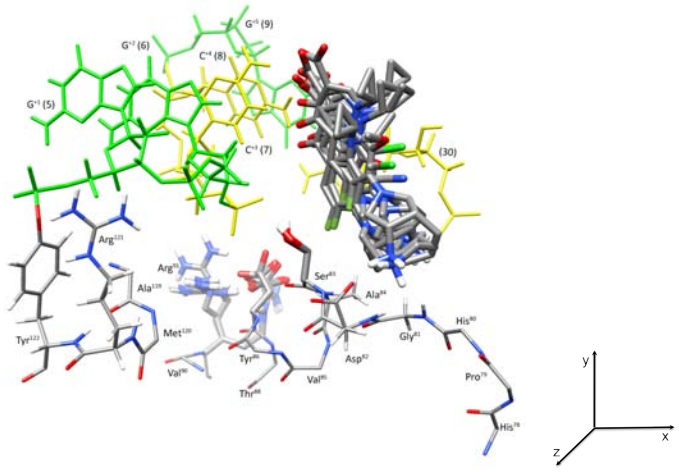

(a)

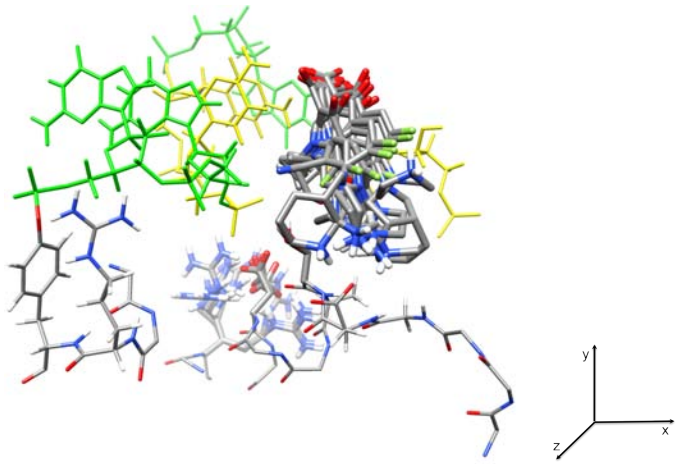

(b)

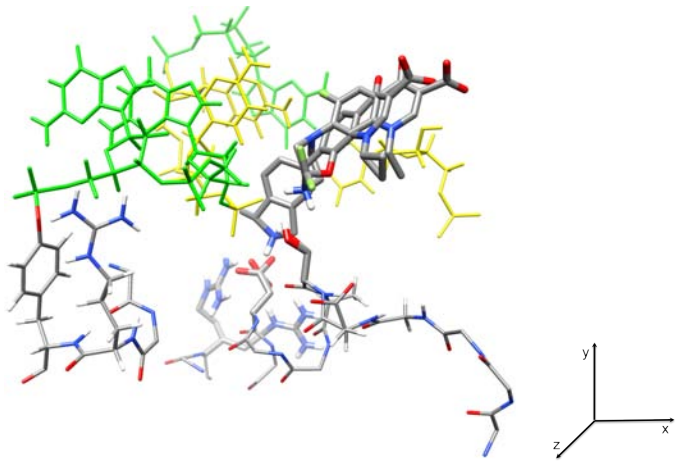

(c)

Figure 5.10: *Quinolone dockings into complex 20 are shown for (a) set A, (b) set B and (c) set C. GyrA59 residues are shown. Different orientations of sidechains that were treated flexible are depicted. Nucleotide colors and numberings (in brackets) as in fig. 5.1. For reasons of clarity, not all hydrogens are shown.*

5.3.2 Docking into target complex 166

The molecular docking of the quinolones into complex 166 was performed with the sidechains of GyrA residues Ser^{83}, Asp^{87}, Arg^{91} and Arg^{121} being flexible. This supported the salt-bridge formation between Asp^{87} and Arg^{91} as well as a hydrogen-bond between Ser^{83} and the phosphate backbone of the cytosine nucleotide 14 (fig. 5.1). Noticeably, from the result of the conformational clustering it could clearly be seen that a high number of clusters was found while the number of conformations in the clusters was decreased (fig. 5.11). Similarly, the number of singletons for each quinolone was significantly raised (tab. 5.2). This characteristic was reflected in the analyses of the three-dimensional docked ligand-target complexes since there was no preference for either a certain binding site or a favored drug conformation. In contrast to complex 20 (section 5.3.1), high scoring docking results were found that also satisfied the characteristics of a plausible docking.
Given the results from the clustering, the representative dockings could be split into subsets A-L of which the latter differed from the others by the possible binding pocket used. Moreover, the conformations in set L were heterogeneous and therefore, even within this set, there was no preference for a particular pose. Aside from this, plausible results were found for each quinolone. However, given the estimated error of the AutoDock4 scoring function, one cannot claim that any pose was better than any other. Thus, results of dockings into the target complex 166 will be exemplarily presented here by sets A, B and L (tab. 5.2, fig. 5.12 and tab. C.2 of the appendix).

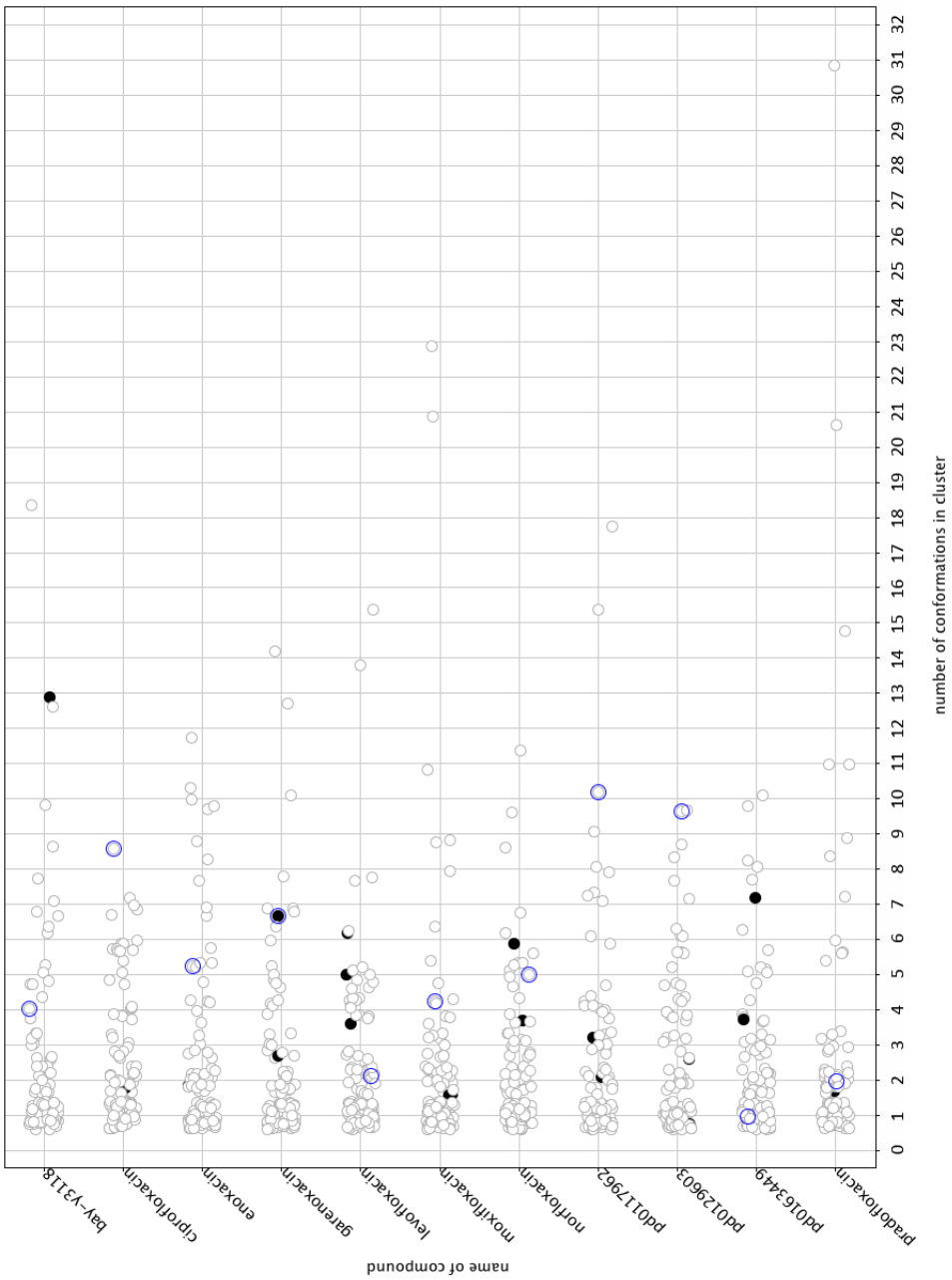

Figure 5.11: *Conformational clustering of docked drug poses for complex 166: A cluster (○) was encircled blue if it contained the pose with the lowest overall energy. A (●) indicated clusters with plausible and selected docking results from sets A, B and L. The number of conformations in each cluster is given for each quinolone.*

Except for enoxacin, moxifloxacin and pd029603, all quinolones were represented in set A. These appeared to be placed into a possible binding pocket formed by the minor groove of DNA and the GyrA α_4-helix. As shown in fig. 5.12 (a), quinolones from this set were located almost isohelical with the minor groove [287–290] and their 3-carboxy-4-oxo moieties oriented towards the DNA helix axis. All representatives of this set were retrieved from the top ten clusters. Although the pose for pd0163449 was found to be scored best for this candidate, it appeared to be classified as a singleton. All dockings were anchored within the gyrase-DNA complex by hydrogen-bonds that were formed between the drugs' carboxyl-groups and the DNA's nucleotide 31. Additionally, hydrogen-bonds were detected between the charged C7-heterocycles and nucleotide 14 as well as the Ser^{83} sidechain oxygens. Furthermore, norfloxacin and pradofloxacin interacted with Arg^{91} via a salt-bridge formed with their carboxyl-moieties. Hydrogen bonds that contributed to the stabilization of the drugs within the proposed binding pocket mainly occurred with nucleotides 14 and 31 and are summarized in tab. C.2 of the appendix.

Set B consisted of eight conformations with two poses found for levofloxacin (tab. 5.2). Not all dockings of this set could be retrieved from the corresponding top ten clusters, but none of them was a singleton. Compared to set A, the docked poses were approximately rotated by $\sim 90^\circ$ around the x-axis (fig. 5.12 (b)). Due to this change in orientation there were no salt-bridge interactions between Arg^{91} and the carboxyl-groups detectable. Moreover, none of these poses interacted with Ser^{83} and all dockings appeared to be stabilized by H-bonds with nucleotides 13 and 33. However, with their positively charged piperazinium substituents at C7, enoxacin, levofloxacin (B3) and norfloxacin formed H-bonds with the the backbone oxygen of His^{80} (tab. C.2). Aside from this, levofloxacin (B4) appeared to be additionally stabilized by an H-bond formed between its C7-substituent and the carboxyl-group of Asp^{82}.

In contrast to sets A and B, the conformations of set L were placed in proximity to Arg^{121}, the active site Tyr^{122} and adenosine nucleotide 15. Although this set was made up of twelve poses, there were only seven different quinolones (tab. 5.2). Moreover, of the twelve reasonable poses, six were clustered as singletons.

For ciprofloxacin, moxifloxacin and pd0129603 two cluster representatives were obtained. For pradofloxacin there were even three plausible drug arrangements. Ciprofloxacin (L1), garenoxacin and pradofloxacin (L10) were found in top 10 clusters. Moreover, garenoxacin and pradofloxacin (L10) were the best scored poses that AutoDock4 was able to find with the given sampling conditions (section 4.3 and appendix A).

Due to the heterogeneity in the quinolone placements within this set, a variety of interaction points between drugs and the target complex were found. All drug arrangements allowed aromatic ring stacking interactions with the adenosine nucleotide 15. Of the other interactions, there were mainly salt-bridges established between Arg^{121} and the COOH groups of the drugs but also between the positively charged C7 quinolone substituents and Asp^{87}. Stabilizing hydrogen-bond anchors between the compounds and DNA predominantly included nucleotides 15, 38 and 39. Interestingly, H-bonds were also formed between the therapeutics and the backbone NHs of Ala^{119} and Met^{120}. A detailed listing of the hydrogen bonds is given in tab. C.2 of the appendix.

no.	**compound**	**cluster analysis**			
		cluster rank$^{(*)}$	**conf. in clust.**	**singletons found**	**energies in [kcal·mol^{-1}] actual / lowest** $^{(\dagger)}$ **/** $\triangle E$
complex 166 set A					
(A1)	bay-y3118	2 / 94	3	51	–5.21 / –5.56 / 0.35
(A2)	ciprofloxacin	6 / 105	1	52	–4.07 / –4.88 / 0.81
(A3)	garenoxacin	5 / 109	3	65	–4.35 / –5.56 / 1.21
(A4)	levofloxacin	6 / 106	4	57	–3.81 / –4.84 / 1.03
(A5)	norfloxacin	8 / 118	4	69	–3.77 / –4.40 / 0.63
(A6)	pd0117962	3 / 98	3	55	–3.80 / –4.48 / 0.68
(A7)	pd0163449	1 / 114	1	62	–4.51 / –4.51 / 0
(A8)	pradofloxacin	2 / 92	2	53	–4.78 / –5.50 / 0.72
complex 166 set B					
(B1)	bay-y3118	3 / 94	13	51	–5.14 / –5.56 / 0.42
(B2)	enoxacin	15 / 99	2	54	–2.71 / –4.36 / 1.65
(B3)	levofloxacin	4 / 106	5	57	–3.88 / –4.84 / 0.96
(B4)	levofloxacin	5 / 106	6	57	–3.84 / –4.84 / 1.00
(B5)	norfloxacin	9 / 118	6	69	–3.67 / –4.40 / 0.73
(B6)	pd0117962	13 / 98	2	55	–3.10 / –4.48 / 1.38

continued on next page

no.	compound	cluster analysis: cluster rank(*)	conf. in clust.	singletons found	energies in [kcal·mol^{-1}] actual / lowest (†) / $\triangle E$
(B7)	pd0129603	11 / 105	3	61	–3.41 / –4.26 / 0.85
(B8)	pd0163449	6 / 114	7	62	–3.77 / –4.51 / 0.74
complex 166 set L					
(L1)	ciprofloxacin	10 / 105	1	52	–3.53 / –4.88 / 1.35
(L2)	ciprofloxacin	56 / 105	2	52	–2.31 / –4.88 / 2.57
(L3)	garenoxacin	1 / 109	7	65	–5.56 / –5.56 / 0
(L4)	moxifloxacin	21 / 105	2	60	–3.64 / –4.81 / 1.17
(L5)	moxifloxacin	37 / 105	2	60	–3.15 / –4.81 / 1.66
(L6)	pd0117962	25 / 98	1	55	–2.76 / –4.48 / 1.72
(L7)	pd0129603	41 / 105	1	61	–2.64 / –4.26 / 1.62
(L8)	pd0129603	86 / 105	1	61	–1.87 / –4.26 / 2.39
(L9)	pd0163449	47 / 114	4	62	–2.66 / –4.51 / 1.85
(L10)	pradofloxacin	1 / 92	2	53	–5.50 / –5.50 / 0
(L11)	pradofloxacin	11 / 92	1	53	–3.90 / –5.50 / 1.60
(L12)	pradofloxacin	29 / 92	1	53	–3.26 / –5.50 / 2.24

Table 5.2: *Results of quinolone docking into complex 20: Each row shows the compound contained in a cluster, listed with the rank of the cluster it was found in and the number of overall clusters found for the compound (*). The number of conformations in this cluster is given with its actual estimated binding energy, the lowest energy of all clusters (†) and their difference $\triangle E$.*

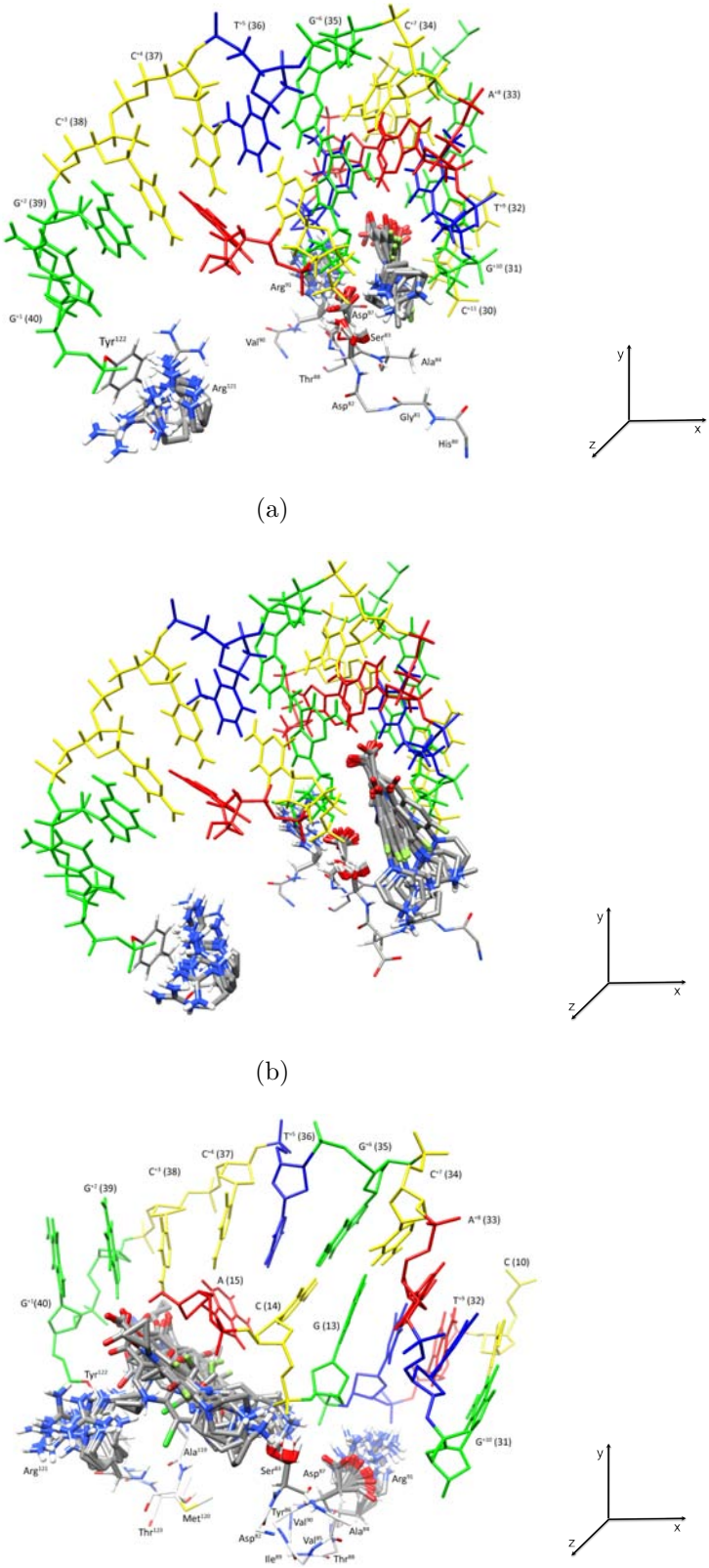

Figure 5.12: *Quinolone dockings into complex 166 are shown for (a) set A, (b) set B and (c) set L. GyrA59 residues are shown. Different orientations of sidechains that were treated flexible are depicted. Nucleotide colors and numberings (in brackets) as in fig. 5.1. For reasons of clarity, not all hydrogens are shown.*

5.4 Protein conservation

Since the docking calculations were carried out, crystal structures of the topoisomerase IV of *S. pneumoniae* in complex with DNA and moxifloxacin and levofloxacin were published [77, 260]. This allowed to set up a reliable homology model for the *E. coli* DNA-gyrase which could be built in an almost trivial exercise (fig. D.1). With more than 60% sequence identity for the GyrB segment to be modelled, there was little scope for error in the underlying sequence alignment.

Some properties of this structural model could be considered by simply looking at residue conservation (entropy S) of GyrB and GyrA. The plots in figures 5.13 and 5.14 represent the conservation / variability across natural species and to some extent, under the influence of antibiotics. Although clinical isolates were not labelled as such, one could clearly see the main influences in the data.

For GyrA the 4000 sequences of highest homology were used (expectation-value $\leq 2{\cdot}10^{-44}$). Thus, the sequences were clearly related and the resulting alignments were unlikely to have any errors. The 4000 sequences that were found using the sequence of the N-terminal domain of *E. coli* GyrA (PDB ID 1ab4) came from 613 genera which could be divided into 1327 different species. There were, of course, biases in the data which could be quantified. The ten species which dominated the data are given in table 5.3. One could say that the worst bias was due to the 100 sequences from *Streptococcus pneumoniae*, some of which have evolved under selection due to antibiotics. At the other end, there were 1054 species with only one or two sequence representatives.

The 4000 sequence homologous (expectation-value $\leq 2{\cdot}10^{-35}$) that were used for GyrB residues 406–543 consisted of 1572 species from 647 different genera. The ten species that dominated this data set are listed in tab. 5.3. Of them 165, sequences of uncultured bacteria and 128 *Listeria monocytogenes* sequences were found. For 1259 species not more than one or two sequences were found.

Quantitatively, sequences from different organisms dominated the results.

gyrase A subunit		gyrase B subunit	
occurrences	**species**	**occurrences**	**species**
100	*Streptococcus pneumoniae*	165	uncultured bacterium
88	*Salmonella enterica*	128	*Listeria monocytogenes*
87	*Bacillus subtilis*	61	*Salmonella enterica*
57	*Campylobacter jejuni*	53	*Bacillus thuringiensis*
53	*Escherichia coli*	52	*Escherichia coli*
52	*Staphylococcus aureus*	43	*Streptococcus pneumoniae*
41	*Bacillus amyloliquefaciens*	42	*Vibrio parahaemolyticus*
36	*Bacillus cereus*	42	*Bacillus cereus*
35	*Clostridium perfringens*	37	*Burkholderia cenocepacia*
32	*Klebsielle pneumoniae*	29	*Vibrio cholerae*

Table 5.3: *Species that dominated the results from BLAST searches*

Rather than simply considering the entropy plots from figs. 5.13 and 5.14, the conservation was also mapped onto the surface of the homology model. The clearest feature from conservation analyses was the band of conserved residues in fig. 5.15 which corresponded to DNA binding residues and could be made clearer. Considering all GyrA amino acids within a 0.5 nm zone of any DNA, levofloxacin and moxifloxacin atom, yielded 30 residues of which ten could have been positively charged depending on pH (His, Lys, Arg). Of these, only two (Lys^{239} and Asn^{272}) were found to vary in evolutionary terms ($S > 2.0$). The GyrB subunit also contacts DNA and fluoroquinolones. Of its five residues within 0.5 nm distance to DNA and drug, all appear to be strongly conserved except for Gln^{465} (figs. 5.14, 5.15 (e,f)). This was most often found to be exchanged to Glu (28%), Asp (11%) and Ala (11%). Interestingly, Gln, Glu and Asp can serve as H-bond acceptors, while Ala lacks this capability. Interesting was also GyrB Glu^{466}. This residue was in salt-bridge interaction distance to the positive charge of amphoteric quinolones. However, this residue could interact with the backbone nitrogen of Lys^{447} and, depending on the rotamer, with the Lys sidechain.

Also amino acids of the classic QRDR could be considered. Interestingly, the only residue of the GyrA QRDR that, in an evolutionary context, appeared to be variable

was Ser^{83}. For the QRDR of GyrB, the conservation analysis showed no highly variable position. If positions with intermediate variability ($1.0 \leq S < 2.0$) were also taken into account, the set of QRDR residues in proximity to the quinolone binding pocket was extended by GyrA residues Ala^{84}, Asp^{87} and Thr^{88} as well as Lys^{447} of GyrB, which was exchanged by an Arg in 53% of the cases. This Lys was spatially neighbored by the two acidic sidechains of GyrB Glu^{466} and Asp^{426}. The latter one was a known resistance mutation. It appeared to be highly conserved ($S = 0.2$) with an Asp found in 97% of the cases. The mutation to Asn was observed in 1.9% of the cases.

There are clear implications for the rise of mutations and the residues which were most likely to be relevant for the development of resistance [148, 160]. Aside from Ser^{83}, the residues closest to DNA or therapeutic were found to be rather conserved.

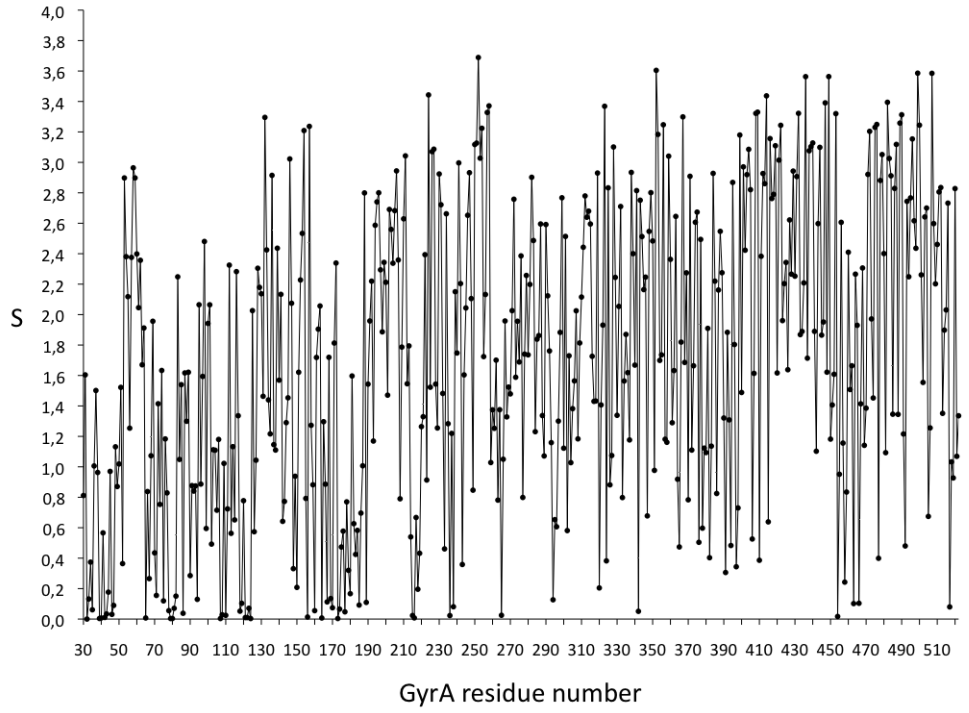

(a)

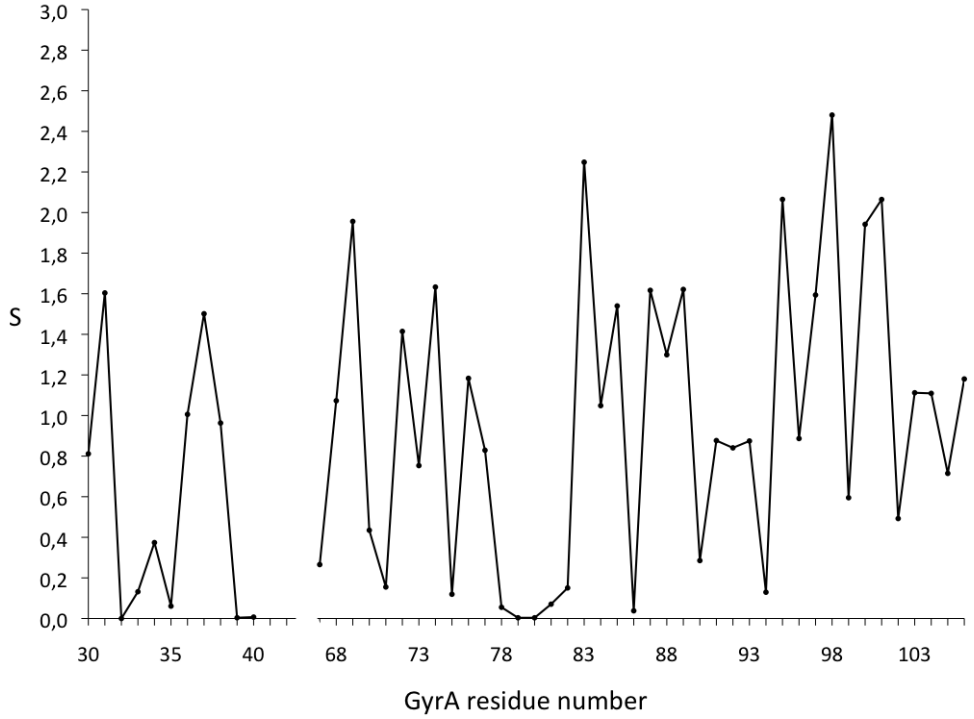

(b)

Figure 5.13: *Conservation S of (a) GyrA residues 30-522 and (b) GyrA residues 30–40 and 67-106*

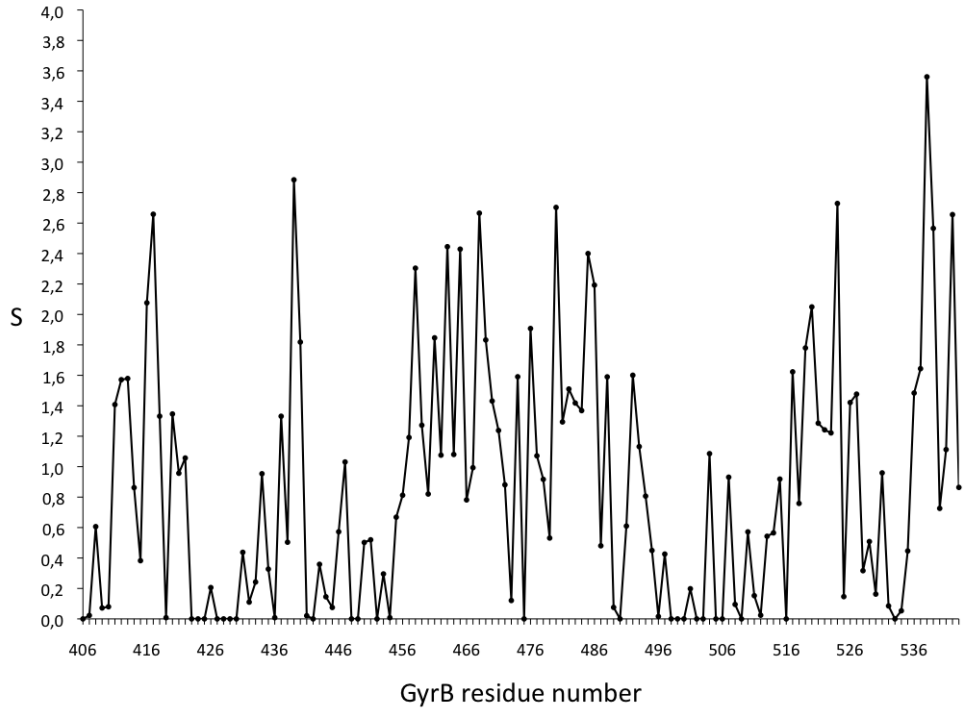

(a)

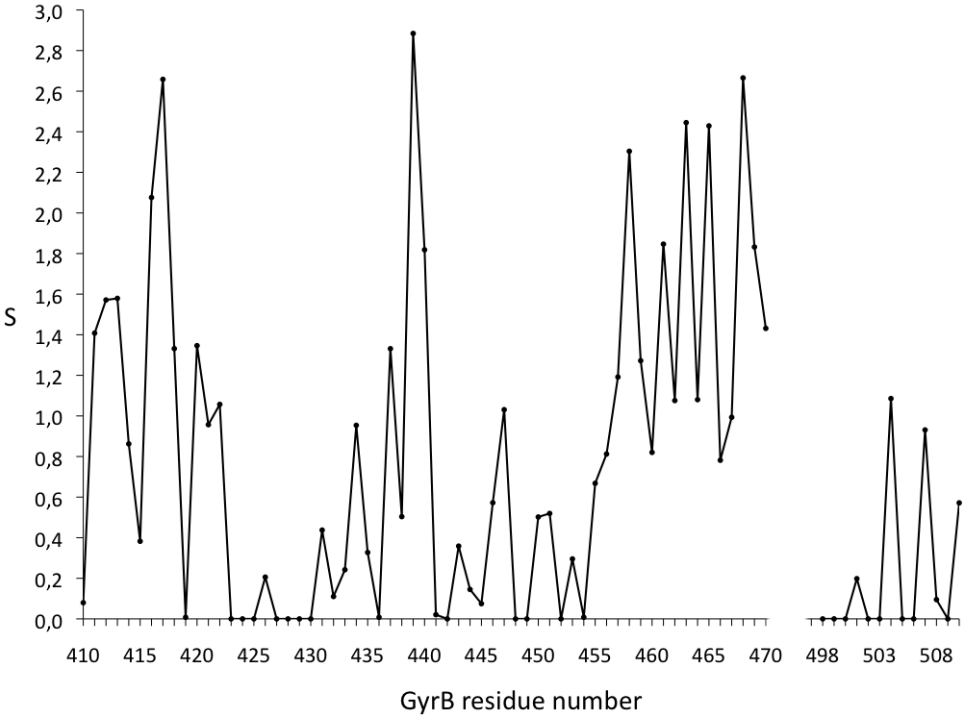

(b)

Figure 5.14: *Conservation S of (a) GyrB residues 406–543 and (b) GyrB residues 410–470 and 498–510*

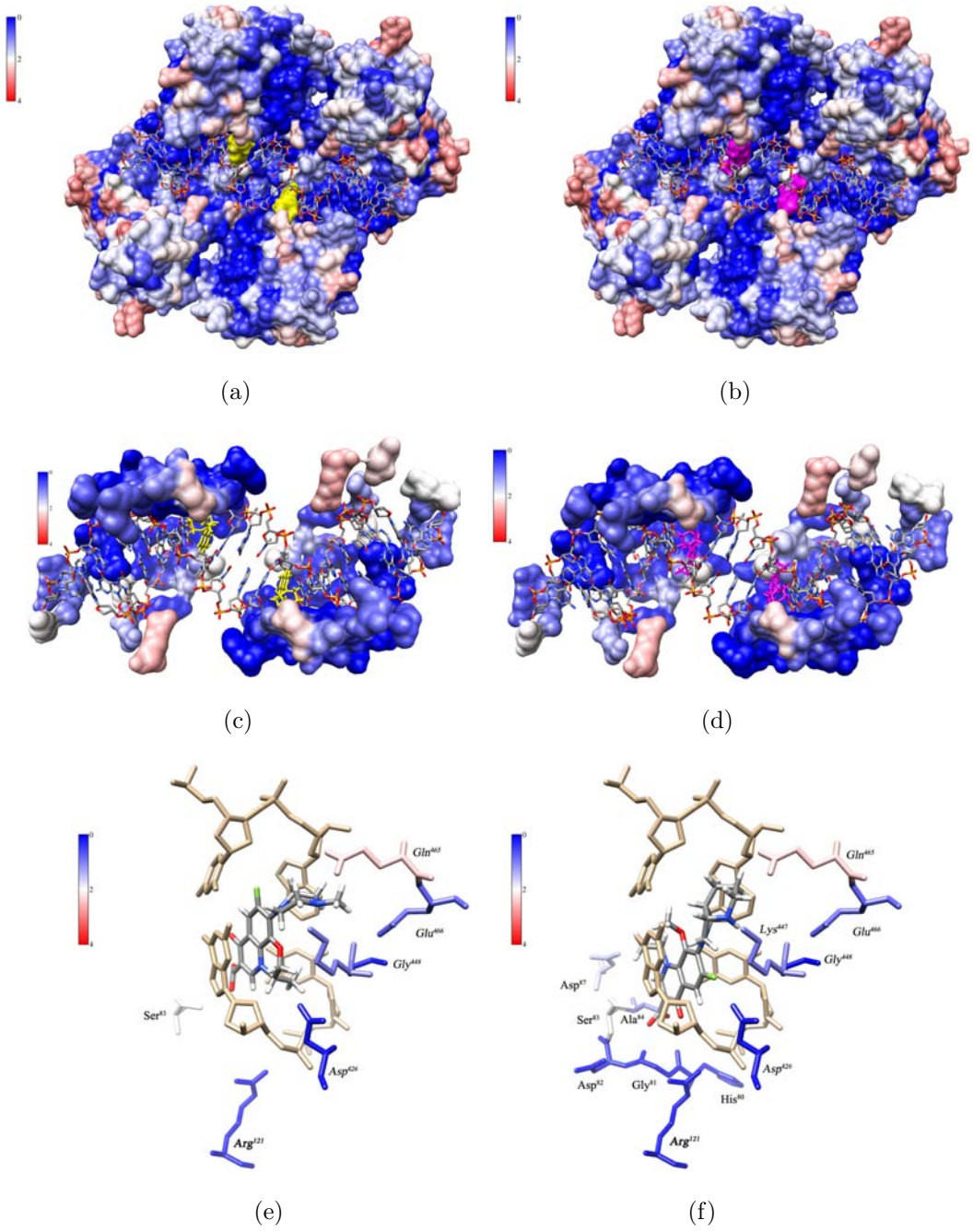

Figure 5.15: *Conservation of amino acids mapped onto the structure of the E.coli gyrase model in complex with DNA (conserved amino acids in blue, variable positions in red): Top view of the model with DNA in capped-sticks representation, (a) levofloxacin (yellow) and (b) moxifloxacin (magenta) depicted in surface representation. (c) View of residues within a 0.5 nm of DNA and levofloxacin as capped sticks and (d) moxifloxacin. (e) Amino acids and DNA (light brown) within a 0.5 nm sphere around levofloxacin and (f) moxifloxacin. GyrB residues are labelled in italics. Arg^{121} belongs to the second GyrA monomer which is not shown.*

5.5 Effect of *E. coli* GyrA mutations on quinolone MIC

Table 5.4 shows the influence of *E. coli* GyrA mutations on MICs for the five quinolones from fig. 5.16. Of them, levofloxacin was the only compound with a substituent at C8 which was additionally fused with the N1-group.
As shown in the table, WT-4 has only a single mutation in ParC and no mutations in GyrA. It has not been seen naturally and was the product of *in-vitro* mutagenesis [198]. However, this ParC $Ser^{80}Ile$ mutation was used in most strains to disable ParC and to highlight the quinolones' effects on DNA-gyrase and all other mutants from tab. 5.4 were obtained from WT-4 via selection experiments [291]. For comparison reasons, the MICs for WT and MI are also listed [199, 205]. If considered individually, the GyrA mutations from the five WT-4 derivatives were all seen in the literature before. But in combination with the ParC $Ser^{80}Ile$ exchange, these mutations and the determined MICs have not been reported yet.

Before examining the effects on gyrase, the relevance of ParC was considered by comparing the WT and WT-4 rows. ParC was important and disabling it usually rendered the bacterium significantly more susceptible to the quinolones.
Next, one could compare the resistance developed to each of the quinolones. Noticeably, the most unusual behaviour was seen with norfloxacin. Even in the wild type, this was one of the weaker therapeutics. With selection, it lost efficacy faster than the other quinolones. The interest however, was more with the structure and correlations with conserved residues. From this point of view the most striking result was the effect of the $Ser^{83}Asn$ mutation. This amino acid substitution increased the MICs of ciprofloxacin, enrofloxacin and norfloxacin 64-fold. For levofloxacin the increase in MIC was lower, but still 16-fold.
It also seemed to be the case that removal of the acidic group from Asp^{87} had a significant effect for all four quinolones. These results raised the questions, discussed below, as to how much the results could be explained by structural considerations.

***E. coli* strain**	**mutation in**		**MIC in μg/mL**				
	GyrA	**ParC**	**CIP**	**ENR**	**LVX**	**NOR**	**PFX**
WT	–	–	0.03	0.03	0.06	0.125	0.25
MI	$Ser^{83}Leu$	–	0.5	1	0.5	1	4/8
WT-4	–	$Ser^{80}Ile$	0.008	0.008	0.015	0.06	0.25
WT-4-M35	$Asp^{87}Gly$	$Ser^{80}Ile$	0.06	0.125	0.125	1	n.d.
WT-4-M37	$Gly^{81}Cys$	$Ser^{80}Ile$	0.125	0.125	0.125	4	n.d.
WT-4-M38	$Asp^{82}Gly$	$Ser^{80}Ile$	0.06	0.06	0.125	1	0.5
WT-4-M71	$Ser^{83}Asn$	$Ser^{80}Ile$	0.5	0.5	0.25	4	n.d.
WT-4-M102	$Asp^{87}Asn$	$Ser^{80}Ile$	0.125	0.25	0.25	2	n.d.

Table 5.4: *Genetic markers for E.coli strains and MICs for five quinolones: Susceptibilities were determined as MICs of ciprofloxacin (CIP), enrofloxacin (ENR), levofloxacin (LVX), norfloxacin (NOR) and pefloxacin (PFX); n.d.: not determined; all mutants were generated and MIC studies were carried out by A. and P. Heisig*

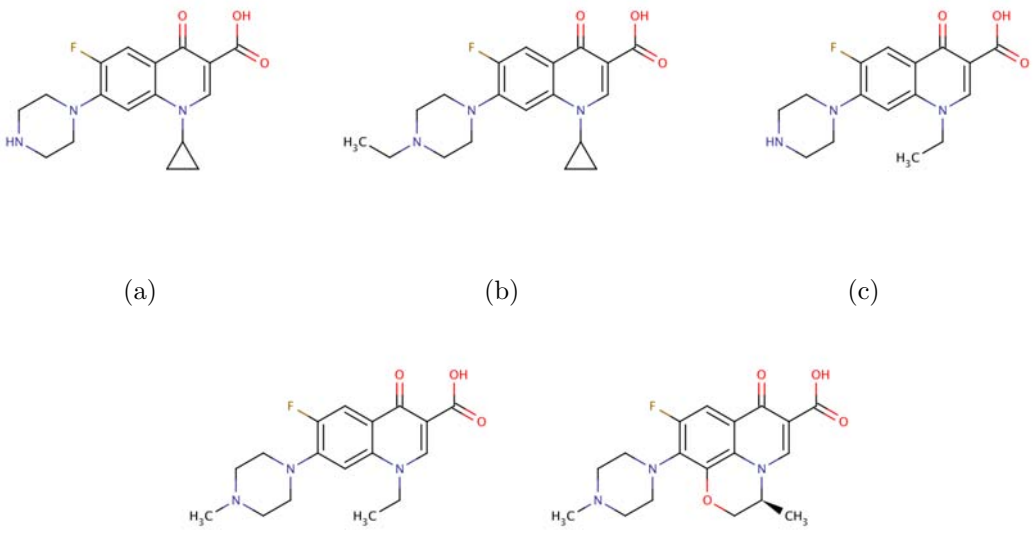

(a) (b) (c)

(d) (e)

Figure 5.16: *Structures of (a) ciprofloxacin, (b) enrofloxacin, (c) norfloxacin, (d) pefloxacin and (e) levofloxacin*

5.6 CoMSIA of Quinolones

Aside from homology modelling and conservation analyses, the recently published crystal structures were used for 3D-QSAR. CoMSIA analyses were carried out based on two different quinolone templates, moxifloxacin (PDB ID 3fof [77]) and levofloxacin (PDB ID 3k9f [260]) and CoMSIA came with the associated caveats. The models used to derive the CoMSIA were not perfect, the experimental data was old and the number of therapeutics was rather small. There were however, two obvious goals of the calculations. First, it was aimed to answer the question whether the CoMSIA model was consistent with newer experimental data (section 5.5). Second, usually calculations might be used to guide the development of new quinolone variations. In this work however, there was a separate question. The crystal structures of

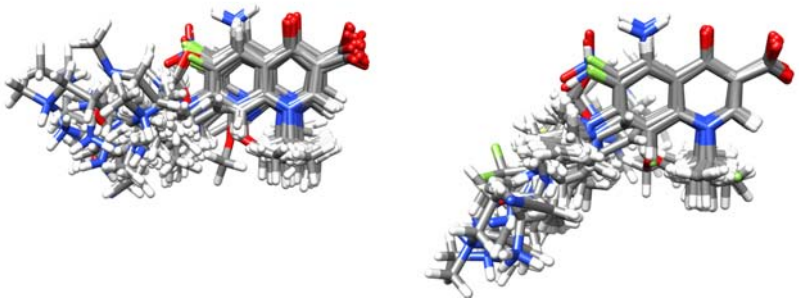

Figure 5.17: *Structural alignment of compounds from the training and test set for CoMSIA based on the 3D-structures of (left) moxifloxacin and (right) levofloxacin*

levofloxacin and moxifloxacin had electron densities in the same part of the structure, but proposed different orientations for the antibiotics. This could be regarded as a flip of 180°, but from a chemical point of view, the two orientations would mean a movement of 0.4 nm for the 3-carboxyl group of moxifloxacin. Moreover, it was possible that both structures were plausible. It was however, more likely that only one of the quinolone orientations in its target was correct. Here, it was attempted to build a CoMSIA model using both orientations.

The CoMSIA model was derived from a set of 49 compounds spanning approximately three orders of magnitude of activity. Although this set consisted of quinolines, pyrido[2,3-d]pyrimidines, 4-pyridones and 1,8-naphtyridines, they will be termed 'quinolones' throughout this analysis. Without any consideration of individual compounds or other details, the question was to analyse from which orientation a plausible model in terms of quality of fit (q^2, F, r^2 and SDR) could be built.
From a statistical point of view the result was a clear preference for the orientation of levofloxacin as given by structure 3k9f (tab. 5.5 , fig. 5.18).

After structural alignment of all compounds to the template therapeutics levofloxacin and moxifloxacin (fig. 5.17), the best CoMSIA models could be derived from a combination of electrostatic, steric, hydrophobic and hydrogen bond acceptor fields. Although eight PLS components were needed to get the smallest $PRESS$ and a

column filtering of 0.5 was needed to derive the most meaningful levofloxacin based CoMSIA model, still better statistics were obtained ($q^2 = 0.59$, $r^2 = 0.95$, $F = 92.47$, $SDR = 0.15$). For the CoMSIA model based on levofloxacin, only compound 2h was found to be a significant outlier and appeared to be underpredicted. Since the deviation of the residual of pefloxacin from the $2SDR$ cut-off was only 0.01 log units of cleavage activity, this compound could be regarded as a border case and was thus not considered as a serious outlier. For the CoMSIA based on the moxifloxacin orientation, the PLS analysis was performed with a column filtering of 0.9 units to reduce the noise and to speed up the calculation. However, using the orientation of moxifloxacin as the template, the statistics could not reach the quality of the levofloxacin-based model ($q^2 = 0.56$, $r^2 = 0.83$, $F = 74.51$, $SDR = 0.27$) and yielded three compounds from the training set that were poorly predicted. Given these results, only calculations based on the orientation of levofloxacin taken from 3k9f were considered.

	moxifloxacin model	**levofloxacin model**
column filtering	0.9	0.5
optimum number of components	3	8
q^2	0.56	0.59
$PRESS$	0.46	0.47
r^2	0.83	0.95
SDR	0.27	0.15
F	74.51	92.47
field contribution		
steric	0.26	0.21
electrostatic	0.18	0.30
hydrophobic	0.44	0.26
acceptor	0.12	0.23

Table 5.5: *Summary of CoMSIA models*

Aside from the statistically more significant leave-one-out calculation, the CoMSIA fields based on the fitting data were used to compute cleavage rates for the six

compounds reserved for testing (tab. E.2). Again, outliers were determined on the basis of the $2SDR$ cut-off of the corresponding training sets. Applying the levofloxacin based CoMSIA model to the test set, only the underpredicted rosoxacin had to be categorized as a real outlier. Its predicted cleavage activity was 0.41 log units above the $2SDR$ threshold.

Given the homology model of the *E. coli* gyrase partial structure in complex with DNA from section 5.4, the steric and electrostatic fields could be analysed in the context of the target structure. These fields contributed 21% and 30%, respectively, to the overall CoMSIA model (tab. 5.18).
The steric fields were visualized for ciprofloxacin as the compound with the highest cleavage activity and 1a' as well as nalidixic acid as examples for weakly active structures (tab. E.1, section 5.19). Regions, where sterically demanding groups increased the cleavage activity (colored green) were placed around the positively charged N4 of the 7-piperazinyl moiety of ciprofloxacin. Isopleths depicting regions in which bulky substituents were disfavored (colored yellow) were found near the cyclopropylic sidechain at N1 as well as in an area beyond the C7 position of ciprofloxacin. The most voluminous sterically disfavored zone was placed in close proximity to the GyrB Gln^{465} residue of the gyrase model but also to the carboxyl-group of GyrB Glu^{466}. This region was occupied by the sidechain of 1a'. However, nalidixic acid does neither fit into the favored nor in the disfavored contour volume. The electrostatic contour maps for ciprofloxacin, 1a' and nalidixic acid are shown in fig. 5.20. The models indicated that a positive electrostatic potential appeared to enhance the drugs' activity if this was placed in the region of the C7-piperazinyl group of ciprofloxacin (fig. 5.20 (a) - blue isopleth). The piperazinium substituent of ciprofloxacin was perfectly located in this region. Moreover, in the context of the target structure, the additional proton of this piperazinium was in H-bonding distance to the sidechain amide oxygen of GyrB Gln^{465}. Additionally, this volume was also near the negative charge of the GyrB Glu^{466} sidechain. 1a' and nalidixic acid lack positive electrostatic potentials in the area of this isopleth (fig. 5.20 (b) and (c)). Moreover, an unprotonated and thus electron-rich piperazinyl-N of 1a' was

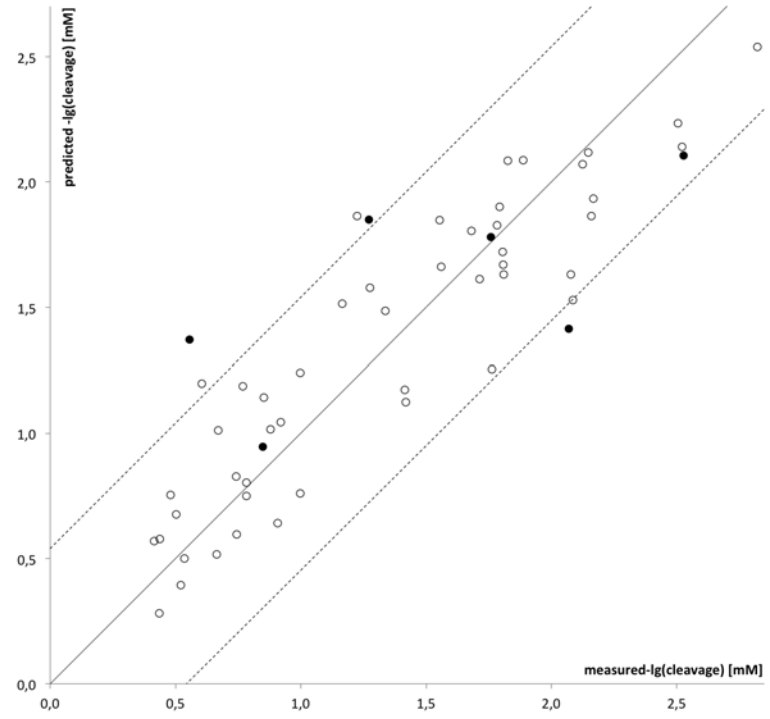

(a)

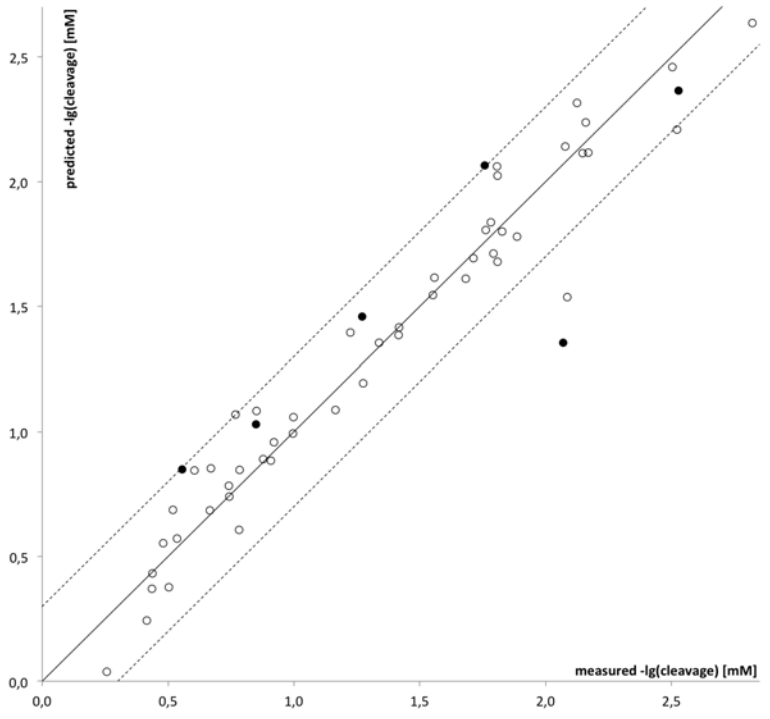

(b)

Figure 5.18: *Plot of predicted -lg(cleavage) [mM] vs. measured -lg(cleavage) [mM] for the training set (○) and test set (●) using (a) moxifloxacin from the 3fof crystal structure and (b) levofloxacin from the 3k9f crystal structure as template. Dashed lines depict the 2SDR cut offs.*

placed within in the blue contour. Additionally, a blue isopleth was also found to be beneficial if placed above the plane of ciprofloxacin's benzene, with its electron-density being decreased by the negative inductive effect of the C6-fluoro atom. Relative to the protein-DNA complex, this contour map was placed parallel to the π-electron system of the adjacent guanine nucleotide.
Positively charged groups however, were found to be unfavorable in proximity to both piperazinyl nitrogens of ciprofloxacin (red isopleth). Although the Lys^{447} sidechain looks as if it was in close contact with this red colored volume, it was in fact more than 0.5 nm away from it (fig. 5.20).

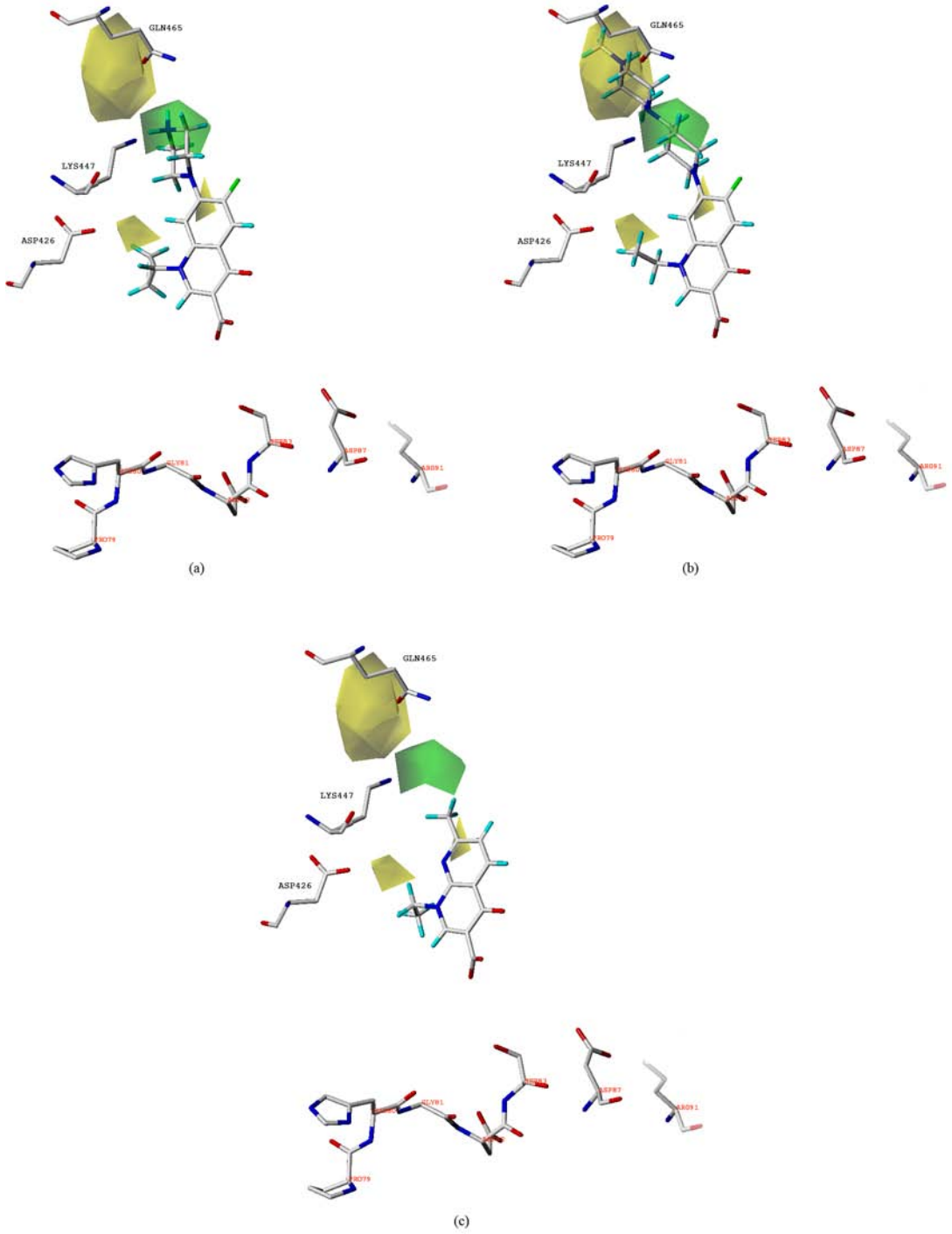

Figure 5.19: *Steric CoMSIA field based on the levofloxacin model shown for (a) ciprofloxacin, (b) 1a' and (c) nalidixic acid. GyrA and GyrB residues are labelled in red and black, respectively. Green isopleths depict sterically favored regions (contour level 0.029), sterically disfavored regions are depicted by yellow isopleths (contour level -0.006), The DNA is not shown for reasons of clarity.*

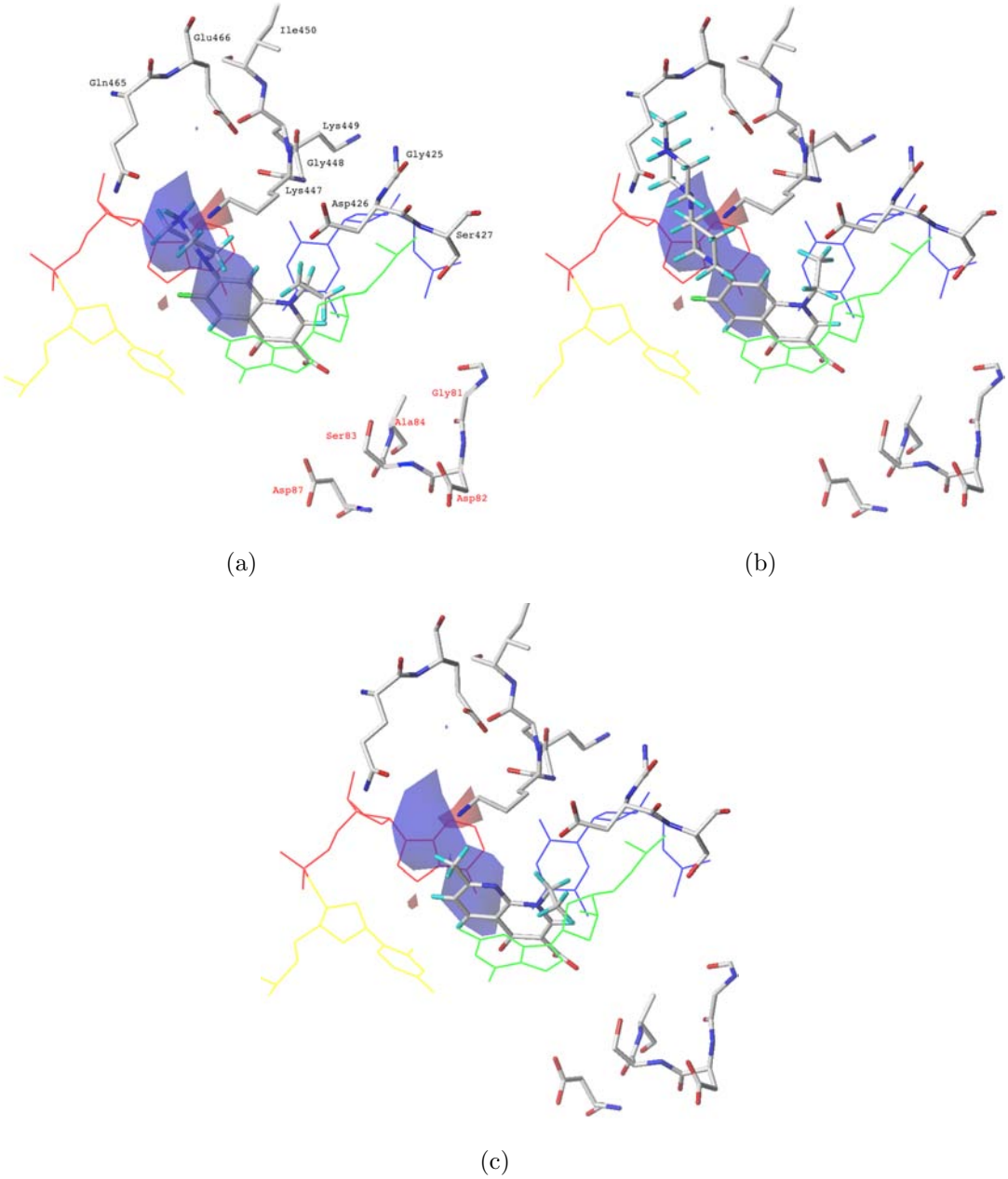

(a) (b)

(c)

Figure 5.20: *Electrostatic CoMSIA field based on levofloxacin model for (a) ciprofloxacin, (b) 1a' and (c) nalidixic acid. GyrA and GyrB residues are labelled in red and black, respectively. Blue isopleths depict regions where a positive charge is favored (contour level 0.012), negatively charged or electronegative groups are favored in the regions of the red isopleth (contour level -0.045). The DNA is colored as in fig. 5.1.*

Chapter 6

Discussion

Due to the lack of crystal structures of the complete *E. coli* gyrase in complex with DNA, the aim of the current work was to use computational methods to build a 3D molecular model in order to gain a better understanding of the quinolone-DNA-gyrase interaction. This model should be able to explain the previously reported resistance mutations [16, 63, 194, 292, 293].
After the calculations were done, crystal structures, homologous to gyrase-DNA-quinolone complexes, were released. Thus, a comparison with the theoretical models could be carried out. Conservation analyses and 3D-QSAR were conducted which, together with molecular modelling, were combined with new mutant selection and inhibition measurements to study the interaction of a series of quinolones with the gyrase-DNA complex from *E. coli*. The conservation analyses and the CoMSIA model were used to explain quinolone effects on steric and electrostatic grounds. However, some mutations that were described here for the first time could not be explained by obvious protein-ligand interactions.

The mechanism of gyrase action was divided into the following steps: In the first step, the DNA approaches the protein non-covalently. Next, the esterification via the Tyr^{122}-DNA bond takes place. Finally, the DNA gap is resealed by a trans-

esterification and subsequent DNA release. Given this simple picture, the intention was to model the DNA approaching the protein first. Subsequently, restrained MD was used to simulate the covalently linked protein-DNA complex. These were finally used for the docking of quinolones. In this chapter the results of the model building will be considered in the context of recently reported crystal structures. Subsequently, conservation analyses and CoMSIA will be discussed.

6.1 Protein-DNA docking

There were no appropriate 3D complexes of the protein-DNA complex that could be used as a basis for a homology modelling. But if the protein-DNA complex was going to be simulated, some idea of how the DNA approaches the protein was needed. Since this could be regarded as a docking problem, plausible protein-DNA complexes were generated by protein-DNA docking. Nevertheless, the selection of plausible and potentially near native dockings was challenging. Due to the lack of any structural information for a type IIA topoisomerase-DNA assembly, a comparison of the docking candidates with known homologous complexes was impossible. In addition, candidates did not necessarily satisfy interactions between DNA and all residues of the reduced docking volume. Furthermore, independent of the underlying docking algorithm, the scoring functions that are used to rank the results are usually the weak point of docking-schemes.

As presented in section 5.1, a docking might yield a plausible complex structure. This complex however, might not necessarily be scored best (fig. 5.2). For this reason the manual assessment of the more than 1000 complex candidates was required. In order to allow the enzyme to alter the topology of the DNA, the Tyr^{122}-residues of both enzyme A-subunits have to be covalently attached to the 5'-ends of the cleaved DNA to form phosphodiesters, especially with the guanine-phosphates of the known cleavage pattern (5'-↓GGCC-3'). Thus, it was claimed that docking solutions had to at least make this linkage possible. In other words, the promising docking candidates had small distances and suitable orientations of the 5'-guanine phosphates with respect to the protein's active site Tyr^{122}. Furthermore, dockings were preferentially

selected by the proximity of the negatively charged DNA backbone to arginines, lysines and histidines of the proposed GyrA DNA binding site. These amino acids are known to be abundant at protein-DNA interfaces where they constitute more than 40% of all amino acids. Especially the positively charged Arg, His and Lys residues seem to play an important role in driving the binding of DNA [294, 295]. The manual inspection according to these selection criteria resulted in 24 remaining complex candidates.

6.2 Molecular Dynamics simulations of protein-DNA complexes

The 24 complexes from the previous docking step represented a reasonable set of protein-DNA complexes with adequate conformational diversity. However, despite the covalent ester-bond to be formed between the protein's Tyr^{122}-OH and the 5'-phosphate of DNA, there was much room for uncertainty. Although the covalent bond restricted the allowed conformational space, it was not sufficient to define the binding mode of DNA. Thus, it was assumed that, in order for the esterification to take place, the DNA had to approach the protein in roughly the right configuration. This kind of molecular recognition implied that protein-DNA complexes from the docking must be somewhat stable, even without the covalent bond. In order to select the most stable complexes, molecular dynamics simulations were carried out for the 24 protein-DNA assemblies. This way, stability and plausibility of the complexes could be assessed and the most reasonable protein-DNA configurations were selected. To save time, the monomeric GyrA59-DNA complex alone rather than the GyrA59-dimer-DNA was simulated. Nevertheless, it should be noted that a partial structure for a homologous gyrase B subunit from *S. cerevisiae* was available when MD runs were conducted [64] (PDB-ID 1bgw). If a GyrB homology model for *E. coli* had been built based on this eukaryotic structure, the region homologous to the QRDR of GyrB was more than 4 nm away from Tyr^{122} and the α_4-helix of GyrA. Because of the size of the system and limited computer time, the MD calculations could only

be carried out on the picosecond time scale. However, this would not have been sufficient to observe the large conformational changes that would have been necessary to place the GyrB residues Asp^{426}, Lys^{447} and Ser^{464} near the QRDR of GyrA. In addition it was known that target mutations in quinolone-resistant bacteria most often occur in GyrA. Moreover, the active site GyrA-Tyr^{122}, proposed quinolone and DNA binding sites as well as amino acids involved in the development of quinolone resistance appear to be positioned in the GyrA subunit where they are in spatial proximity to each other [63].
Due to the limitations in computer time and to the important role of the GyrA subunit, it was not arbitrary to neglect the B subunit in the MD calculations although it was assumed that it is also involved in quinolone and DNA binding [70, 82]. Therefore, the focus was put on the complex formed by the 59 kDa N-terminal domain of the *E. coli* GyrA subunit in complex with DNA.

After the systems were equilibrated, five candidates from the first set of MD simulations satisfied the threshold distance. These structures were taken from the MD trajectories, so the conformations are accessible at room temperature. The 0.8 nm cut-off was the first criterion to look at and was used to select reasonable protein-DNA complexes. On the one hand it was chosen to exclude candidates for which it could not be anticipated that MD simulations would bring the guanine 5'-phosphates and the Tyr^{122}-OH into binding distance. On the other hand it still retained a sufficient variability of potential complex geometries.
The known preferred cleavage pattern 5'-↓GGCC-3' was included fourfold in the DNA model (fig. 5.1). Hence, for each of the 24 candidates four distance pairs were narrowly tracked and plotted. However, if the DNA was going to be covalently attached to the protein's Tyr^{122}-OH, only the linkage to nucleotides 5 and 40, respectively, would have resulted in remaining DNA fragment sizes that could be assumed to be sufficiently stabilized by interactions with the protein. Hence, of the five candidates satisfying the selection criterion from the first set of MD simulations, only two candidates, complexes 20 and 166, were picked for the subsequent steps. These could be distinguished by the orientation of the QRDRs α_4-helix with respect to the

DNA. Both models however, were consistent with proposals from the literature. The first complex placed α_4 in the major groove of the DNA as proposed by Liddington, whereas complex 166 supported the model of Laponogov with the α_4-helix in the minor groove of DNA (fig. 5.2) [63, 76].

Concerning the distances from figs. 5.4 and 5.5, it could be argued that for complex 20, a short distance between Tyr^{122}-OH and DNA was less favorable than for complex 166. However, there were several factors that governed the outcome of the MD simulations. These could be the choice of the force field parameters, treatment of non-bonded interactions, solvation effects, boundary conditions, treatment of temperature and pressure, integration method or the time step [210, 211, 213–215]. But most important was the initial configuration since it determines the system to be simulated. This means that calculation results of the MD simulations also strongly depended on those from protein-DNA dockings. In fact, the distance between Tyr^{122}-OH and nucleotide 5 in complex 20 was roughly 1 nm. In complex 166 however, the corresponding distance was already 0.8 nm when the simulation started. Both complexes were stable within the simulation parameters and were subjected to the intermediate and third set of MD calculations.

Before considering any structural details, the stability of the final covalently linked protein-DNA models was assessed by monitoring the *rmsd* and the radii of gyration r_g. Figures 5.6 and 5.7 showed that the extent to which the structures changed and the compactness of the structures equilibrated without any unfolding or detachment of the DNA from the protein. This was also verified by visualization of the trajectories. However, one must always bear in mind that the simulations could be too short. If any unfolding event occurs on the microsecond time-scale, it will not be seen in a nanosecond time-scale simulation. Moreover, looking at monitored simulation properties, neither of the two complexes could be regarded to be more likely than the other. One could compare potential energies of the two systems. But this would completely neglect entropic effects. Better than comparing potential energies would have been to compare the complexes with respect to their differences in free energy $\triangle$G. Free energy perturbation methods however, would only have been feasible for comparing very similar states and could not be applied since a rearrangement was

required to go between the different conformations [296].
If the complexes were also considered with respect to resistance data, there was in fact an indication for preferring complex 20 to complex 166: The known resistance mediating Ser^{83}Trp exchange in complex 166 might not only influence quinolone binding. It might also interfere with the overall DNA binding mode. But since both complexes appeared to be stable, at least under the simulation conditions, they were examined more closely. In this context, the focus was put on potential quinolone binding pockets.

The results of the structural analysis of complex 20 and the experimental findings suggested that a possible quinolone binding pocket could be found in a region confined by the overhanging tetranucleotide and residues of the α_4-helix of the QRDR [63, 138, 160]. This potential binding pocket appeared to be stabilized by several protein-DNA interactions. Most interesting were contacts between the DNA and the positively charged sidechains of Arg^{91} and Arg^{121} of which the latter one might aid Tyr^{122} in covalently linking the DNA.
Arg^{91} might contribute to the stabilization of the cut DNA within its potential binding site of GyrA. This amino acid formed a salt-bridge with Asp^{87} and could thus be regarded as a main stabilizer of the potential quinolone binding pocket. Moreover, resistance mutations of Asp^{87} to non-acidic residues could be explained by the resulting loss of salt-bridge interaction with Arg^{91} and the possibly resulting destabilization of the binding pocket and a change in the binding pocket's electrostatics [160].
Of the two serines Ser^{83} and Ser^{116}, the former one was known to contribute to the development of resistance to quinolones. The known resistance mutation Ser^{83}Trp could be explained by steric effects. The bulky tryptophan would decrease the available binding volume that could otherwise be taken up by a quinolone.
Since H-bonds open and close at room temperature, the function of Ser^{83} in H-bonding with DNA as well as the different roles of Ser^{116} in H-bonding between complex 20 and complex 166 is better evaluated in the context of averaged structures from the complete trajectories. However, here only snapshots from the trajectories

were taken.
Considering complex 166 on a structural basis revealed that the orientation of the DNA with respect to α_4-helix yielded two potential quinolone binding sites (fig. 5.8 (b)). The first cavity was formed by the α_4-helix and the minor groove of the DNA. The stabilization of this potential quinolone binding site could be carried out by Arg^{91} and Ser^{83} as described above. But apart from the salt-bridge formed between Arg^{91} and Asp^{87}, the former amino acid could also establish a second salt-bridge with the DNA and thus influence the DNA binding mode. The second potential quinolone binding volume in this complex was bounded by the α_4-helix, the overhanging tetranucleotide and Arg^{121}. As with complex 20, Arg^{121} could stabilize the orientation of the DNA.

6.3 Docking of quinolones

The docking of quinolones was carried out using the potential binding sites of both complexes as discussed in section 6.2. The goal was to see how the drugs might interact with their molecular target and of even greater interest, how resistance mutations could be explained.
The docking analyses for complexes 20 and 166 started with the conformational clustering of the 250 conformations that AutoDock proposed for each of the eleven quinolones (figs. 5.9, 5.11). Ideally, the clusters with the most members should have been assigned the lowest AutoDock binding energies. Moreover, these clusters should reflect the most reasonable dockings. This means, the quinolone conformations from such clusters should have been placed in the proposed binding site and satisfy the desired interactions with residues of the α_4-helix and the DNA. But the best scored drug pose might not have been the most plausible one. Moreover, the results from the dockings into the complexes showed that there were conformations of the same drug that appeared to be in more than one set. This means that they showed significant differences regarding their binding modes (tables 5.1, 5.2). If the differences in the estimated binding energies were within the expected error of the AutoDock4

scoring function (3 kcal·mol^{-1}), they could not be distinguished. In other words, if a compound appeared to be in more than one set but the pairwise comparisons of its scores was within the error, there was no chance to tell which of the poses really was the better one. Hence, the AutoDock4 scoring function could not be used to distinguish the dockings under consideration into good or bad models. Thus, manual assessment of all predicted ligand poses could not be avoided. Rather than finding the ideal case of conformational clustering, it was observed that none of the best scored dockings showed both, plausible interactions with DNA and residues of the α_4-helix.
For the interpretation of the results it was important to keep in mind that all dockings were carried out using snapshots from the MD trajectories rather than averaged structures. Additionally, the dockings were carried out without considering explicit waters molecules or magnesium ions.

6.3.1 Docking of quinolones into complex 20

It was worth considering that the binding site itself and the orientation of the DNA in complex 20 might facilitate the binding of quinolones by contributing to H-bonds and stacking interactions between DNA bases and the aromatic core of the drugs. Taking this as a criterion for the selection of promising poses, plausible dockings could be divided into three sets (A, B and C) on the basis of their orientation. The $\triangle E$ values for each compound from sets A and B clearly show that these could not be differentiated from the best scored conformations for the compound under consideration that was suggested by AutoDock4.
The plausible drug poses were placed within the same binding cavity, but there were noticeable differences with respect to their orientations. Compared to set A, the conformations from set B appeared to be rotated by $\sim$180° (fig. 5.10). Aside from this, the compounds from both sets were mainly anchored within the protein-DNA complex by hydrogen bonds between the 3-carboxy-4-oxo function and cytosine C^{+3} and C^{+4}. Furthermore, salt-bridges were found between the drugs' protonated C7-substituents and the sidechain of Asp^{82}. This was of particular interest since a

mutation of Asp^{82} to Gly was a known cause of resistance to quinolones if associated with a Gly^{81}Asp exchange [193]. Although the influence of the Asp^{82}Gly mutation on the quinolone efficacy could be explained by the removal of negative charge, the Gly^{81}Asp mutation could not be explained. Aside from this, resistance to quinolones due to mutations of Ser^{83} to Trp or Leu could be explained on sterical grounds. In the current models, such amino acid exchanges could decrease the accessible binding volume for the drugs. The models would also provide a reasonable explanation for the increased resistance due to Ser^{83}, Asp^{87} double mutations. In addition to the steric hindrance caused by mutations at position 83, an Asp^{87} exchange that might disturb the salt-bridge with Arg^{91}, would further destabilize the potential quinolone binding site.

Compounds from set C were interesting for two reasons. First, the orientation of the drugs strikingly differed from sets A and B (5.10) with the 3-carboxy-4-oxo structures of norfloxacin and pradofloxacin pointing out of the proposed binding pocket. Given this however, the importance of this moiety for the quinolones' activity could not be explained. Second, and as a consequence of that, the C7-substituent of garenoxacin directly interacted with the Asp^{87} sidechain. Hence, an exchange of this residue to a non-acidic amino acid would directly disturb the interaction with the drug. And as discussed for sets A and B, it would also lead to a loss of the interaction with Arg^{91}. A contact with Asp^{87} was not observed for norfloxacin which carries a smaller C7-heterocycle and protruded slightly further from the binding pocket. Although norfloxacin did not seem to be very stabilised in its pocket, one could not rule out this orientation on energetic grounds. The scoring function is not that accurate (tab. 5.1). This means that cluster ranks and energies for the example of norfloxacin did not provide a basis for an interpretation.
Aside from this, the drug orientations could provide an explanation for the resistance caused by mutations of Ser^{83}. As with the previously discussed docking models, this could simply be due to steric hindrance if the small and polar serine appears to be exchanged by the big and apolar tryptophan. Apart from the placement of the 3-carboxy-4-keto groups, another drawback of this model was its inability to explain the influence of the Gly^{81}Asp, the Asp^{82}Gly and the Gly^{81}Asp / Asp^{82}Gly double

mutation. A possible explanation could be a change of the electrostatic properties within the binding site.
Considering the docking scores of the compounds of each set, a general disadvantage of the given models was their inability to directly clarify the important role of Mg^{2+} ions for quinolone action [85, 297]. In particular, a potential direct interaction between quinolones, gyrase A subunit and Mg^{2+} ions could not be deduced from the dockings. Nevertheless, there was still the chance that an interaction takes place between quinolones, the ions and residues of the B-subunit which was not taken into account for modelling.

6.3.2 Docking of quinolones into complex 166

As the conformational clustering and the subsequent manual assessment of the ligand-target complexes showed, the results of the quinolone docking to complex 166 were rather heterogenous (section 5.3.2). One explanation for this observation was the size of the docking volume, which, in contrast to complex 20, was set large enough to include both possible binding pockets (section 6.2).
For the possible binding pocket defined by the α_4-helix and the minor groove of the DNA, one could assume that quinolones act similarly to the minor groove binder DAPI (4',6-diamidino-2-phenylindol) [287, 289] (PDB ID 1d30). This assumption was met by the eight compounds from set A as depicted in fig. 5.12 (a). This particular pose provides a simple explanation for the importance of the 3-carboxy-4-keto and the N-containing heterocycle at the drugs' C7. While the former anchored the drugs in the target via hydrogen-bonding with DNA and a salt-bridge with Arg^{91}, the latter, in its protonated form, interacted with the backbone of the DNA and the Ser^{83}–OH. Aside from this, Ser^{83} was interesting for the following reason: The dockings provided a possible reason for the important role of Ser^{83} for the development of resistance. This could, on the one hand, simply be attributed to steric hindrances caused by Ser^{83}Trp substitutions. Nevertheless, considering the actual target structure, such steric reasons could be widened to explain Ser^{83}Trp mutations for a broad spectrum of quinolone dockings to this particular pocket. On the other hand, the Ser^{83}Ile

mutations could be explained by the resulting loss of a H-bond acceptor. However, since structural snapshots of the target structure were used this has to be considered with adequate care.
Although the current dockings do not account for resistance mutations at position Asp^{87}, they highlight the plausible importance of Arg^{91}.

Even if the eight quinolones from set B were placed into the same cavity as compounds from set A, they were not placed in a DAPI like fashion. Moreover, the compounds were rotated around the horizontal axis by about 90° and protruded out of the cavity, with a distance between the quinolones and Arg^{91} of approximately 0.7 nm (fig. 5.12 (b)). As a consequence, the quinolones' 3-carboxyl feature was not involved in salt-bridge interactions with Arg^{91} any more. The structures were found to be stabilized within their target by H-bonds with DNA, the His^{80} backbone-carbonyl and the Asp^{82}–COOH, respectively (tab. C.2). But they were not able to explain important resistance features like the $Gly^{81}Asp$ / $Asp^{82}Gly$ double mutation. Moreover, given the model under consideration, it was rather hard to explain the substantial contribution of the $Ser^{83}Leu$ / $Asp^{87}Gly$ double mutation to the development of resistance against fluoroquinolones [205]. It could be argued that in this scenario, position 83 would no longer be available as an H-bond acceptor. Such proposals should be regarded with caution. Easier to interpret would be an exchange of Asp^{87} to Gly, since this could affect the overall shape and the electrostatics of the binding pocket by a potential impairment of the Asp^{87} / Arg^{91} interplay. This way, long range electrostatic interactions might influence the binding of quinolones.
Considering the importance of the drugs' 3-carboxy-4-keto group, the structurally unknown role of Mg^{2+} and the impact of a $Ser^{83}Leu$ / $Asp^{87}Gly$ double mutation, creates room for speculations. A Mg^{2+} might be complexed by the 3-carboxy-4-keto moiety of the quinolones, whereas the quinolone cores could stack with the DNA as already proposed [27, 277]. In contrast to this proposal, the ion might on the other end be complexed by the sidechains of Ser^{83} and Asp^{87}. Hence, there is an indirect quinolone-gyrase interaction which appears to be mediated by Mg^{2+}. A $Ser^{83}Leu$ / $Asp^{87}Gly$ substitution would in the light of such model not be able to complex the magnesium ion any more. Thus, the quinolones will lose the capability to indirectly

interact with the gyrase A subunit. However, a quinolone docking that satisfied this assumption was not found.

Before considering set L, it should be noticed that the main reason for compiling it was the different binding pocket that was addressed compared to sets A and B. In contrast to conformations found in the latter sets, the twelve poses considered here, were very diverse and did not show any clear-cut conformation that might have presented a preferential binding mode. Moreover, this heterogeneity was also reflected by the fact that 50% of the conformations from this set were clustered as singletons. Due to the aforementioned limitations that were associated with the scoring function, it was not even possible to take the top ranked poses of garenoxacin and pradofloxacin as references for a common conformation (tab. C.2). But yet, there were still some interesting features that should be mentioned. All conformations from this set could contribute to stacking interactions with the adenine nucleotide 15 (fig. 5.12 (c)). Interestingly, it was found that some conformations from this set appeared to be stabilized via interactions between their carboxyl-groups and Arg^{121}. This residue was reported before to be potentially involved in the interaction with quinolones [298]. Occasionally, the carboxyl-group of the drugs was also found to be in contact with the backbone amines of Ala^{119} and Met^{120}. However, for most conformations of this set, the carboxyl-groups formed H-bonds with DNA bases. Although interactions were found between positively charged C7-substituents of the drugs and the sidechains of Ser^{83} and Asp^{87} (tab. C.2), this was not sufficient to be used for a reasonable explanation of gyrase residues involved in the development of resistance.

One could generally state that none of the current dockings allowed the presence of Mg^{2+} ions. Even more interesting was the observation that Ser^{83} and Arg^{91} in complex 166 were involved in the binding of DNA and in the potential binding of quinolones. Hence, one might finally argue that mutations that directly or indirectly interfere with these residues might not result in a decreased susceptibility to quinolones alone. Such mutations might also disturb the protein's ability to bind DNA, at least with respect to the binding mode under consideration. This way, it was assumed that complex 166 was less likely since mutations might negatively affect the natural

function of DNA-gyrase.

6.3.3 Docking of quinolones: general considerations

Because a family of drugs was used, it should have been possible to exploit the assumption that the drugs must bind similarly to have similar biological effects. Moreover, dockings began with the idea that the best drug pose should be common to each drug. Unfortunately, neither the subsets shown for docking into complex 20 nor for complex 166 contained all eleven drugs (tab. 5.1, fig. 5.10). Given these observations, it could be argued that this was mainly due to the different chemical structures of the quinolones. With respect to complex 20, this could be used as an explanation for finding all (1*S*, 6*S*)-2,8-diazabicyclo[4.3.0] non-8-yl carrying compounds (bay-y3118, moxifloxacin and pradofloxacin) in the same set. However, it could not be used as an explanation for the absence of enoxacin and pd0163449 from any set. This was particularly interesting because pd0163449 only differs from pd0117962 and pd0129603 by its halogen-substituent at C8. A similar finding was made for complex 166. Aside from enoxacin and moxifloxacin, it was not possible to explain the lack of pd0129603 from set A.

It was more likely that other reasons had a bigger influence. First, AutoDock picked random initial coordinates for the ligands. These were subsequently changed by the non-deterministic genetic docking algorithm to create different quinolone orientations and were spread throughout the entire docking volume. Second, given the selected docking volume, only 250 conformations could be generated within a reasonable period of time and the cluster sizes were rather small. But this might not have been sufficient to exhaustively sample the entire docking volume. One option could have been to sample ten times more conformations in order to obtain ten times more compounds in each cluster. However, this would have been computationally very expensive.

One could also reduce the docking volume. But this would have needed for a more precise prior knowledge of the binding site. Furthermore, the docking volume could have been divided into several smaller overlapping grids. Although this would have decreased the time needed to dock into each such volume, the number of dockings would have been increased at the same time. Thus, the total time spent would not

have been substantially decreased.

6.4 Comparison with crystal structures

The crystal structures of a *S. pneumoniae* topoIV-DNA-quinolone complex (PDB-ID 3k9f) represented excellent opportunities for further computational work [77, 260]. Given the plausible structures from the docking, it was thus, from a methodological point of view, of great interest to compare the docking results with a recently published crystal structure. When considering the ParC monomer of the *S. pneumoniae* structure bound to DNA, it was on the one hand striking to see that there was a four basepairs staggered DNA break, but the DNA strands were not separated (fig. 6.1 (a)). On the other hand, the crystal structure clearly showed quinolones interacting with the ParE subunit, homologous to GyrB, too (fig. 6.1 (b)). It was also shown that each such topoIV monomer induces a 75° bend in its associated part of the dsDNA [77, 89, 260]. This seems to be supported by an isoleucine sidechain (*S. pneumoniae* Ile^{170}) that sits in between the basepairs at the bend.
The crystal structure supports the models presented here with respect to the stabilization of the protein-DNA complex. This is mainly carried out by electrostatic and van der Waals interactions. In addition, the consideration of the ParC-ParC dimer of topoIV (PDB ID 3k9f) shows that the previously mentioned Arg^{121} of the first ParC monomer could interact with DNA and the drug bound to the DNA-ParC assembly of the second monomer. Their distance was roughly 0.5 nm.
But there were fundamental differences concerning the theoretical models that were built and presented in this work. First, the built models were neither based on a cleaved but double stranded DNA nor could they simulate the A-geometry or the bend. Second, modelling was based on a GyrA monomer rather than the dimer. And third, the models were built without taking the GyrB subunit into account.

The structural alignment of 451 atom pairs of a ParC monomer of 3k9f and the protein-part of complex 166 resulted in an *rmsd* of 0.23 nm [224]. Nevertheless, this superposition showed substantial differences in the position and orientation of the

DNA with respect to the α_4-helix (fig. 6.1 (c)). While in complex 166 this helix pointed into the minor groove of the DNA, it was opposed to the C^{+4} and A^{+5} nucleotides of the DNA in the crystal structure. It thus confirmed the assumption that the proposed complex was less likely (section 6.3.2). Therefore, complex 166 was not considered for further discussion.

In contrast to complex 166 however, the modeling of the protein-DNA assembly in complex 20 was significantly closer to the crystal structure. The structural alignment of the GyrA59 based part of complex 20 and 3k9f yielded an *rmsd* of 0.24 nm over 453 atom pairs. As depicted in fig. 6.1 (d), the DNA binding modes in complex 20 and 3k9f were similar, especially regarding the orientation of the protein's α_4-helix with respect to the DNA's cleavage site. Although the *E. coli* protein-DNA model in complex 20 also showed the sidechain of Ile^{174} (*S. pneumoniae* Ile^{170}) sitting between basepairs of the DNA, the associated DNA bend was missing. Aside from this, the most striking difference was the distorted DNA geometry of the four overhanging bases in complex 20. Their backbone atoms were on average about 1 nm away from their 3k9f counterparts and appeared to be pushed towards the A subunit resulting in a larger binding pocket. This was most likely due to the fact that simulations were carried out with this part of the DNA being single stranded. Hence, the H-bond interactions that would normally stabilize the dsDNA were missing.

From the comparison of quinolone binding modes in the model and the crystal structure as shown in fig. 6.2, it could clearly be seen that the 3-carboxy-4-keto function of levofloxacin from 3k9f pointed towards positions Ser^{79} and Asp^{83} of ParC (Ser^{83} and Asp^{87} in GyrA). Its C7-substituent directly interacted with the ParE subunit of topoIV, resulting in a slight protrusion from the binding pocket built from DNA and ParC [77, 260]. The most promising docking poses however showed the drug being flipped by about 180° and more receded into the GyrA-DNA binding pocket.

Moreover, the quinolone pose in 3k9f allowed the presence of a Mg^{2+} ion that can be coordinated by the drugs and the sidechains of Ser^{79} and Asp^{83}. However, such drug pose was not found amongst the dockings into complex 20.

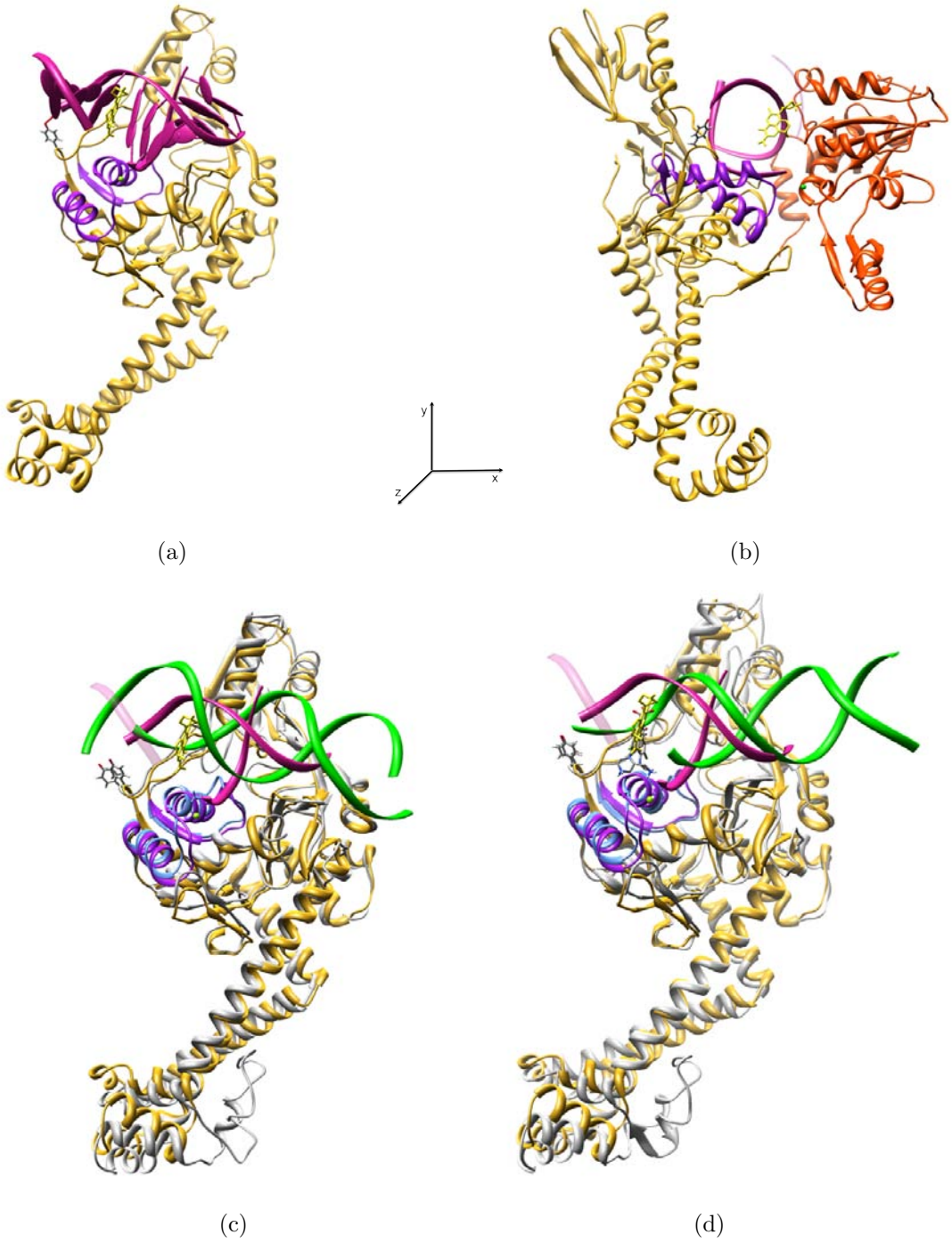

Figure 6.1: *(a) ParC monomer of the topoIV crystal structure of S. pneumoniae (gold) in complex with DNA (magenta) and levofloxacin (yellow) (PDB ID 3k9f). The region analogue to GyrA QRDR is highlighted (purple) and Mg^{2+} is shown as a sphere (green). (b) The same structures is rotated 90° around the y-axis and the ParE subunit is depicted in orange. (c) Structural alignment of 3k9f and complex 166 (grey) with GyrA QRDR (lightblue) and DNA (green). (d) Structural alignment of 3k9f and complex 20 with docked levofloxacin and ciprofloxacin. Colors as in (c).*

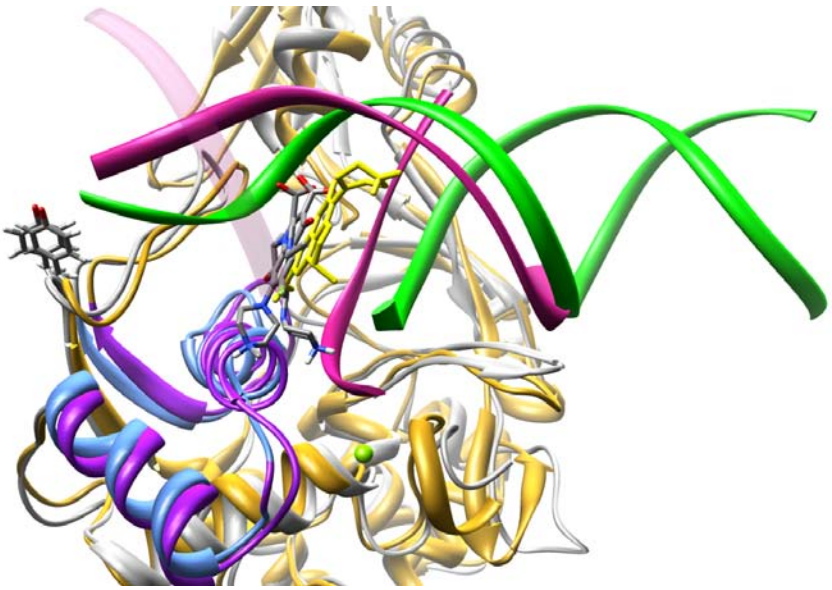

(a)

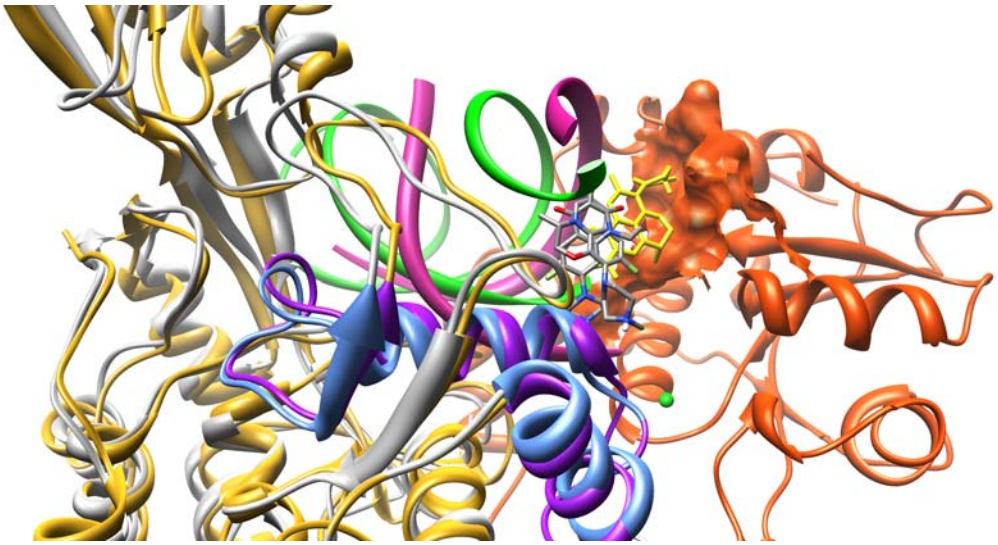

(b)

Figure 6.2: *Close ups of (a) complex 20 from fig. 6.1(d) and (b) fig. 6.1(d) with ParE rotated by 90° around the y-axis. Colors as in fig. 6.1. In addition to the co-crystallized levofloxacin (yellow), norfloxacin from set A and levofloxacin from set B are depicted and colored by their atom types.*

One could argue that the docking algorithm was inappropriate for this particular kind of docking problem. This lead to the most concrete proposal to test if the eleven drugs could successfully be docked into the known quinolone binding site of 3k9f to recover known conformations and interactions. To see if the calculations were at all feasible, a 're-docking' was carried out. The ligand was removed from the crystal structure and the quinolones were docked into this binding site. Under these artificial and ideal conditions, the docking seems to be reliable and the correct location and orientation could be retrieved. But the correct docking ranked in first place was seen in less than half the calculations.
This again emphasized on the importance of manual assessment of docking results.

compound	**search for (near-) native conformations - cluster analysis**			
	cluster rank$^{(*)}$	**rank in cluster**	**conformations in cluster**	**energies in [kcal·mol^{-1}] actual / lowest**$^{(\dagger)}$ **/** $\triangle E$
redocking into 3k9f				
bay-y3118	1 / 44	6	11	–7.95 / –8.41 / 0.46
ciprofloxacin	2 / 26	1	1	–7.4 / –7.89 / 0.49
enoxacin	3 / 37	2	14	–5.93 / –6.84 / 0.91
garenoxacin	1 / 29	3	15	–9.23 / –9.34 / 0.11
levofloxacin	7 / 21	6	8	–6.71 / –8.0 / 1.29
moxifloxacin	2 / 47	5	7	–7.18 / –7.95 / 0.77
norfoxacin	5 / 31	16	27	–6.65 / –7.78 / 1.13
pd0117962	2 / 24	1	7	–7.49 / –7.89 / 0.4
pd0129603	2 / 24	8	11	–6.67 / –7.72 / 1.05
pd0163449	1 / 25	13	13	–6.57 / –8.03 / 1.46
pradofloxacin	1 / 37	7	12	–8.39 / –8.92 / 0.53

Table 6.1: *Results of the redocking into 3k9f: Each row shows the compound contained in a cluster, listed with the rank of the cluster it was found in and the number of overall clusters found for the compound (*). The rank of the compound within that cluster is given with the number of overall conformations in this cluster. The actual estimated binding energy, the lowest energy of all clusters (†) and their difference* $\triangle E$ *is given.*

The problems in recovering native or near-native quinolone conformations by docking into the theoretical models were not due to a poor performance of AutoDock4. It was rather shown that docking results were very susceptible to the target geometry. The modelling results were very close to the published structure. This was quite surprising given the practical limitations. Because of the system size, it was not even possible to include the complete target structure. From a methodological point of view, the results are especially encouraging. The selection of candidate structures and the gradual introduction of the covalent linkage appear to be a more than reasonable protocol.
In summary, it can be stated that docking into a known and well defined binding site with a bound drug is a promising approach. But if this level of structural detail is missing, the results from molecular dockings have always to be interpreted very carefully. They can only be regarded as starting points for subsequent work.

6.5 Mapping Protein conservation and Resistance Mutations

The assessment of residue conservation on an entropy-like basis as used in this work is a common way to analyse multiple sequence alignments within a protein family [262]. Conserved residues are likely to be important for maintaining the protein's structure and thus its functionality [299, 300]. This characteristic can be useful for the development of drugs that interfere with such proteins but also implies that any drug design should be tolerant of the exact sidechains at the less conserved and highly variable positions.
The results from the conservation analyses depicted in figs. 5.13, 5.14, 5.15 and summarised in table 6.2 indicate that most residues that directly correlate with DNA binding were largely conserved. This strongly suggested that these positions are functionally important [301]. Especially the positively charged Arg, His and Lys residues seem to play an important role in driving the binding of DNA. Furthermore,

recent analysis showed that arginines induce specific electrostatic patterns on the protein and DNA site that are important for recognition and binding of the nucleic acids [302]. Arg^{121} in GyrA for instance was found to be highly conserved. This strengthened the assumption that Arg^{121} plays a pivotal role in obtaining the spatial orientation of the DNA. In this role it might guide the DNA towards the active site Tyr^{122} and may serve as a kind of stabilizer that eases the attack of Tyr^{122} to the DNA [64, 249]. Furthermore, this residue might be involved in quinolone binding as shown in fig. 5.15(e, f). However, of the positively charged residues in proximity to the DNA that were not near the quinolone binding site, Arg^{91} appeared to be conserved and involved in DNA binding. But it was most interesting to further look at the variable positions Lys^{239} and Arg^{272}. The analysis of the alignments from the BLAST searches revealed that Lys^{239} in GyrA was most often exchanged by an arginine in 40 % of the homologous sequences. Since Lys and Arg share similar physicochemical properties and are thus able to carry out similar functions, this was no surprise. A similar behavior was observed for Arg^{272} which was most frequently substituted by a Lys. However, also exchanges to the polar but uncharged Asn were found in 11% of the cases. Although the physicochemical properties of Asn are different compared to Arg, both can serve as H-bond donors. Hence, both are able to interact with the negatively charged backbone of the DNA.

In contrast to the basic amino acids, Ser^{172}, Gln^{325} and Ser^{329} were also found to be less conserved. But since these residues do not occur in vicinity to the fluoroquinolone inhibitors, they were not taken into account for further discussion.

The low conservation of Ser^{83} and Asp^{87} of GyrA was no surprise, either. These positions are known to be among the most common resistance mutations in *E. coli* GyrA [190]. Surprisingly, Asp^{87} was not within 0.5 nm of any DNA or drug. This may support the possible role of water or a magnesium ion in bridging the distance between drug and this amino acid.

Aside from these known resistance mutations, it was more interesting to find Gln^{465} of GyrB to be a variable residue. From the structural model in fig. 5.15 it can be seen that the positively charged C7-substituents of amphoteric quinolones could interact with GyrB Gln^{465}. Given the results from the conservation analysis, one could

argue that the most frequently observed mutations ($Gln^{465}Glu$ and $Gln^{465}Asp$) might strengthen the interaction between the drugs and GyrB. This way the susceptibility of gyrase against amphoteric quinolones would be increased which one should be able to measure. The also frequently found replacement to Ala could be expected to have the opposite effect. Aside from the aforementioned GyrB residues, GyrB Ser^{464} is a known resistance mediating position. It was not within a 0.5 nm sphere around the quinolone, but within 0.5 nm of the DNA. Mutations to Phe, Tyr or Asn have been previously reported [196, 303]. These mutations might influence the shape and the electrostatics of the quinolone binding site within GyrB and can lead to steric hindrance due to their sidechain sizes.

In contrast to the positions near the quinolone binding pocket that vary, it was worthwhile looking at the highly conserved positions which were located near the drug binding site. Starting from the BLAST searches, GyrA residues Gly^{81} and Asp^{82} statistically rarely vary (figs. 5.13, 5.14 5.15). Nevertheless, it was already known from the literature that mutants carrying a $Gly^{81}Asp$ or $Asp^{82}Gly$ exchange show resistances against some but not all fluoroquinolones while they remain susceptible to nalidixic acid. By contrast, the presence of a $Gly^{81}Asp$ / $Asp^{82}Gly$ double mutation in GyrA mediates resistance to fluoroquinolones and nalidixic acid [193, 304]. With respect to the crystal structures this might be due to remodelling of the electrostatics in the quinolone binding site. Additionally, His^{80} was highly conserved and experiments indicate that this residue is not directly involved in quinolone binding but in the gyrase cleavage-religation reaction [301, 305]. In addition, Ile^{174} is also a conserved residue. It is placed in between DNA bases and seems to play an important role in bending the DNA. Due to this role it was not surprising to find it to be highly conserved [80, 89, 260].

With respect to GyrB, the residues that appeared to be close to levofloxacin and moxifloxacin were the same. Of them Gly^{448} statistically was the most conserved amino acid followed by Asp^{426} and Glu^{466}. The former one was interesting. Together with Lys^{447} from the PLKGK motif of GyrB, Asp^{426} was a known position of resistance mutations. Asp^{426} appeared to be highly conserved and if mutated, exchanges

to Asn were observed most often. This was consistent with experimental findings [70] since quinolone use creates selection pressure favoring this mutation. Of even greater interest was the former residue, GyrB Glu^{466}. Although the model shows that this position might be involved in an interaction with the positive charges of the quinolones' C7-moieties, it was rather conserved. However, one could assume that mutations at this position might be one plausible way for bacteria to lower the impact of amphoteric drugs on the gyrase.

Also of interest were the findings for GyrB position 447. This residue is moderately conserved. The frequent mutation to Arg is no surprise since the similar properties of these side chains cannot be expected to have a major effect on the structure. Curiously however, the mutation to Glu described by Yoshida [192] was not found in the database at all. A GyrB $Lys^{447}Glu$ mutation however, was known to confer resistance against acidic quinolones like oxolinic acid if mutated to Glu. This mutation also results in a slight hypersensitivity to amphoteric quinolones like ciprofloxacin [70, 192]. This can be attributed to electrostatic repulsion between the negatively charged Glu sidechain and electron rich atoms at the acidic quinolones' C7-substituents. The positively charged C7-moieties of amphoteric drugs however, would benefit from this mutation due to the possible formation of a salt-bridge. These explanations were clearly supported by the recent crystal structures.

The flexibility of the positively charged GyrB Lys^{447} sidechain allows this residue to adopt different spatial orientations. One such placement substantiated the idea of Heddle and Maxwell that Lys^{447} forms a salt-bridge with GyrB Asp^{426}. In contrast to the mutation of Lys^{447} however, the reason for decreased susceptibilities to acidic and amphoteric drugs in the case of an $Asp^{426}Asn$ exchange remains anyone's guess. Heddle and Maxwell suggested that: "The positively charged Lys at 447 is proposed to interact with the negatively charged carboxyl group of Asp^{426}, providing a neutral environment for binding hydrophobic groups. Thus, the wild-type pocket binds both types of quinolone. In the quinolone resistance mutation GyrB $Asp^{426}Asn$, a negative charge is neutralized, and so binding of both types of drug is reduced" [70]. While the strength of an interaction between the side chains at positions 447 and 426 would most likely be decreased, a resulting binding pocket would still be far from neutral.

residue	conservation S	note	close to DNA*	close to drug†
Gyrase A subunit				
His^{80}	0.0	potentially involved in cleavage-religation reaction	√	
Gly^{81}	0.1	known resistance mutation		
Asp^{82}	0.2	known resistance mutation		
Ser^{83}	2.1	known resistance mutation possibly involved in coordination of Mg^{2+} / H_2O		√
Asp^{87}	1.4	known resistance mutation possibly involved in coordination of Mg^{2+} / H_2O		
Arg^{91}	0.3	conserved; involved in DNA binding	√	
Arg^{121}	0.0	may support Tyr^{122} in DNA binding	√	√
Tyr^{122}	0.0	covalently linked to DNA	√	
Ser^{172}	2.1	variable; not close to drug	√	
Ile^{174}	0.1	conserved; role in DNA bending	√	
Lys^{239}	2.1	variable; not close to drug	√	
Arg^{272}	2.7	variable; not close to drug	√	
Gln^{325}	2.3	variable; not close to drug	√	
Ser^{329}	2.0	variable; not close to drug	√	
Gyrase B subunit				
Asp^{426}	0.2	known resistance mutation conserved; close to drug		√
Lys^{447}	1.0	known resistance mutation moderately conserved close to drug		√
Gly^{448}	0.0	conserved; close to drug		√
Ser^{464}	1.0	known resistance mutation moderately conserved	√	
Gln^{465}	2.4	variable; close to drug		√
Glu^{466}	0.8	conserved; close to drug		√

Table 6.2: *Residues within a 0.5 nm sphere around DNA (*) and levofloxacin (†) of the E. coli gyrase model. Conservation of amino acids can range from 0 (highly conserved) to 4.3 (not conserved)*

6.6 MIC studies

There are several ways to interpret the mutants and MIC values in table 5.4. All of them were generously provided by A. Heisig and P. Heisig (unpublished data): The results are just a small sample of the bacterial response to ciprofloxacin challenge and they are not exactly what one would expect in the light of the conservation analysis. The results for the quinolones could be interpreted in chemical terms. Some could also be interpreted in the light of the structural model. The four sites at which mutations were seen (Gly^{81}, Asp^{82}, Ser^{83} and Asp^{87}) were all in the α_4-helix, but involved in different kinds of interactions. Here, the focus is primarily on properties of the GyrA protein.

The first two lines of the table 5.4 refer to the native bacterium or a mutant thereof (WT, MI). The rest of the table is based on results from the WT-4 strain carrying a mutation which renders the topoIV resistant to quinolones. This allows one to focus on GyrA.

The start of the table shows a single mutation of Ser^{83}Leu which has been discussed previously (MI) [199]. It is listed in the table for comparison. The *E. coli* mutants were selected by confrontation with ciprofloxacin and their resistance to all five tested fluoroquinolones was markedly increased.

Five mutations are seen at four sites. Individually, these have been reported previously [194, 205, 292, 293]. However, such single site *E. coli* GyrA amino acid substitutions in combination with a mutation in ParC, leading to an exchange of Ser^{80} by Ile, have not been described yet. From an evolutionary point of view, the mutations are interesting. In 4000 related sequences, residues Gly^{81} and Asp^{82} were very conserved. Hence, there might be some fitness cost associated with their mutation. At the same time, in this work and other literature studies, these residues mutated in the face of an antibiotic challenge. On the basis of the conservation measures discussed in section 6.5, one might say that there was a large fitness cost associated with the mutations. On the basis of the *in-vitro* studies, this cost is smaller than the artificial

selection pressure.

The structures of the used fluoroquinolones slightly differ by their substitutions at C7 and N1 (fig. 5.16). The only compound substituted at C8 was levofloxacin. The additional electron-withdrawing C8 substituent decreases the electron-density of the benzene ring and might thus increase the stacking with DNA bases. Moreover, the flexibility of the N1 substituents in this drug was significantly decreased by ring-fusion between C8 and N1. The stereochemistry forces the N1 substituent to point into the direction of the less obstructed space around the thymine nucleotide and the C^{α} atom of the highly conserved GyrB Gly^{448}. These chemical properties of levofloxacin might explain that the effect of the mutations on this drug was weaker on average.

Table 5.4 lists two mutations affecting GyrA Ser^{83}. The Ser^{83}Leu substitution in the MI mutant and a Ser^{83}Asn replacement for WT-4-M71. Compared to serine, such substitutions introduce steric hindrance and fill the volume normally available to the quinolone. This way, the drugs might get pushed away from the GyrA α_4-helix towards a sterically disfavored volume confined by residues Lys^{447}, Gln^{465} and Glu^{466} of the GyrB subunit. This could increase the MICs. Moreover, the displacement induced by Ser^{83}Asn might also diminish the strength of DNA base stacking of the quinolone skeletons. Furthermore, the proximity to Gln^{465} and Glu^{466} of GyrB would suggest that drugs like ciprofloxacin and norfloxacin with unsubstituted piperazinyl moieties at C7 would interact with these GyrB residues (fig. 5.15). Unfortunately, the present MIC studies did not investigate this hypothesis. Otherwise it would be expected that a GyrA mutation like Ser^{83}Asn would have a lesser impact on ciprofloxacin and norfloxacin than on the 4-piperazinyl-substituted fluoroquinolones. Aside from the steric hindrance, it was also important to notice that the polarity at position 83 was changed by exchanges of the hydrophilic Ser^{83} by small and apolar amino acids like Ala or Leu [190, 249]. This could be explained by the presence of water or Mg^{2+}: The distance of roughly 0.4 nm between Ser^{83} and levofloxacin in our model could either be bridged by water or by Mg^{2+}. Such interactions would be disturbed by Ser^{83}Ala or Ser^{83}Leu. Thus, a replacement of serine by leucine or asparagine might not only change the shape of the quinolone binding pocket,

but could also alter its physicochemical properties and its ability to interact with potential water molecules or magnesium ions. Aside from these considerations, a displacement of the quinolones by a $Ser^{83}Trp$ mutations might also decrease the aromatic ring stacking ability of the therapeutics with the DNA.
Concerning position 87 of the gyrase A subunit, all quinolones under consideration showed a more pronounced increase of the MICs if the acidic Asp^{87} was exchanged to the polar but uncharged asparagine as in WT-4-M102 than the complete truncation of the sidechain ($Asp^{87}Gly$ in WT-4-M35). The $Asp^{87}Asn$ exchange resulted in a 16-fold MIC increase for ciprofloxacin. The same mutant however increased the MIC of enrofloxacin 32-fold although the drugs only differ by an ethyl-group at the piperazinyl-substituent. These differences might be explained by the change of the electrostatics in the binding site. Although a substitution of Asp^{87} by Gly would impair the possible coordination of water or Mg^{2+} it would also increase the volume accessible for ciprofloxacin and enrofloxacin. An exchange to Asn however, would not only impair such coordination ability, but would also decrease the space available for the drugs. This might push ciprofloxacin and enrofloxacin towards the GyrB residues of the binding pocket and thus, cause steric clashes. Due to its N-ethyl-piperazine substituent, these would be stronger for enrofloxacin than for ciprofloxacin and might explain the differences in their MICs.
In contrast to the orientation of levofloxacin in fig. 5.15(e), the set of residues within a 0.5 nm distance around moxifloxacin (fig. 5.15 (f)) also covers GyrA positions Gly^{81}, Asp^{82} and Asp^{87}. Thus, the binding mode of moxifloxacin might have been more useful to explain mutations at these positions. However, since the moxifloxacin orientation was only poorly defined in the crystal structure (PDB ID 3fof), the current studies were focussed on the levofloxacin orientation as in 3k9f. However, regardless of the exact binding mode of the drugs and the accuracy of the model, there was no way the mutation of Asp^{82} in GyrA could be in proximity to the quinolone. Remarkably, the $Asp^{82}Gly$ exchange as in WT-4-M38 rendered all quinolones an order of magnitude less effective.
Gly^{81} and Asp^{82} could both play some part in the functioning of the native enzyme, as suggested by the conservation data. More specifically, the structural model in fig.

5.15 suggests that they are in close proximity to DNA. This makes at least one of the observed mutations all the more surprising. Removing the negatively charged aspartate might cost the bacterium some fitness, but it was not absolutely essential.

Given the modelled *E.coli* gyrase-DNA-quinolone complex, some mutations were rather easy to explain on the basis of steric hindrance and alterations of polarity. Nevertheless, our models were not able to explain every mutation by means of the drug structure and the corresponding influence on the MIC. This became especially apparent for norfloxacin. Although this compound lost its effectiveness faster than the other drugs, this effect could not be explained in terms of the given target and drug structures. This suggests that there might be an alternative quinolone binding mode or a yet unknown mechanism of action that influences the MICs. A similar suggestion was recently made by Malik [156].
In general, model building should be looked at with adequate care. The B-factors of the template structures are rather high and two interpretations have been published (3fof, 3k9f). Also, the ionisation is debatable and due to the presence of several rotatable bonds in each structure, the exact geometry may differ from the one in the crystal structures. This should not only be kept in mind for the interpretation of the results from the MIC studies but also for the outcome of the CoMSIA.

6.7 CoMSIA of Quinolones

Structure-activity relationships for quinolone antibacterials often utilizes MICs to determine biological activity [278, 306]. Although the MIC is a standard parameter to quickly assess the activity of antibacterial drugs, it is determined against whole bacteria and therefore depends on a variety of different factors. Ideally, QSAR analysis are grounded on biological activities that are as simple as possible. These are often given by IC_{50} values measured on isolated target structures [20]. Since IC_{50} values were not available, the aim of the current CoMSIA study was to build a model based on cleavage activities. This model should have been suitable for predicting

the cleavage activities for a set of quinolone compounds and to derive features that could be correlated with the model of the gyrase-DNA-quinolone complex. The best statistical values for the CoMSIA for the levofloxacin and the moxifloxacin model resulted in q^2 values above 0.5. This indicated the usability of the respective models in the prediction of the cleavage activity of the quinolones in the targets. However, the levofloxacin based model performed much better with respect to q^2, r^2 and the SDR (fig. 5.18, tab. E). Nevertheless, one should bear in mind that the number of compounds used was rather small and the cleavage activities only covered approximately 2.6 log units.

The quality of the structural alignment of the drugs is crucial for the outcome of the CoMSIA [307]. As shown in fig. 5.17, the alignment based on levofloxacin was superior to the moxifloxacin based one. This was also reflected in the statistical analyses of the models. Regardless of the good statistics of the levofloxacin based CoMSIA, there was one outlier in the training set (2h) and one from the test set (rosoxacin). These could be explained: With its C7-pyrrolidine substituent, 2h was the only 1,8-naphtyridin with a 5-membered saturated heterocycle at C7 that carried only one heteroatom. Accordingly, such structures were not well represented in the training set. Hence, it was no surprise to find 2h being underpredicted. The underrepresentation of rosoxacin from the training set could be explained on a similar basis. This drug was the only one with a 6-membered aromatic substituent at C7. Moreover, since it was part of the test set, it could not be expected to find this compound well predicted at all.

Aside from the statistical parameters, the graphical visualization of the results from the CoMSIA could be used for the interpretation of the models. From a subjective and possibly biased point of view, it was easiest to interpret the steric and electrostatic fields of the levofloxacin based CoMSIA model. By this means, the CoMSIA models could partly be reconciled with the findings from the MIC studies and vice versa: Some sterical problems that were found in the context of our molecular model appeared to be consistent with the steric CoMSIA fields (fig. 5.19). On the target site, an exchange of smaller residues in the proposed drug-binding pocket by amino acids with bulkier sidechains as observed for $Ser^{83}Asn$, would push the drugs into

the disfavored region of the steric field and thus induce steric clashes with Gln^{465} of GyrB. From the therapeutics' point of view, very voluminous C7-substituents as in 1a' should have an impact that is comparable to an exchange of Ser^{83} by sterically demanding residues. However, given the MIC data and the results from the CoMSIA analysis, one could argue that a combination of such Ser^{83} substitutions and voluminous C7-substituents should result in an even bigger impairment of quinolone activity. In addition, the disfavored steric volume in proximity to the quinolones' N1 also supports the observations from the MIC studies that large and flexible N1-substituents could cause steric clash with the adjacent nucleotides by protrusion into this volume (section 6.6). Aside from the disfavored regions, the favored steric isopleth was also compatible with the MIC findings when the sterically disfavored volume remains free. With respect to the target structure, voluminous groups in this region could support the formation of interactions between the drug and the protein-DNA complex.

Aside from the steric CoMSIA fields, the isopleths for the electrostatic one also reflect the chemical properties within the quinolone binding pocket very well. Moreover, the electrostatic field further strengthened the observation made for the steric field. As shown in fig. 5.20, the region where positive potentials increase the drugs' effectiveness coincides with the volume that favors sterically demanding groups (fig. 5.19). Again, this perfectly reconciled observations from the MIC studies since it prefers positive charges within a defined distance to the negative charge around GyrB Glu^{466} and Gln^{465} which can serve as an H-bond donor. Thus, quinolones like enrofloxacin that lack a positive charge in this area were found to be less effective than compounds like ciprofloxacin. The volume that favors positive potentials in a region between the quinolones' benzene and the aromatic DNA bases can be interpreted in terms of the electron-withdrawing effects of groups attached to the quinolone skeletons: It is known that a C6-fluoro substitution increases the effectiveness of the drugs. This could be due to its negative inductive effect by which the electron-density of the ring system is decreased (fig. 6.3). This way, the ring stacking interaction between the therapeutics and the adjacent DNA bases is increased. Moreover, this could also explain the better performance of levofloxacin in the MIC studies, since the

additional electron-withdrawing group at C8 further decreases the drugs' electron density. Such considerations could not only be used to explain the good activity of difluoro-quinolones 1p and 1q (tables E.1, E.2). It could also be used to explain the effectiveness of the desfluoro-quinolone garenoxacin: Since the lack of the C6-fluoro substitution is compensated by a difluoromethoxy moiety at C8, the electron-density of the aromatic ring is still sufficiently low to increase the stacking interaction with the DNA.
But yet, QSAR models are only of interest if they are used in a predictive context. Hence, the levofloxacin based CoMSIA model was used for the prediction of the cleavage activity of levofloxacin and enrofloxacin. Although these drugs were used in the MIC studies, they were not part of the training and test set used for the CoMSIA analysis. The prediction of their cleavage activities followed the same strategy as applied for the test set compounds. For levofloxacin and enrofloxacin our prediction yielded –lg cleavage activities of 1.98 mmol/L and 1.85 mmol/L, respectively (tab. E.3). They were thus ranked among the top 30% compared to the compounds that were used to derive the CoMSIA model. Unfortunately, there was no cleavage data available that could be used for comparison with the predicted values.

In principle, QSAR analyses have always to be interpreted with care. In this work for example, the protonation states of the compounds used for the 3D-QSAR analysis was estimated. However, for the interpretation of the CoMSIA analysis, the protonation of the compounds is as crucial as their structural alignment. Changes of protonations of compounds or of the structural alignments would lead to results that certainly differ from the ones presented here. Due to a possible interaction of such a positive charge with acidic residues and H-bond acceptors in the target structure, this lead also to the question if a positive charge at the drugs' C7-substituents would generally be necessary for their effectiveness. The differences in the quinolones' chemistry causes differences in their pK_a values. Given particular pH conditions in the quinolone binding pocket, such pK_a differences would cause differing proportions of protonated and unprotonated drugs according to the Henderson-Hasselbalch equation. This way one could explain why some drugs are less active than others.

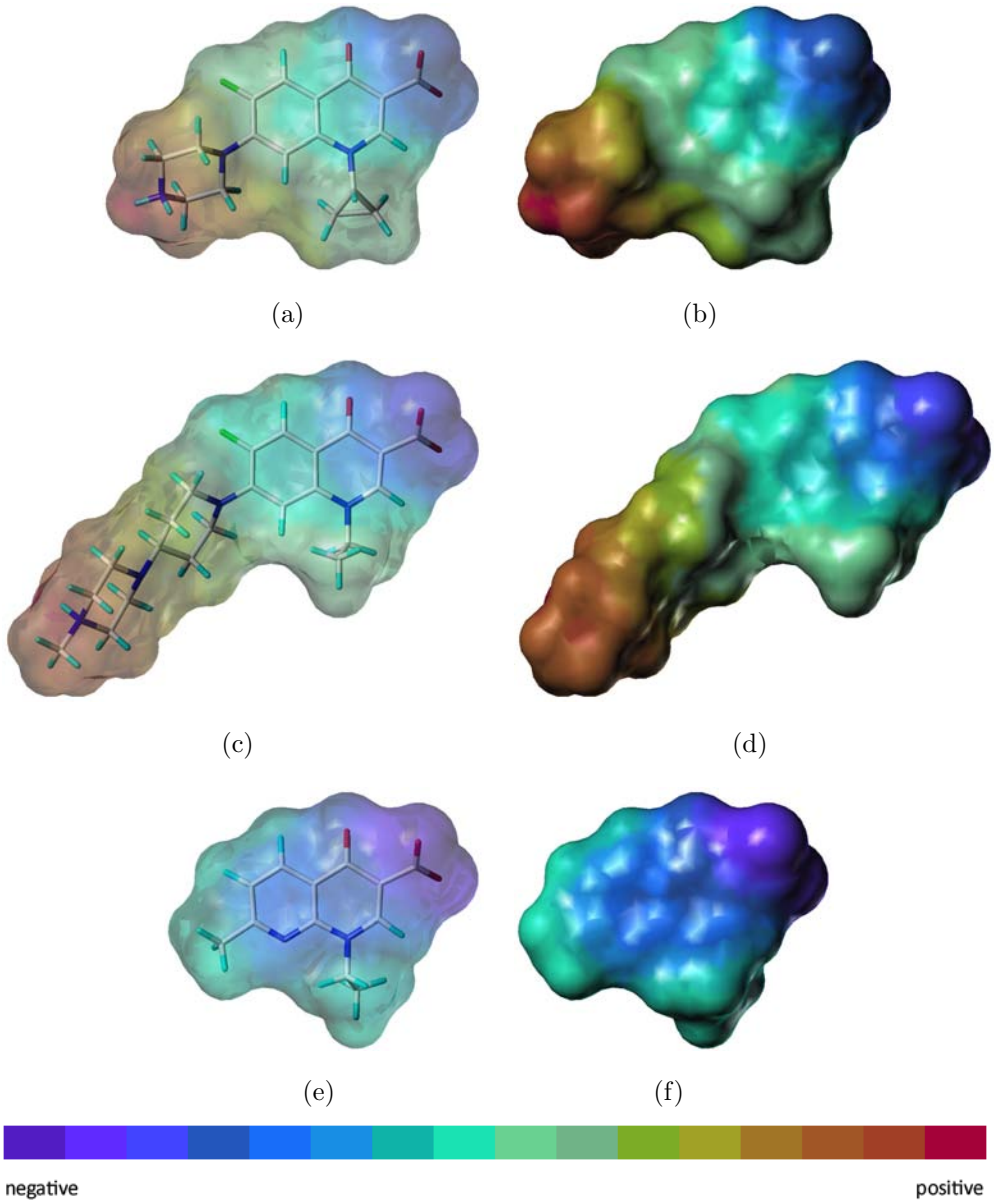

Figure 6.3: *MOLCAD generated electrostatic surface property maps based on AM1 charges of (a, b) ciprofloxacin, (c, d) 1a' and (e, f) nalidixic acid [227]. Due to the presence of C6-fluoro substituents in ciprofloxacin and 1a', their aromatic rings appear less negative than in nalidixic acid.*

6.8 Outlook

In the present work molecular modelling methods were used to build a three-dimensional model of the covalently linked *E. coli* GyrA-DNA assembly in complex with quinolones. It was shown that the applied model building protocol was very promising. It might thus be a reasonable approach for future modelling exercises if smaller and less sophisticated target structures are considered.

One way to gather more information of the gyrase-DNA-drug complex would be to carry out *in-vitro* mutagenesis experiments. Here, the results from the modelling, CoMSIA and the conservation analysis suggest the involvement of GyrB residues Gln^{465} and Glu^{466} in quinolone binding which are both are just outside the known GyrB QRDR. In this context, it would be interesting to see how a Gln^{465}Ala substitution influences the effectiveness of quinolones. However, it would be of even greater interest to see how mutations of the well conserved Glu^{466} might influence the antibacterial effect of quinolones. Here, an exchange to an aspartate would be expected to have a lesser impact than an inversion of the charge by a Glu^{466}Arg mutation or at least the loss of the negative sidechain charge through a substitution by alanine. Furthermore, due to its high conservation, Glu^{466} could be targeted by more interactions.
Aside from these GyrB residues, the possible role of GyrA Arg^{121} in quinolone binding and DNA cleavage is particularly interesting. It might thus be a reasonable position for further *in-vitro* mutagenesis experiments: First, one might analyse the mutation's impact on the quinolone effectiveness. Second, the ability of the mutant to bind DNA might be examined in an electrophoretic mobility shift assay [308]. Third, the influence of the mutations on the bacterial fitness should be looked at. This may be done in terms of the bacterial generation-time or the supercoiling capability. In general, such analyses may contribute to a deeper understanding of this residue and the mechanism of DNA cleavage. Moreover, due to the high conservation of Arg^{121}, it might also be an interesting residue from the angle of antibacterial drug design. If *in-vitro* mutagenesis would be able to demonstrate its importance for the enzyme,

targeting this residue with prospective drugs would be expected to be even more beneficial.

Since the gyrase activity requires the adoption of a variety of different gyrase and DNA geometries, a comparison of the built models with published crystal structures cannot exclude that the modelled gyrase-DNA complexes might occur during the catalytic cycle. Given the models from the docking (section 6.3), it might be postulated that sidechains of Asp^{87} and Arg^{91} form a salt-bridge. One might assume that this salt-bridge is involved in maintaing the shape, stability and electrostatics of potential binding-cavities and contributes to the binding of DNA. Based on these assumptions, another prospect of this work could thus be to test the influence of GyrA positions 87 and 91 on the effectiveness of quinolones, the DNA binding capability and the bacterial fitness by *in-vitro* mutageneses experiments. This may lead to a better understanding of mechanistic gyrase aspects.

More concrete, the overall idea could be to follow two different routes of *in-vitro* mutageneses (fig. 6.4). One such approach for the introduction of the mutations is schematically depicted in fig. 6.4. Following route A, first an $Asp^{87}Lys$ exchange could be introduced. This way, the resulting Lys^{87} would be adjacent to the likewise positively charged Arg^{91}. In a second step, this Arg^{91} could be mutated to an acidic Glu. Route B might be used to establish the $Arg^{91}Glu$ exchange first. As opposed to route A, this introduces two negatively charged sidechains at positions 87 and 91 of GyrA. Via the second mutation, $Asp^{87}Lys$, this could be reversed. The two approaches should therefore be used, to generate mutants, which show two closely spaced positive (route A) and negative charges (route B) in the α_4-helix. The second step of both routes, would pursue the goal to cancel out these repulsive effects, but with the positions of the charges reversed.

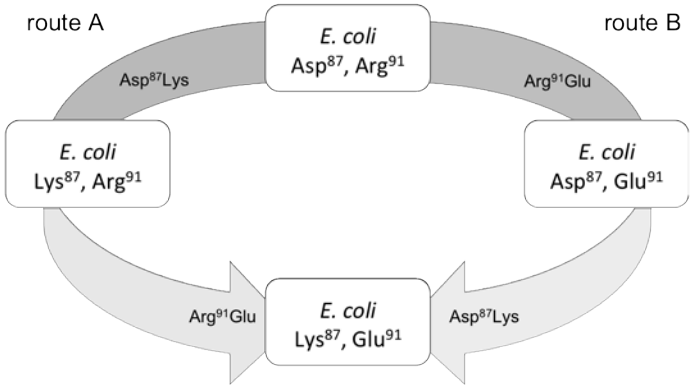

Figure 6.4: *Experimental routes for insertion of mutations. The routes differ in the order that the mutations are introduced.*

Also, the potential role of Mg^{2+} in quinolone and DNA binding was very recently confirmed in crystal structures [79, 80]. Apart from the magnesium-ion that is necessary for drug binding, the structures also revealed the role of the GyrB Asp^{498}-x-Asp^{500}-x-Asp^{502} motif in Mg^{2+} mediated DNA binding. This pattern plays a key role in DNA cleavage and appears to be highly conserved. Hence, the availability of high-resolution structures of the gyrase holoenzyme would be ideal for structure-based drug design to search for new antibiotic lead structures that target this motif [309]. One such approach would be the virtual screening of large compound libraries to find starting points for the development of novel antibacterial agents [310, 311]. This concept can be generalized to search for potential candidates that also target other sites of gyrase, e.g. in closer proximity to GyrA Arg^{121}. One should bear in mind that virtual high-throughput screening methods have to be fast in order to process large compound libraries in a short time. The increased speed is often accompanied by less extensive sampling of the ligands' conformational space and a loss of docking accuracy. This makes such methods even less reliable than pure docking approaches. However, newer approaches try to address this conflict by well chosen preprocessing steps [312].

Another prospect of this work is to combine the outcomes of the CoMSIA and the conservation analyses for the synthesis of new compounds. These could be tested with respect to their activities while the results could in turn be used to improve the CoMSIA model and its predictive value in an iterative fashion. This could help to develop a rational basis for the design of new or improved inhibitors of DNA-gyrase.

Finally however, it is more likely that it will be the combination of biological, chemical, physical and computational methods that leads to the development of new and potent antibiotic drugs that are refractory to resistance.

Summary

Fluoroquinolones are losing their effectiveness due to emerging bacterial resistance. One known reason for this is the alteration of the drugs' molecular target, the DNA-gyrase in complex with DNA. But due to the lack of crystal structures of the complete gyrase-holoenzyme, this work aimed to build a 3D complex by using molecular modelling techniques.

A protein-DNA-docking method was initially used to search for plausible complexes of the crystal structure of a 59 kDa fragment of the *E. coli* GyrA N-terminal domain (GyrA59) and a 21 bp dsDNA. In order for the ester bond to form, the DNA must approach the protein in roughly the right configuration. Therefore, starting from the docking step, molecular dynamics (MD) simulations of the plausible non-covalent protein-DNA complexes were carried out. Promising complexes were picked after manual assessment and subjected to further simulations with the covalent bond in place. Finally, two covalently linked protein-DNA complexes that differed by their DNA binding modes were picked: The GyrA59 α_4-helix of complex 20 pointed towards the major groove of the DNA while it was oriented towards the minor groove in complex 166. Both complexes provided evidence for a possible role of Arg^{91} for the binding of DNA and the formation of a potential quinolone binding pocket.

Although complex 20 could better reconcile existing biochemical data, both complexes were used as target structures for the molecular docking of eleven quinolones. All dockings showed ring stacking interactions but significantly differed with respect to the drugs' orientations and the resulting interactions with DNA and the α_4-helix. Dockings into complex 20 yielded three sets with different drug poses. The placement of quinolones within complex 166 were much more heterogenous and yielded twelve subsets with different drug orientations. Although some poses were able to explain the influence of known resistance mutations on drug binding, none was able to explain all resistance mutations and the important role of Mg^{2+}.

A recently released crystal structure of *S. pneumoniae* topoIV in complex with DNA and quinolone was used to evaluate the theoretical models. The orientation of the

drugs in the theoretical models could not exactly reproduce the crystal structure, but the results for complex 20 were very close to the experimental data. This showed the applied method to be a very reasonable protocol.

Crystal structures were also taken to derive a CoMSIA model based on cleavage activities. This was subsequently examined on the basis of a homology model built for the *E. coli* gyrase-DNA-quinolone complex. It could be used to explain quinolone effects on steric and electrostatic grounds: Substituents at the quinolones' C7 are favorable if they reach a volume that, in the light of ciprofloxacin, is located around the N4 of the 7-piperazinyl moiety. Moreover, the models indicate that a positive electrostatic potential enhances the drugs' activity if it is placed in the same region. This allows interactions with negative electrostatic potentials of GyrB residues Gln^{465} and Glu^{466}. By contrast, substituents that protrude from this volume lead to steric clash with the same GyrB residues and decrease quinolone activity. Additionally, electron-withdrawing substituents like C6-fluoro or C8-methoxy were found to be beneficial. They decrease the electron-density of the quinolones' ring system and thus increase ring stacking interaction between the therapeutics and the adjacent DNA bases.

Together with the CoMSIA, the results of a conservation analysis of gyrase residues could partly reconcile mutation data and MIC measurements that were generously provided by A. and P. Heisig. Thus, the significant increase of MICs for different quinolones resulting from a GyrA Ser^{83}Asn mutation could be explained. Such exchange pushes the drugs into the disfavored steric region. This induces steric clashes with GyrB Gln^{465} and Glu^{466} of which the former one was found to be variable while the latter one appeared to be conserved. Interestingly, Gln^{465} is most often exchanged to Glu and Asp. Such mutations may strengthen the interaction with amphoteric drugs and increase the susceptibility of gyrase. Nevertheless, some mutations could not be explained by simple protein-drug interactions. From the analyses however one could suggest that Gln^{465} and Glu^{466} of GyrB and the conserved GyrA Arg^{121} which is also close to the bound quinolone, might be useful residues to target with drugs.

Zusammenfassung

Aufgrund zunehmender Resistenzen verlieren Fluorchinolone an Wirksamkeit. Ein Grund dafür sind Mutationen, die zur Veränderung ihrer molekularen Zielstruktur, dem Komplex aus DNA und Gyrase, führen. Aufgrund fehlender Strukturen des vollständigen Holoenzyms, wurde in dieser Arbeit ein 3D-Strukturmodell des Gyrase-DNA-Chinolon Komplexes mit Hilfe von Molecular Modelling Techniken erstellt.
Zunächst wurde ein Protein-DNA Docking Verfahren verwendet, um ausgehend von der 59 kDa Partialstruktur der N-terminalen GyrA Domäne (GyrA59) von *E. coli* und einer 21 bp dsDNA, Protein-DNA Komplexe zu erzeugen. Ausgehend von der Annahme, dass sich die DNA dem Protein in einer geeigneten Weise nähern muss, damit es zur Ausbildung der kovalenten Protein-DNA Verknüpfung kommt, wurden nachfolgend Moleküldynamik (MD) Simulationen der plausibelsten nicht-kovalent gebundenen Protein-DNA Komplexe durchgeführt. Die aussichtsreichsten Kanditen wurden manuell ausgewählt und für weitere MD Simulationen von kovalent verbundenen Komplexen aus GyrA59 und DNA verwendet. Die zwei resultierenden GyrA59-DNA Komplexe unterschieden sich hinsichtlich ihrer DNA Bindungsmodi: Während die GyrA59 α_4-Helix des Komplexes 20 in die große Furche der DNA ragte, zeigte diese Helix in Komplex 166 in die kleine Furche. Beide Komplexe lieferten Hinweise auf eine mögliche Rolle von GyrA Arg^{91} für die Bindung der DNA und die Ausbildung einer potentiellen Chinolon-Bindetasche.
Existierende biochemische Daten ließen sich zwar besser mit Komplex 20 in Einklang bringen. Dennoch wurden beide Komplexe als Zielstrukturen für das Docking von elf Chinolonen verwendet. Alle Ergebnisse zeigten zwar Ring-Stacking Wechselwirkungen mit DNA Basen, unterschieden sich jedoch signifikant hinsichtlich der Chinolon-Orientierungen und der daraus resultierenden Wechselwirkungen mit DNA und Protein. Ein Docking in Komplex 20 lieferte drei verschiedene Posen, während 12 für Komplex 166 gefunden wurden. Obwohl manche Posen eine Erklärung für den Einfluss bekannter Resistenzmutationen ermöglichen, war keine Orientierung in der Lage, alle Resistenzmutationen sowie die wichtige Rolle von Mg^{2+} zu erklären.

Der Vergleich der theroretischen Modelle mit einer kürzlich publizierten Struktur eines TopoIV-DNA-Chinolon Komplexes aus *S. pneumoniae* zeigte zwar, dass die Orientierung der Chinolone in den Kristallstrukturen nicht exakt reproduziert werden konnte. Dennoch lag das Modell für Komplex 20 sehr nah an den experimentellen Strukturen, wodurch gezeigt werden konnte, dass der hier gewählte Ansatz eine geeignete Methode zur Modellierung von Proteinstrukturen darstellt.
Die Kristallstrukturen wurden auch für die Erstellung eines auf Cleavage-Daten basierenden CoMSIA Modells verwendet. Dieses wurde anschließend auf der Basis eines Homologiemodells des *E. coli* Gyrase-DNA-Chinolon Komplexes analysiert und konnte die Chinolon-Aktivität aus sterischer und elektrostatischer Sicht erläutern: Substituenten an C7 zeigen einen positiven Effekt auf die Aktivität wenn sie in ein Volumen ragen, welches bezogen auf Ciprofloxacin, um das N4 der 7-Piperazinyl Gruppe lokalisiert ist. Ein positives elektrostatisches Potential in diesem Bereich verstärkt die Aktivität. Hierdurch werden Interaktionen mit negativen elektrostatischen Potentialen der GyrB Positionen Gln^{465} and Glu^{466} ermöglicht. Ragen C7-Reste über dieses Volumen hinaus, kommt es zu sterischen Problemen mit diesen GyrB Positionen. Zusätzlich bewirken elektronenziehende Reste wie C6-Fluor oder C8-Methoxy eine Verringerung der Elektronendichte im Chinolon-Ringsystem und verstärken dadurch das Stacking mit benachbarten DNA Basen.
Zusammen mit dem CoMSIA-Modell konnte die Analyse der Konservierung von Gyrase teilweise mit Daten aus Selektions- und MHK-Versuchen von A. and P. Heisig in Einklang gebracht werden. So war zum Beispiel der deutliche MHK Anstieg verschiedener Chinolone das Ergebnis einer GyrA Ser^{83}Asn Mutation. Diese drückt die Arzneistoffe in die sterisch ungünstige Region und induziert Konflikte mit der variablen GyrB Gln^{465} und der konservierten Glu^{466} Position. Gln^{465} ist dabei meistens durch Glu oder Asp ersetzt. Solche Austausche könnten die Interaktion mit amphoteren Chinolonen verstärken und deren Wirksamkeit erhöhen. Jedoch konnten nicht alle Mutationen durch Protein-Ligand Wechselwirkungen erklärt werden. Die Analysen zeigen jedoch, dass Gln^{465} und Glu^{466} in GyrB sowie das sich in Chinolon-Nähe befindliche und konservierte GyrA Arg^{121}, interessante Positionen für den Angriff durch neue Arzneistoffen darstellen könnten.

Bibliography

[1] G L Armstrong, L A Conn, and R W Pinner. Trends in infectious disease mortality in the United States during the 20th century. *JAMA*, 281(1):61–6, Jan 1999. 11

[2] W Stille, H-R Brodt, A Groll, and G Just-Nuebling. *Antibiotika-Therapie: Klinik und Praxis der antiinfektioesen Therapie*. Schattauer, Stuttgart, 11., kompl. akt. u. erw. Aufl. edition, 2006. 11, 14

[3] C Walsh. Where will new antibiotics come from? *Nat Rev Microbiol*, 1(1):65–70, Oct 2003. 11, 12

[4] G Lesher, E Froelich, M Gruett, J Bailey, and R Brundage. 1,8-naphtyridine derivatives - a new class of chemotherapeutic agents. *J Med Pharm Chem*, 91:1063–1065, 1962 Sep. 11, 28

[5] G E Zurenko, C W Ford, D K Hutchinson, S J Brickner, and M R Barbachyn. Oxazolidinone antibacterial agents: development of the clinical candidates eperezolid and linezolid. *Expert Opin Investig Drugs*, 6(2):151–8, Feb 1997. 12

[6] U Holzgrabe. Antiobiotika-Entwicklung gestern und heute. *Chemotherapie Journal*, 13(3):142–147, 2004. 12, 15

[7] W E Rose and M J Rybak. Tigecycline: first of a new class of antimicrobial agents. *Pharmacotherapy*, 26(8):1099–110, Aug 2006. 12

[8] S Heinzl. Neue Antibiotika: Bericht von der 45 th ICAAC, Washington, DC, 16. bis 19. Dezember 2005. *Chemotherapie Journal*, 15(2):40–44, 2006. 12

[9] K J Simmons, I Chopra, and C W G Fishwick. Structure-based discovery of antibacterial drugs. *Nat Rev Microbiol*, 8(7):501–10, Jul 2010. 12

[10] E P Abraham and E Chain. An enzyme from bacteria able to destroy penicillin. *Rev Infect Dis*, 10(4):677–8, 1988. 13

[11] W A Goss, W H Deitz, and T M Cook. Mechanism of action of nalidixic acid on Eschrichia coli - II - Inhibition of deoxyribonucleic acid synthesis. *J Bacteriol*, 89:1068–1074, 1965. 13, 31

[12] W A Goss, W H Deitz, and T M Cokk. Mechanism of action of nalidixic acid on Eschrichia coli - I. *J Bacteriol*, 88(4):1112–8, Oct 1964. 13, 31

[13] T M Cook, W A Goss, and W H Deitz. Mechanism of action of nalidixic acid on Escherichia coli - V - Possible Mutagenic Effect. *J Bacteriol*, 91(2):780–783, Feb 1966. 13

[14] T M Cook, W H Deitz, and W A Goss. Mechanism of action of nalidixic acid on Escherichia coli - IV - Effects on the stability of cellular constituents. *J Bacteriol*, 91(2):774–9, Feb 1966. 13

[15] W H Deitz, T M Cook, and W A Goss. Mechanism of action of nalidixic acid on Escherichia coli - III - Conditions required for lethality. *J Bacteriol*, 91(2):768–73, Feb 1966. 13

[16] P Heisig. Mechanismen bakterieller Resistenz gegen Antibiotika. *Arzneimitteltherapie*, Sonderdruck, 1994. 13, 99

[17] C Walsh. *Antibiotics: actions, origins, resistance*. ASM Press, Washington, D.C., 2003. 13

[18] U Schmidt, I Aigner, and A Schavan. DART - Deutsche Antibiotika Resistenz Strategie. *Bundesministerium fuer Gesundheit*, November 2008. 13

[19] T Clarke. Drug companies snub antibiotics as pipeline threatens to run dry. *Nature*, 425(6955):225, Sep 2003. 13

[20] G Klebe. *Wirkstoffdesign - Entwurf und Wirkung von Arzneistoffen*. Spektrum Akademischer Verlag Heidelberg, 2nd edition, 2009. 15, 42, 126

[21] G L Patrick. *An introduction to medicinal chemistry*. Oxford University Press, Oxford, 3rd ed edition, 2005. 15

[22] R Bax, N Mullan, and J Verhoef. The millennium bugs–the need for and development of new antibacterials. *Int J Antimicrob Agents*, 16(1):51–9, Sep 2000. 15

[23] J Cairns. The chromosome of Escherichia coli. *Cold Spring Harb. Symp. Quant. Biol.*, 28:43–46, 1963. 16

[24] J D Watson and F H Crick. Molecular structure of nucleic acids; a structure for deoxyribose nucleic acid. *Nature*, 171(4356):737–738, 1953. 16

[25] J C Wang. Helical repeat of DNA in solution. *Proc Natl Acad Sci U S A*, 76(1):200–3, Jan 1979. 16

[26] D Rhodes and A Klug. Helical periodicity of DNA determined by enzyme digestion. *Nature*, 286(5773):573–8, Aug 1980. 16

[27] R J Reece and A Maxwell. DNA gyrase: structure and function. *Crit Rev Biochem Mol Biol*, 26(3-4):335–375, 1991. 16, 109

[28] F H Crick. Linking numbers and nucleosomes. *Proc Natl Acad Sci U S A*, 73(8):2639–43, Aug 1976. 16

[29] J White. Self-linking and the Gauss integral in higher dimensions. *American Journal of Mathematics*, 91:693–728, 1969. 16

[30] A Schoeffler and J Berger. DNA topoisomerases: harnessing and constraining energy to govern chromosome topology. *Q Rev Biophys*, 41(1):41–101, Feb 2008. 17, 18, 19, 20, 21

[31] J Vinograd, J Lebowitz, R Radloff, R Watson, and P Laipis. The twisted circular form of polyoma viral DNA. *Proc Natl Acad Sci U S A*, 53(5):1104–11, May 1965. 17

[32] F Charbonnier and P Forterre. Comparison of plasmid DNA topology among mesophilic and thermophilic eubacteria and archaebacteria. *J Bacteriol*, 176(5):1251–9, Mar 1994. 17, 27

[33] A Worcel and E Burgi. On the structure of the folded chromosome of Escherichia coli. *J Mol Biol*, 71(2):127–47, Nov 1972. 17, 27

[34] M Gellert. DNA Topoisomerases. *Annual Review of Biochemistry*, 50:879–910, 1981. 17

[35] J C Wang. DNA Topoisomerases. *Annual Review of Biochemistry*, 65(1):635–692, 1996. PMID: 8811192. 17, 18, 19, 20, 27

[36] J C Wang. DNA Topoisomerases. *Annual Review of Biochemistry*, 54(1):665–697, 1985. PMID: 2992360. 17, 19

[37] K Drlica. Control of bacterial DNA supercoiling. *Mol Microbiol*, 6(4):425–33, Feb 1992. 17

[38] L F Liu and J C Wang. Supercoiling of the DNA template during transcription. *Proc Natl Acad Sci U S A*, 84(20):7024–7, Oct 1987. 18

[39] J C Wang. Cellular roles of DNA topoisomerases: a molecular perspective. *Nat Rev Mol Cell Biol*, 3(6):430–40, Jun 2002. 18, 19, 20, 27

[40] J C Wang. *Untangling the double helix: DNA entanglement and the action of the DNA topoisomerases*. Cold Spring Harbor Laboratory Press, Cold Spring Harbor, N.Y., 2009. 19

[41] C J Dorman and C P Corcoran. Bacterial DNA topology and infectious disease. *Nucleic Acids Res*, 37(3):672–8, Feb 2009. 19, 34

[42] J Dale and S Park. *Molecular Genetics of Bacteria*. John Wiley and Sons, 4th edition, 2004. 19

[43] J J Champoux. Proteins that affect DNA conformation. *Annual Review of Biochemistry*, 47:449–479, 1978. 19

[44] K Drlica and J Rouviere-Yaniv. Histonelike proteins of bacteria. *Microbiol Rev*, 51(3):301–19, Sep 1987. 19

[45] D E Pettijohn. Histone-like proteins and bacterial chromosome structure. *J Biol Chem*, 263(26):12793–6, Sep 1988. 19

[46] D Kamashev and J Rouviere-Yaniv. The histone-like protein HU binds specifically to DNA recombination and repair intermediates. *EMBO J*, 19(23):6527–35, Dec 2000. 19

[47] J Rouvière-Yaniv, M Yaniv, and J E Germond. E. coli DNA binding protein HU forms nucleosome-like structure with circular double-stranded DNA. *Cell*, 17(2):265–74, Jun 1979. 19

[48] D Kamashev, A Balandina, A K Mazur, P B Arimondo, and J Rouviere-Yaniv. HU binds and folds single-stranded DNA. *Nucleic Acids Res*, 36(3):1026–36, Feb 2008. 19

[49] M Malik, A Bensaid, J Rouviere-Yaniv, and K Drlica. Histone-like protein HU and bacterial DNA topology: suppression of an HU deficiency by gyrase mutations. *J Mol Biol*, 256(1):66–76, Feb 1996. 19

[50] K N Kreuzer and N R Cozzarelli. Escherichia coli mutants thermosensitive for deoxyribonucleic acid gyrase subunit a: effects on deoxyribonucleic acid replication, transcription, and bacteriophage growth. *J Bacteriol*, 140(2):424–435, 1979. 19

[51] J L Nitiss. Investigating the biological functions of DNA topoisomerases in eukaryotic cells. *Biochim Biophys Acta*, 1400(1-3):63–81, Oct 1998. 19, 30

[52] J Champoux. DNA topoisomerases: structure, function, and mechanism. *Annual Review of Biochemistry*, 70:369–413, 2001. 19, 20, 25

[53] J E Lindsley and J C Wang. On the coupling between ATP usage and DNA transport by yeast DNA topoisomerase II. *J Biol Chem*, 268(11):8096–104, Apr 1993. 19

[54] D S Horowitz and J C Wang. Mapping the active site tyrosine of Escherichia coli DNA gyrase. *J Biol Chem*, 262(11):5339–5344, 1987. 19, 22, 48

[55] J C Wang. DNA topoisomerases: why so many? *J Biol Chem*, 266(11):6659–62, Apr 1991. 20

[56] J C Wang and K Becherer. Cloning of the gene topA encoding for DNA topoisomerase I and the physical mapping of the cysB-topA-trp region of Escherichia coli. *Nucleic Acids Res*, 11(6):1773–90, Mar 1983. 20

[57] B Alberts and F J Stusser. *Mechanistic studies of DNA replication and genetic recombination: proceedings of the 1980 ICN-UCLA Symposia on Mechanistic Studies of DNA and Genetic Recombination held in Keystone, Colorado, March 16-21, 1980*, volume v. 19. Academic Press, New York, 1980. 20

[58] M Trucksis and R E Depew. Identification and localization of a gene that specifies production of Escherichia coli DNA topoisomerase I. *Proc Natl Acad Sci U S A*, 78(4):2164–8, Apr 1981. 20

[59] E Massé and M Drolet. Relaxation of transcription-induced negative supercoiling is an essential function of Escherichia coli DNA topoisomerase I. *J Biol Chem*, 274(23):16654–8, Jun 1999. 20

[60] J Kato, Y Nishimura, R Imamura, H Niki, S Hiraga, and H Suzuki. New topoisomerase essential for chromosome segregation in E. coli. *Cell*, 63(2):393–404, Oct 1990. 21, 23, 25

[61] J G Heddle, T Lu, X Zhao, K Drlica, and A Maxwell. gyrB-225, a mutation of DNA gyrase that compensates for topoisomerase I deficiency: investigation of its low activity and quinolone hypersensitivity. *J Mol Biol*, 309(5):1219–1231, 2001. 21

[62] G J Pruss, S H Manes, and K Drlica. Escherichia coli DNA topoisomerase I mutants: increased supercoiling is corrected by mutations near gyrase genes. *Cell*, 31(1):35–42, Nov 1982. 21

[63] J H Cabral, A P Jackson, C V Smith, N Shikotra, A Maxwell, and R C Liddington. Crystal structure of the breakage-reunion domain of DNA gyrase. *Nature*, 388(6645):903–906, 1997. 22, 48, 99, 102, 103, 104

[64] J M Berger, S J Gamblin, S C Harrison, and J C Wang. Structure and mechanism of DNA topoisomerase II. *Nature*, 379(6562):225–232, 1996. 22, 101, 119

[65] J M Berger, D Fass, J C Wang, and S C Harrison. Structural similarities between topoisomerases that cleave one or both DNA strands. *Proc Natl Acad Sci U S A*, 95(14):7876–7881, 1998. 22

[66] D Strumberg, J L Nitiss, J Dong, J Walker, M C Nicklaus, K W Kohn, J G Heddle, A Maxwell, S Seeber, and Y Pommier. Importance of the fourth alpha-helix within the CAP homology domain of type II topoisomerase for DNA cleavage site recognition and quinolone action. *Antimicrob Agents Chemother*, 46(9):2735–2746, 2002. 22

[67] L Costenaro, J Grossmann, C Ebel, and A Maxwell. Small-angle X-ray scattering reveals the solution structure of the full-length DNA gyrase a subunit. *Structure*, 13(2):287–296, 2005. 22, 23

[68] K D Corbett, R K Shultzaberger, and J M Berger. The C-terminal domain of DNA gyrase A adopts a DNA-bending beta-pinwheel fold. *Proc Natl Acad Sci U S A*, 101(19):7293–7298, 2004. 22

[69] A J Ruthenburg, D M Graybosch, J C Huetsch, and G L Verdine. A superhelical spiral in the Escherichia coli DNA gyrase A C-terminal domain imparts unidirectional supercoiling bias. *J Biol Chem*, 280(28):26177–26184, 2005. 22

[70] J G Heddle and A Maxwell. Quinolone-binding pocket of DNA gyrase: role of GyrB. *Antimicrob Agents Chemother*, 46(6):1805–1815, 2002. 22, 102, 121

[71] L Costenaro, J Grossmann, C Ebel, and A Maxwell. Modular structure of the full-length DNA gyrase B subunit revealed by small-angle X-ray scattering. *Structure*, 15(3):329–339, 2007. 22, 23, 26

[72] D B Wigley, G J Davies, E J Dodson, A Maxwell, and G Dodson. Crystal structure of an N-terminal fragment of the DNA gyrase B protein. *Nature*, 351(6328):624–629, 1991. 22

[73] L Brino, A Urzhumtsev, M Mousli, C Bronner, A Mitschler, P Oudet, and D Moras. Dimerization of Escherichia coli DNA-gyrase B provides a structural mechanism for activating the ATPase catalytic center. *J Biol Chem*, 275(13):9468–9475, 2000. 22

[74] S C Kampranis and A Maxwell. Conformational changes in DNA gyrase revealed by limited proteolysis. *J Biol Chem*, 273(35):22606–22614, 1998. 22

[75] C G Noble and A Maxwell. The role of GyrB in the DNA cleavage-religation reaction of DNA gyrase: a proposed two metal-ion mechanism. *J Mol Biol*, 318(2):361–71, Apr 2002. 22

[76] I Laponogov, D A Veselkov, M K Sohi, X Pan, A Achari, C Yang, J Ferrara, L M Fisher, and M Sanderson. Breakage-Reunion Domain of Streptococcus pneumoniae Topoisomerase IV: Crystal Structure of a Gram-Positive Quinolone Target. *PLoS ONE*, 2:e301, 2007. 22, 23, 53, 103

[77] I Laponogov, M K Sohi, D A Veselkov, X Pan, R Sawhney, A W Thompson, K E McAuley, L M Fisher, and M R Sanderson. Structural insight into the quinolone-DNA cleavage complex of type IIA topoisomerases. *Nat Struct Mol Biol*, May 2009. 22, 23, 53, 82, 90, 113, 114

[78] B H Schmidt, A B Burgin, J E Deweese, N Osheroff, and J M Berger. A novel and unified two-metal mechanism for DNA cleavage by type II and IA topoisomerases. *Nature*, 465(7298):641–4, Jun 2010. 22, 23

[79] A Wohlkonig, P F Chan, A P Fosberry, P Homes, J Huang, M Kranz, V R Leydon, T J Miles, N D Pearson, R L Perera, A J Shillings, M N

Gwynn, and B D Bax. Structural basis of quinolone inhibition of type IIA topoisomerases and target-mediated resistance. *Nat Struct Mol Biol*, 17(9):1152–3, Sep 2010. 22, 23, 133

[80] B D Bax, P F Chan, D S Eggleston, A Fosberry, D R Gentry, F Gorrec, I Giordano, M M Hann, A Hennessy, M Hibbs, J Huang, E Jones, J Jones, K Brown, C J Lewis, E W May, M R Saunders, O Singh, C E Spitzfaden, C Shen, A Shillings, A F Theobald, A Wohlkonig, N D Pearson, and M N Gwynn. Type IIA topoisomerase inhibition by a new class of antibacterial agents. *Nature*, Aug 2010. 22, 23, 120, 133

[81] S T Rao and M G Rossmann. Comparison of super-secondary structures in proteins. *J Mol Biol*, 76(2):241–56, May 1973. 22

[82] L Aravind, D D Leipe, and E V Koonin. Toprim–a conserved catalytic domain in type IA and II topoisomerases, DnaG-type primases, OLD family nucleases and RecR proteins. *Nucleic Acids Res*, 26(18):4205–4213, 1998. 22, 24, 26, 102

[83] A Maxwell, L Costenaro, S Mitelheiser, and A D Bates. Coupling ATP hydrolysis to DNA strand passage in type IIA DNA topoisomerases. *Biochem Soc Trans*, 33(Pt 6):1460–4, Dec 2005. 23

[84] D Lockshon and D R Morris. Sites of reaction of Escherichia coli DNA gyrase on pBR322 in vivo as revealed by oxolinic acid-induced plasmid linearization. *J Mol Biol*, 181(1):63–74, Jan 1985. 23, 47, 48

[85] C G Noble, F M Barnard, and A Maxwell. Quinolone-DNA interaction: sequence-dependent binding to single-stranded DNA reflects the interaction within the gyrase-DNA complex. *Antimicrob Agents Chemother*, 47(3):854–862, 2003. 23, 47, 48, 69, 108

[86] L M Fisher, H A Barot, and M E Cullen. DNA gyrase complex with DNA: determinants for site-specific DNA breakage. *EMBO J*, 5(6):1411–8, Jun 1986. 23, 47, 48

[87] A Sugino, C L Peebles, K N Kreuzer, and N R Cozzarelli. Mechanism of action of nalidixic acid: purification of Escherichia coli nalA gene product and its relationship to DNA gyrase and a novel nicking-closing enzyme. *Proc Natl Acad Sci U S A*, 74(11):4767–4771, 1977. 23, 28, 54

[88] M Gellert, K Mizuuchi, M H O'Dea, T Itoh, and J I Tomizawa. Nalidixic acid resistance: a second genetic character involved in DNA gyrase activity. *Proc Natl Acad Sci U S A*, 74(11):4772–4776, 1977. 23, 28

[89] K Dong and J M Berger. Structural basis for gate-DNA recognition and bending by type IIA topoisomerases. *Nature*, 450(7173):1201–1205, 2007 Dec 20. 23, 113, 120

[90] M K Sohi, D A Veselkov, I Laponogov, X Pan, M Fisher, and M Sanderson. The difficult case of crystallization and structure solution for the ParC55 breakage-reunion domain of topoisomerase IV from Streptococcus pneumoniae. *PLoS ONE*, 3(9):e3201, 2008. 23, 53

[91] P Rezacova, D Borek, S F Moy, A Joachimiak, and Z Otwinowski. Crystal structure and putative function of small Toprim domain-containing protein from Bacillus stearothermophilus. *Proteins*, 70(2):311–319, 2008 Feb 1. 23

[92] H Peng and K J Marians. The interaction of Escherichia coli topoisomerase IV with DNA. *J Biol Chem*, 270(42):25286–90, Oct 1995. 23

[93] B Rost. Twilight zone of protein sequence alignments. *Protein Eng*, 12(2):85–94, 1999. 23, 53

[94] E L Zechiedrich, A B Khodursky, S Bachellier, R Schneider, D Chen, D M Lilley, and N R Cozzarelli. Roles of topoisomerases in maintaining steady-state DNA supercoiling in Escherichia coli. *J Biol Chem*, 275(11):8103–13, Mar 2000. 23, 25

[95] K S Srivenugopal, D Lockshon, and D R Morris. Escherichia coli DNA topoisomerase III: purification and characterization of a new type I enzyme. *Biochemistry*, 23(9):1899–906, Apr 1984. 25

[96] R J DiGate and K J Marians. Molecular cloning and DNA sequence analysis of Escherichia coli topB, the gene encoding topoisomerase III. *J Biol Chem*, 264(30):17924–30, Oct 1989. 25

[97] R J DiGate and K J Marians. Identification of a potent decatenating enzyme from Escherichia coli. *J Biol Chem*, 263(26):13366–73, Sep 1988. 25

[98] P Nurse, C Levine, H Hassing, and K J Marians. Topoisomerase III can serve as the cellular decatenase in Escherichia coli. *J Biol Chem*, 278(10):8653–60, Mar 2003. 25

[99] H Hiasa and K J Marians. Topoisomerase III, but not topoisomerase I, can support nascent chain elongation during theta-type DNA replication. *J Biol Chem*, 269(51):32655–9, Dec 1994. 25

[100] B J Peter, C Ullsperger, H Hiasa, K J Marians, and N R Cozzarelli. The structure of supercoiled intermediates in DNA replication. *Cell*, 94(6):819–27, Sep 1998. 25

[101] M A Schofield, R Agbunag, M L Michaels, and J H Miller. Cloning and sequencing of Escherichia coli mutR shows its identity to topB, encoding topoisomerase III. *J Bacteriol*, 174(15):5168–70, Aug 1992. 25

[102] H Peng and K J Marians. Escherichia coli topoisomerase IV. Purification, characterization, subunit structure, and subunit interactions. *J Biol Chem*, 268(32):24481–90, Nov 1993. 25

[103] E Mossessova, C Levine, H Peng, P Nurse, S Bahng, and K J Marians. Mutational analysis of Escherichia coli topoisomerase IV. I. Selection of dominant-negative parE alleles. *J Biol Chem*, 275(6):4099–103, Feb 2000. 25

[104] P Nurse, S Bahng, E Mossessova, and K J Marians. Mutational analysis of Escherichia coli topoisomerase IV. II. ATPase negative mutants of parE induce hyper-DNA cleavage. *J Biol Chem*, 275(6):4104–11, Feb 2000. 25

[105] S Bahng, E Mossessova, P Nurse, and K J Marians. Mutational analysis of Escherichia coli topoisomerase IV. III. Identification of a region of parE involved in covalent catalysis. *J Biol Chem*, 275(6):4112–7, Feb 2000. 25

[106] E L Zechiedrich and N R Cozzarelli. Roles of topoisomerase IV and DNA gyrase in DNA unlinking during replication in Escherichia coli. *Genes Dev*, 9(22):2859–69, Nov 1995. 25

[107] N J Crisona, T R Strick, D Bensimon, V Croquette, and N R Cozzarelli. Preferential relaxation of positively supercoiled DNA by E. coli topoisomerase IV in single-molecule and ensemble measurements. *Genes Dev*, 14(22):2881–92, Nov 2000. 25, 27

[108] R W Deibler, S Rahmati, and E L Zechiedrich. Topoisomerase IV, alone, unknots DNA in E. coli. *Genes Dev*, 15(6):748–761, 2001 Mar 15. 25

[109] A Luttinger. The twisted 'life' of DNA in the cell: bacterial topoisomerases. *Mol Microbiol*, 15(4):601–6, Feb 1995. 25

[110] R Menzel and M Gellert. Regulation of the genes for E. coli DNA gyrase: homeostatic control of DNA supercoiling. *Cell*, 34(1):105–13, Aug 1983. 27

[111] J Snoep, C van der Weijden, H Andersen, H Westerhoff, and P Jensen. DNA supercoiling in Escherichia coli is under tight and subtle homeostatic control, involving gene-expression and metabolic regulation of both topoisomerase I and DNA gyrase. *Eur J Biochem*, 269(6):1662–9, Mar 2002. 27

[112] S Neumann and A Quinones. Discoordinate gene expression of gyrA and gyrB in response to DNA gyrase inhibition in Escherichia coli. *J Basic Microbiol*, 37(1):53–69, 1997. 27

[113] Y C Tse-Dinh. Regulation of the Escherichia coli DNA topoisomerase I gene by DNA supercoiling. *Nucleic Acids Res*, 13(13):4751–63, Jul 1985. 27

[114] Y C Tse-Dinh and R K Beran. Multiple promoters for transcription of the Escherichia coli DNA topoisomerase I gene and their regulation by DNA supercoiling. *J Mol Biol*, 202(4):735–42, Aug 1988. 27

[115] S Sengupta and V Nagaraja. YacG from Escherichia coli is a specific endogenous inhibitor of DNA gyrase. *Nucleic Acids Res*, 36(13):4310–4316, 2008 Aug. 27

[116] C Li, K uand Pasternak, E Haertig, K Haberzettl, A Maxwell, and G Klug. Thioredoxin can influence gene expression by affecting gyrase activity. *Nucleic Acids Res*, 32(15):4563–75, 2004. 27

[117] S Khrapunov, H Cheng, S Hegde, J Blanchard, and M Brenowitz. Solution structure and refolding of the Mycobacterium tuberculosis pentapeptide repeat protein MfpA. *J Biol Chem*, 283(52):36290–9, Dec 2008. 27

[118] A Nakanishi, T Oshida, T Matsushita, S Imajoh-Ohmi, and T Ohnuki. Identification of DNA gyrase inhibitor (GyrI) in Escherichia coli. *J Biol Chem*, 273(4):1933–1938, 1998. 27

[119] M Chatterji and V Nagaraja. GyrI: a counter-defensive strategy against proteinaceous inhibitors of DNA gyrase. *EMBO Rep*, 3(3):261–7, Mar 2002. 27

[120] M Ashiuchi, E Kuwana, T Yamamoto, K Komatsu, K Soda, and H Misono. Glutamate racemase is an endogenous DNA gyrase inhibitor. *J Biol Chem*, 277(42):39070–3, Oct 2002. 27

[121] S Sengupta, M Shah, and V Nagaraja. Glutamate racemase from Mycobacterium tuberculosis inhibits DNA gyrase by affecting its DNA-binding. *Nucleic Acids Res*, 34(19):5567–76, 2006. 27

[122] S Hegde, M W Vetting, S L Roderick, L A Mitchenall, A Maxwell, H E Takiff, and J S Blanchard. A fluoroquinolone resistance protein from Mycobacterium tuberculosis that mimics DNA. *Science*, 308(5727):1480–3, Jun 2005. 27

[123] C J Dorman, G C Barr, N N Bhriain, and C F Higgins. DNA supercoiling and the anaerobic and growth phase regulation of tonB gene expression. *J Bacteriol*, 170(6):2816–26, Jun 1988. 27, 34

[124] E Goldstein and K Drlica. Regulation of bacterial DNA supercoiling: plasmid linking numbers vary with growth temperature. *Proc Natl Acad Sci U S A*, 81(13):4046–50, Jul 1984. 27

[125] L S Hsieh, R M Burger, and K Drlica. Bacterial DNA supercoiling and [ATP]/[ADP]. Changes associated with a transition to anaerobic growth. *J Mol Biol*, 219(3):443–50, Jun 1991. 27

[126] L S Hsieh, J Rouviere-Yaniv, and K Drlica. Bacterial DNA supercoiling and [ATP]/[ADP] ratio: changes associated with salt shock. *J Bacteriol*, 173(12):3914–7, Jun 1991. 27

[127] V L Balke and J D Gralla. Changes in the linking number of supercoiled DNA accompany growth transitions in Escherichia coli. *J Bacteriol*, 169(10):4499–506, Oct 1987. 27

[128] A Maxwell. The molecular-basis of quinolone action. *Journal of Antimicrobial Chemotherapy*, 30(4):409–414, October 1992. 28

[129] A Y Chen and L F Liu. DNA topoisomerases: essential enzymes and lethal targets. *Annu Rev Pharmacol Toxicol*, 34:191–218, 1994. 28

[130] P B Fernandes, R Menzel, D J Hardy, Y C Tse-Dinh, A Warren, and D A Elsemore. Microbial resistance: novel screens for a contemporary problem. *Med Res Rev*, 19(6):559–68, Nov 1999. 28

[131] M Gellert, M H O'Dea, T Itoh, and J Tomizawa. Novobiocin and coumermycin inhibit DNA supercoiling catalyzed by DNA gyrase. *Proc Natl Acad Sci U S A*, 73(12):4474–8, Dec 1976. 28, 34

[132] N R Cozzarelli. DNA gyrase and the supercoiling of DNA. *Science*, 207(4434):953–60, Feb 1980. 28

[133] A Maxwell. The interaction between coumarin drugs and DNA gyrase. *Mol Microbiol*, 9(4):681–6, Aug 1993. 28

[134] F T Tsai, O M Singh, T Skarzynski, A J Wonacott, S Weston, A Tucker, R A Pauptit, A L Breeze, J P Poyser, R O'Brien, J E Ladbury, and D B Wigley. The high-resolution crystal structure of a 24-kDa gyrase B fragment from E. coli complexed with one of the most potent coumarin inhibitors, clorobiocin. *Proteins*, 28(1):41–52, 1997. 28

[135] S C Kampranis, N A Gormley, R Tranter, G Orphanides, and A Maxwell. Probing the binding of coumarins and cyclothialidines to DNA gyrase. *Biochemistry*, 38(7):1967–1976, 1999. 28

[136] M Cotten, D Bresnahan, S Thompson, L Sealy, and R Chalkley. Novobiocin precipitates histones at concentrations normally used to inhibit eukaryotic type II topoisomerase. *Nucleic Acids Res*, 14(9):3671–86, May 1986. 28

[137] H J Edenberg. Novobiocin inhibition of simian virus 40 DNA replication. *Nature*, 286(5772):529–31, Jul 1980. 28

[138] P Heisig. Inhibitors of bacterial topoisomerases: mechanisms of action and resistance and clinical aspects. *Planta Med*, 67(1):3–12, 2001 Feb. 28, 104

[139] K G Naber and D Adam. Classification of fluoroquinolones. *Int J Antimicrob Agents*, 10(4):255–7, Nov 1998. 29, 30

[140] F Vogel, KG Naber, D Adam, KF Bodmann, C Lebert, A Rodloff, and F Sörgel. Aktuelle Bewertung der Fluorchinolone. *Arzneimitteltherapie*, 23(4):130–136, 2005. 29, 30

[141] J G Zijlstra, S de Jong, E G de Vries, and N H Mulder. Topoisomerases, new targets in cancer chemotherapy. *Med Oncol Tumor Pharmacother*, 7(1):11–8, 1990. 30

[142] J Nitiss. Targeting DNA topoisomerase II in cancer chemotherapy. *Nat Rev Cancer*, 9(5):338–50, May 2009. 30

[143] J Nitiss. DNA topoisomerase II and its growing repertoire of biological functions. *Nat Rev Cancer*, 9(5):327–337, 2009 May. 30

[144] T R Hammonds, S R Foster, and A Maxwell. Increased sensitivity to quinolone antibacterials can be engineered in human topoisomerase IIalpha by selective mutagenesis. *J Mol Biol*, 300(3):481–91, Jul 2000. 30

[145] J R Pohlhaus and K N Kreuzer. Norfloxacin-induced DNA gyrase cleavage complexes block Escherichia coli replication forks, causing double-stranded breaks in vivo. *Mol Microbiol*, 56(6):1416–1429, 2005. 31

[146] K Drlica and X Zhao. DNA gyrase, topoisomerase IV, and the 4-quinolones. *Microbiol Mol Biol Rev*, 61(3):377–392, 1997. 31

[147] K Drlica. Mechanism of fluoroquinolone action. *Curr Opin Microbiol*, 2(5):504–508, 1999 Oct. 31

[148] K Drlica, H Hiasa, R Kerns, M Malik, A Mustaev, and X Zhao. Quinolones: Action and Resistance Updated. *Curr Top Med Chem*, Sep 2009. 31, 84

[149] C J Willmott, S E Critchlow, I C Eperon, and A Maxwell. The complex of DNA gyrase and quinolone drugs with DNA forms a barrier to transcription by RNA polymerase. *J Mol Biol*, 242(4):351–363, 1994. 31

[150] I Phillips, E Culebras, F Moreno, and F Baquero. Induction of the SOS response by new 4-quinolones. *J Antimicrob Chemother*, 20(5):631–8, Nov 1987. 31

[151] A M Chaudhury and G R Smith. Role of Escherichia coli RecBC enzyme in SOS induction. *Mol Gen Genet*, 201(3):525–8, 1985. 31

[152] D G Anderson and S C Kowalczykowski. Reconstitution of an SOS response pathway: derepression of transcription in response to DNA breaks. *Cell*, 95(7):975–9, Dec 1998. 31

[153] J W Little. LexA cleavage and other self-processing reactions. *J Bacteriol*, 175(16):4943–50, Aug 1993. 31

[154] M Schnarr, P Oertel-Buchheit, M Kazmaier, and M Granger-Schnarr. DNA binding properties of the LexA repressor. *Biochimie*, 73(4):423–31, Apr 1991. 31

[155] X Wang, X Zhao, M Malik, and K Drlica. Contribution of reactive oxygen species to pathways of quinolone-mediated bacterial cell death. *J Antimicrob Chemother*, Jan 2010. 31

[156] M Malik, K R Marks, H A Schwanz, N German, K Drlica, and R J Kerns. Effect of N-1/C-8 ring fusion and C-7 ring structure on fluoroquinolone lethality. *Antimicrob Agents Chemother*, Sep 2010. 31, 32, 126

[157] M Malik, X Zhao, and K Drlica. Lethal fragmentation of bacterial chromosomes mediated by DNA gyrase and quinolones. *Mol Microbiol*, 61(3):810–825, 2006. 31

[158] H Ikeda, K Aoki, and A Naito. Illegitimate recombination mediated in vitro by DNA gyrase of Escherichia coli: structure of recombinant DNA molecules. *Proc Natl Acad Sci U S A*, 79(12):3724–8, Jun 1982. 31

[159] H Ikeda, I Kawasaki, and M Gellert. Mechanism of illegitimate recombination: common sites for recombination and cleavage mediated by E. coli DNA gyrase. *Mol Gen Genet*, 196(3):546–9, 1984. 31

[160] B Wiedeman and P Heisig. Bakterielle Resistenz gegenüber Chinolonen (Ciprofloxacin). *Chemotherapie Journal*, 8(3):99–107, 1999. 32, 33, 84, 104

[161] G A Jacoby. Mechanisms of resistance to quinolones. *Clin Infect Dis*, 41 Suppl 2:S120–6, Jul 2005. 32

[162] S K Morgan-Linnell, L Becnel Boyd, D Steffen, and L Zechiedrich. Mechanisms accounting for fluoroquinolone resistance in Escherichia coli clinical isolates. *Antimicrob Agents Chemother*, 53(1):235–41, Jan 2009. 32

[163] M T. Madigan, J M Martinko, and J Parker. *Brock – Biology of Microorganisms*. Prentice Hall/Pearson Education, Upper Saddle River, NJ, 10th edition, 2003. 32

[164] S W Cowan, R M Garavito, J N Jansonius, J A Jenkins, R Karlsson, N König, E F Pai, R A Pauptit, P J Rizkallah, and J P Rosenbusch. The structure of OmpF porin in a tetragonal crystal form. *Structure*, 3(10):1041–50, Oct 1995. 32

[165] D C Hooper, J S Wolfson, K S Souza, E Y Ng, G L McHugh, and M N Swartz. Mechanisms of quinolone resistance in Escherichia coli: characterization of nfxB and cfxB, two mutant resistance loci decreasing norfloxacin accumulation. *Antimicrob Agents Chemother*, 33(3):283–90, Mar 1989. 32

[166] K Hirai, H Aoyama, S Suzue, T Irikura, S Iyobe, and S Mitsuhashi. Isolation and characterization of norfloxacin-resistant mutants of Escherichia coli K-12. *Antimicrob Agents Chemother*, 30(2):248–53, Aug 1986. 32

[167] K Hirai, H Aoyama, T Irikura, S Iyobe, and S Mitsuhashi. Differences in susceptibility to quinolones of outer membrane mutants of Salmonella typhimurium and Escherichia coli. *Antimicrob Agents Chemother*, 29(3):535–8, Mar 1986. 32

[168] S P Cohen, D C Hooper, J S Wolfson, K S Souza, L M McMurry, and S B Levy. Endogenous active efflux of norfloxacin in susceptible Escherichia coli. *Antimicrob Agents Chemother*, 32(8):1187–91, Aug 1988. 32

[169] J Andersen, S A Forst, K Zhao, M Inouye, and N Delihas. The function of micF RNA. micF RNA is a major factor in the thermal regulation of OmpF protein in Escherichia coli. *J Biol Chem*, 264(30):17961–70, Oct 1989. 32

[170] S P Cohen, L M McMurry, D C Hooper, J S Wolfson, and S B Levy. Cross-resistance to fluoroquinolones in multiple-antibiotic-resistant (Mar) Escherichia coli selected by tetracycline or chloramphenicol: decreased drug accumulation associated with membrane changes in addition to OmpF reduction. *Antimicrob Agents Chemother*, 33(8):1318–25, Aug 1989. 32

[171] D C Hooper, J S Wolfson, M A Bozza, and E Y Ng. Genetics and regulation of outer membrane protein expression by quinolone resistance loci nfxB, nfxC, and cfxB. *Antimicrob Agents Chemother*, 36(5):1151–4, May 1992. 32

[172] N Delihas and S Forst. MicF: an antisense RNA gene involved in response of Escherichia coli to

global stress factors. *J Mol Biol*, 313(1):1–12, Oct 2001. 32

[173] D Ma, D N Cook, M Alberti, N G Pon, H Nikaido, and J E Hearst. Genes acrA and acrB encode a stress-induced efflux system of Escherichia coli. *Mol Microbiol*, 16(1):45–55, Apr 1995. 33

[174] H Okusu, D Ma, and H Nikaido. AcrAB efflux pump plays a major role in the antibiotic resistance phenotype of Escherichia coli multiple-antibiotic-resistance (Mar) mutants. *J Bacteriol*, 178(1):306–8, Jan 1996. 33

[175] K Poole. Efflux-mediated resistance to fluoroquinolones in gram-negative bacteria. *Antimicrob Agents Chemother*, 44(9):2233–41, Sep 2000. 33

[176] K Poole. Efflux-mediated resistance to fluoroquinolones in gram-positive bacteria and the mycobacteria. *Antimicrob Agents Chemother*, 44(10):2595–9, Oct 2000. 33

[177] H Nikaido and H I Zgurskaya. AcrAB and related multidrug efflux pumps of Escherichia coli. *J Mol Microbiol Biotechnol*, 3(2):215–8, Apr 2001. 33

[178] L Piddock. Clinically relevant chromosomally encoded multidrug resistance efflux pumps in bacteria. *Clin Microbiol Rev*, 19(2):382–402, Apr 2006. 33

[179] S Grkovic, M H Brown, and R A Skurray. Regulation of bacterial drug export systems. *Microbiol Mol Biol Rev*, 66(4):671–701, table of contents, Dec 2002. 33

[180] T M Barbosa and S B Levy. The impact of antibiotic use on resistance development and persistence. *Drug Resist Updat*, 3(5):303–311, Oct 2000. 33

[181] H Hächler, S P Cohen, and S B Levy. marA, a regulated locus which controls expression of chromosomal multiple antibiotic resistance in Escherichia coli. *J Bacteriol*, 173(17):5532–8, Sep 1991. 33

[182] A Robicsek, J Strahilevitz, G Jacoby, M Macielag, D Abbanat, C Park, K Bush, and D Hooper. Fluoroquinolone-modifying enzyme: a new adaptation of a common aminoglycoside acetyltransferase. *Nat Med*, 12(1):83–88, 2006. 33

[183] J H Tran and G A Jacoby. Mechanism of plasmid-mediated quinolone resistance. *Proc Natl Acad Sci U S A*, 99(8):5638–42, Apr 2002. 33

[184] G A Jacoby, K E Walsh, D M Mills, V J Walker, H Oh, A Robicsek, and D C Hooper. qnrB, another plasmid-mediated gene for quinolone resistance. *Antimicrob Agents Chemother*, 50(4):1178–82, Apr 2006. 33

[185] J Tran, G Jacoby, and D Hooper. Interaction of the plasmid-encoded quinolone resistance protein Qnr with Escherichia coli DNA gyrase. *Antimicrob Agents Chemother*, 49(1):118–25, Jan 2005. 33

[186] L Poirel, T Vu Nguyen, A Weintraub, C Leviandier, and P Nordmann. Plasmid-mediated quinolone resistance determinant qnrS in Enterobacter cloacae. *Clin Microbiol Infect*, 12(10):1021–3, Oct 2006. 33

[187] J Strahilevitz, G A Jacoby, D C Hooper, and A Robicsek. Plasmid-mediated quinolone resistance: a multifaceted threat. *Clin Microbiol Rev*, 22(4):664–89, Oct 2009. 33

[188] L Martínez-Martínez, A Pascual, I García, J Tran, and G A Jacoby. Interaction of plasmid and host quinolone resistance. *J Antimicrob Chemother*, 51(4):1037–9, Apr 2003. 33

[189] P Heisig. Mechanismen und Epidemiologie hoher Fluorchinolonresistenz bei Escherichia coli und anderen Gram-negativen Bakterien, 1997. 33

[190] H Yoshida, M Bogaki, M Nakamura, and S Nakamura. Quinolone resistance-determining region in the DNA gyrase gyrA gene of Escherichia coli. *Antimicrob Agents Chemother*, 34(6):1271–1272, 1990. 33, 35, 119, 124

[191] H Yoshida, T Kojima, J Yamagishi, and S Nakamura. Quinolone-resistant mutations of the gyrA gene of Escherichia coli. *Mol Gen Genet*, 211(1):1–7, 1988. 33, 48

[192] H Yoshida, M Bogaki, M Nakamura, L M Yamanaka, and S Nakamura. Quinolone resistance-determining region in the DNA gyrase gyrB gene of Escherichia coli. *Antimicrob Agents Chemother*, 35(8):1647–1650, 1991. 33, 121

[193] Q C Truong, J C Nguyen Van, D Shlaes, L Gutmann, and N J Moreau. A novel, double mutation in DNA gyrase A of Escherichia coli conferring resistance to quinolone antibiotics. *Antimicrob Agents Chemother*, 41(1):85–90, Jan 1997. 33, 107, 120

[194] P Heisig. Genetic evidence for a role of parC mutations in development of high-level fluoroquinolone resistance in Escherichia coli. *Antimicrob Agents Chemother*, 40(4):879–885, 1996. 33, 34, 99, 123

[195] I Guillemin, V Jarlier, and E Cambau. Correlation between quinolone susceptibility patterns and sequences in the A and B subunits of DNA gyrase in mycobacteria. *Antimicrob Agents Chemother*, 42(8):2084–8, Aug 1998. 33

[196] L M Weigel, G J Anderson, and F C Tenover. DNA gyrase and topoisomerase IV mutations associated with fluoroquinolone resistance in Proteus mirabilis. *Antimicrob Agents Chemother*, 46(8):2582–7, Aug 2002. 33, 120

[197] A B Khodursky, E L Zechiedrich, and N R Cozzarelli. Topoisomerase iv is a target of quinolones in escherichia coli. *Proc Natl Acad Sci U S A*, 92(25):11801–5, Dec 1995. 33

[198] S Bagel, V Hullen, B Wiedemann, and P Heisig. Impact of gyrA and parC mutations on quinolone resistance, doubling time, and supercoiling degree of Escherichia coli. *Antimicrob Agents Chemother*, 43(4):868–875, 1999. 34, 88

[199] P Heisig and R Tschorny. Characterization of fluoroquinolone-resistant mutants of Escherichia coli selected in vitro. *Antimicrob Agents Chemother*, 38(6):1284–1291, 1994 Jun. 34, 88, 123

[200] J Vila, J Ruiz, F Marco, A Barcelo, P Goñi, E Giralt, and T Jimenez de Anta. Association between double mutation in gyrA gene of ciprofloxacin-resistant clinical isolates of Escherichia coli and MICs. *Antimicrob Agents Chemother*, 38(10):2477–9, Oct 1994. 34

[201] X S Pan and L M Fisher. Targeting of DNA gyrase in Streptococcus pneumoniae by sparfloxacin: selective targeting of gyrase or topoisomerase IV by quinolones. *Antimicrob Agents Chemother*, 41(2):471–4, Feb 1997. 34

[202] X S Pan and L M Fisher. DNA gyrase and topoisomerase IV are dual targets of clinafloxacin action in Streptococcus pneumoniae. *Antimicrob Agents Chemother*, 42(11):2810–6, Nov 1998. 34

[203] X S Pan and L M Fisher. Streptococcus pneumoniae DNA gyrase and topoisomerase IV: overexpression, purification, and differential inhibition by fluoroquinolones. *Antimicrob Agents Chemother*, 43(5):1129–36, May 1999. 34

[204] V Aleixandre, G Herrera, A Urios, and M Blanco. Effects of ciprofloxacin on plasmid DNA supercoiling of Escherichia coli topoisomerase I and gyrase mutants. *Antimicrob Agents Chemother*, 35(1):20–3, Jan 1991. 34

[205] P Heisig, H Schedletzky, and H Falkenstein-Paul. Mutations in the gyrA gene of a highly fluoroquinolone-resistant clinical isolate of Escherichia coli. *Antimicrob Agents Chemother*, 37(4):696–701, 1993 Apr. 34, 88, 109, 123

[206] C J Dorman. DNA topology and the global control of bacterial gene expression: implications for the regulation of virulence gene expression. *Microbiology*, 141 (Pt 6):1271–80, Jun 1995. 34

[207] C J Willmott and A Maxwell. A single point mutation in the DNA gyrase A protein greatly reduces binding of fluoroquinolones to the gyrase-DNA complex. *Antimicrob Agents Chemother*, 37(1):126–127, 1993. 35

[208] E Fischer. Einfluss der Konfiguration auf die Wirkung der Enzyme. *Berichte der Deutschen Chemischen Gesellschaft*, 3(27):2985–2993, 1894. 37

[209] D Schneidmann-Duhovny, R Nussinov, and H J Wolfson. Efficient unbound docking of rigid molecules. In Gusfield, editor, *Proceedings of the 2'nd Workshop on Algorithms in Bioinformatics (WABI), Rome, Italy*, pages 185–200. Springer Verlag, 2002. 38, 45, 48, 59

[210] A Leach. *Molecular Modelling - Principles and Applications*. Pearson Prentice Hall, 2nd edition, 2001. 39, 40, 52, 54, 103

[211] D Frenkel and B Smit. *Understanding molecular simulation: from algorithms to applications*, volume 1 of *Computational science series*. Academic Press, San Diego, 2nd ed edition, 2002. 39, 103

[212] A Hinchliffe. *Molecular modelling for beginners*. Wiley, Chichester, West Sussex, England, 2003. 39

[213] D Van Der Spoel, E Lindahl, B Hess, G Groenhof, A E Mark, and H J C Berendsen. GROMACS: fast, flexible, and free. *J Comput Chem*, 26(16):1701–1718, 2005. 39, 45, 49, 103

[214] D Van Der Spoel, B Hess, and E Lindahl. *GROMACS- Groningen Machine for Chemical Simulations - user manual*. The GROMACS development team, version 3.3 edition. 39, 41, 45, 52, 103

[215] D Van Der Spoel, B Hess, and E Lindahl. *GROMACS user manual - Groningen Machine for Chemical Simulations*. The GROMACS development team, version 3.2 edition. 39, 103

[216] H Kubinyi. QSAR and 3D QSAR in drug design - Part 2: applications and problems. *Drug Discovery Today*, 2(12):538–546, December 1997. 42

[217] H Kubinyi. QSAR and 3D QSAR in drug design - Part 1: methodology. *Drug Discovery Today*, 2(11):457–467, November 1997. 42

[218] H Kubinyi, G Folkers, and Y Martin. *3D QSAR in drug design*, volume v. 2 of *QDSAR*. Kluwer Academic, Dordrecht, 1998. 42

[219] G Klebe, U Abraham, and T Mietzner. Molecular similarity indices in a comparative analysis (comsia) of drug molecules to correlate and predict their biological activity. *J Med Chem*, 37(24):4130–46, Nov 1994. 42

[220] M Böhm, J Stuerzebecher, and G Klebe. Three-dimensional quantitative structure-activity relationship analyses using comparative molecular field analysis and comparative molecular similarity indices analysis to elucidate selectivity differences of inhibitors binding to trypsin, thrombin, and factor Xa. *J Med Chem*, 42(3):458–77, Feb 1999. 42

[221] G Schüürmann, R Ebert, J Chen, and R Kühne. External validation and prediction employing the predictive squared correlation coefficient test set activity mean vs training set activity mean. *J Chem Inf Model*, 48(11):2140–5, Nov 2008. 43

[222] V Consonni, D Ballabio, and R Todeschini. Comments on the definition of the Q2 parameter for QSAR validation. *J Chem Inf Model*, 49(7):1669–78, Jul 2009. 43

[223] G S Couch, D K Hendrix, and T E Ferrin. Nucleic acid visualization with UCSF Chimera. *Nucleic Acids Res*, 34(4):e29, 2006. 45, 58, 69

[224] E Meng, E Pettersen, G Couch, C Huang, and T Ferrin. Tools for integrated sequence-structure analysis with ucsf chimera. *BMC Bioinformatics*, 7:339, 2006. 45, 69, 113

[225] E Pettersen, T Goddard, C Huang, G Couch, D Greenblatt, E Meng, and T Ferrin. UCSF Chimera–a visualization system for exploratory research and analysis. *J Comput Chem*, 25(13):1605–1612, 2004. 45, 69

[226] The New Tripos. SYBYL-X. 45, 54

[227] The New Tripos. SYBYL 8. 45, 54, 130

[228] Tripos International. Sybyl 7.7. 45, 47

[229] D Schneidmann-Duhovny, Y Inbar, H Benyamini, R Nussinov, and H J Wolfson. Taking geometry to its edge: fast unbound rigid (and hinge-bent) docking. *Proteins*, 52(1):107–112, 2003. 45, 48

[230] D Schneidman-Duhovny, Y Inbar, R Nussinov, and H J Wolfson. PatchDock and SymmDock: servers for rigid and symmetric docking. *Nucleic Acids Res*, 33(Web Server issue):W363–7, 2005. 45, 48

[231] M Shatsky, O Dror, D Schneidman-Duhovny, R Nussinov, and H J Wolfson. BioInfo3D: a suite of tools for structural bioinformatics. *Nucleic Acids Res*, 32(Web Server issue):W503–7, 2004. 45

[232] G M Morris, R Huey, W Lindstrom, M F Sanner, R K Belew, D S Goodsell, and A J Olson. AutoDock4 and AutoDockTools4: Automated docking with selective receptor flexibility. *J Comput Chem*, 30(16):2785–91, Dec 2009. 45, 49, 72

[233] R Huey, G Morris, A Olson, and D Goodsell. A semiempirical free energy force field with charge-based desolvation. *J Comput Chem*, 28(6):1145–1152, 2007. 45, 49

[234] W.L. DeLano. The PyMOL Molecular Graphics System. Technical report, DeLano Scientific LLC, Palo Alto, CA, USA. http://www.pymol.org, 2008. 45

[235] N A Baker, D Sept, S Joseph, M J Holst, and J A McCammon. Electrostatics of nanosystems: application to microtubules and the ribosome. *Proc Natl Acad Sci U S A*, 98(18):10037–10041, 2001 Aug 28. 45

[236] L Bordoli, F Kiefer, K Arnold, P Benkert, J Battey, and T Schwede. Protein structure homology modeling using SWISS-MODEL workspace. *Nat Protoc*, 4(1):1–13, 2009. 45, 53

[237] F Kiefer, K Arnold, M Kuenzli, L Bordoli, and T Schwede. The SWISS-MODEL Repository and associated resources. *Nucleic Acids Res*, 37(Database issue):D387–92, Jan 2009. 45, 53

[238] K Arnold, L Bordoli, J Kopp, and T Schwede. The SWISS-MODEL workspace: a web-based environment for protein structure homology modelling. *Bioinformatics*, 22(2):195–201, Jan 2006. 45, 53

[239] M J Frisch, G W Trucks, H B Schlegel, G E Scuseria, M A Robb, J R Cheeseman, J A Montgomery, Jr., T Vreven, K N Kudin, J C Burant, J M Millam, S S Iyengar, J Tomasi, V Barone, B Mennucci, M Cossi, G Scalmani, N Rega, G A Petersson, H Nakatsuji, M Hada, M Ehara, K Toyota, R Fukuda, J Hasegawa, M Ishida, T Nakajima, Y Honda, O Kitao, H Nakai, M Klene, X Li, J E Knox, H P Hratchian, J B Cross, V Bakken, C Adamo, J Jaramillo, R Gomperts, R E Stratmann, O Yazyev, A J Austin, R Cammi, C Pomelli, J W Ochterski, P Y Ayala, K Morokuma, G A Voth, P Salvador, J J Dannenberg, V G Zakrzewski, S Dapprich, A D Daniels, M C Strain, O Farkas, D K Malick, A D Rabuck, K Raghavachari, J B Foresman, J V Ortiz, Q Cui, A G Baboul, S Clifford, J Cioslowski, B B Stefanov, G Liu, A Liashenko, P Piskorz, I Komaromi, R L Martin, D J Fox, T Keith, M A Al-Laham, C Y Peng, A Nanayakkara, M Challacombe, P M W Gill, B Johnson, W Chen, M W Wong, C Gonzalez, and J A Pople. Gaussian 03, revision e.01. Gaussian, Inc., Wallingford, CT, 2004. 45, 52

[240] J J Stewart. MOPAC: a semiempirical molecular orbital program. *J Comput Aided Mol Des*, 4(1):1–105, Mar 1990. 45, 54

[241] T S Rush, 3rd, J A Grant, L Mosyak, and A Nicholls. A shape-based 3-D scaffold hopping method and its application to a bacterial protein-protein interaction. *J Med Chem*, 48(5):1489–95, Mar 2005. 45, 55

[242] P C D Hawkins, A G Skillman, and A Nicholls. Comparison of shape-matching and docking as virtual screening tools. *J Med Chem*, 50(1):74–82, Jan 2007. 45, 55

[243] Y Inbar, H Benyamini, R Nussinov, and H Wolfson. Prediction of multimolecular assemblies by multiple docking. *J Mol Biol*, 349(2):435–447, 2005. 48

[244] G M Morris, D S Goodsell, R Huey, W Hart, R Belew, and A J Olson. Automated Docking Using a Lamarckian Genetic Algorithm and an Empirical Binding Free Energy Function. *J Comput Chem*, 19:1639–1662, 1998. 49

[245] G M Morris, D S Goodsell, and A J Olson. *AutoDock - Automated Docking of Flexible Ligands into Receptors*. The Scripps Research Institute, Molecular Graphics Laboratory, Department of Molecular Biology, Mail Drop MB-5, 10550 North Torrey Pines Road, La Jolla, CA 92037-1000, U.S.A., 3.0.5 edition, November 2001. 49

[246] D S Goodsell, G M Morris, and A J Olson. Automated docking of flexible ligands: applications of AutoDock. *J Mol Recognit*, 9(1):1–5, 1996. 49

[247] G M Morris, D S Goodsell, R Huey, and A J Olson. Distributed automated docking of flexible ligands to proteins: parallel applications of AutoDock 2.4. *J Comput Aided Mol Des*, 10(4):293–304, 1996. 49

[248] K Onodera, K Satou, and H Hirota. Evaluations of molecular docking programs for virtual screening. *J Chem Inf Model*, 47(4):1609–1618, 2007. 49

[249] F M Barnard and A Maxwell. Interaction between DNA gyrase and quinolones: effects of alanine mutations at GyrA subunit residues Ser(83) and Asp(87). *Antimicrob Agents Chemother*, 45(7):1994–2000, 2001. 50, 119, 124

[250] E J Sorin and V S Pande. Exploring the helix-coil transition via all-atom equilibrium ensemble simulations. *Biophys J*, 88(4):2472–2493, 2005. 49

[251] HJC Berendsen, JPM Postma, W F Van Gunsteren, A Dinola, and JR Haak. Molecular dynamics with coupling to an external bath. *Journal of Chemical Physics*, 81(8):3684–3690, 1984. 49

[252] W Jorgensen, J Chandrasekhar, JD Madura, RW Impey, and ML Klein. Comparison of simple potential functions for simulating liquid water. *Journal of Chemical Physics*, 79(2):926–935, 1983. 49

[253] U Essmann, L Perera, ML Berkowitz, T Darden, H Lee, and LG Pedersen. A smooth Particle Mesh Ewald method. *Journal of Chemical Physics*, 103(19):8577–8593, November 1995. 51

[254] T Darden, D York, and L Pedersen. Particle Mesh Ewald - an N log(N) method for Ewald sums in large systems, June 1993. Journal of Chemical Physics. 51

[255] B Hess, H Bekker, HJC Berendsen, and JGEM Fraaije. LINCS: A linear constraint solver for molecular simulations. *Journal of Computational Chemistry*, 18(12):1463–1472, SEP 1997. 51

[256] S H Vosko, L Wilk, and M Nusair. Accurate spin-dependent electron liquid correlation energies for local spin density calculations: a critical analysis. *Canadian Journal of Physics*, 58(8):1200–1211, 1980. 52

[257] C Lee, W Yang, and RG Parr. Development of the colle-salvetti correlation-energy formula into a functional of the electron density. *Phys Rev B Condens Matter*, 37(2):785–789, 1988 Jan 15. 52

[258] A D Becke. Density-functional thermochemistry. III. The role of exact exchange. *Journal of Chemical Physics*, 98:5648–5652, 1993. 52

[259] P J Stephens, F J Devlin, C F Chabalowski, and M J Frisch. Ab Initio Calculation of Vibrational Absorption and Circular Dichroism Spectra Using Density Functional Force Fields. *Journal of Physical Chemistry*, 98(45):11623–11627, 1994. 52

[260] I Laponogov, X Pan, D A Veselkov, K E McAuley, L M Fisher, and M R Sanderson. Structural basis of gate-DNA breakage and resealing by type II topoisomerases. *PLoS One*, 5(6):e11338, 2010. 53, 82, 90, 113, 114, 120

[261] C Sander and R Schneider. Database of homology-derived protein structures and the structural meaning of sequence alignment. *Proteins*, 9(1):56–68, 1991. 53

[262] L A Mirny and E I Shakhnovich. Universally conserved positions in protein folds: reading evolutionary signals about stability, folding kinetics and function. *J Mol Biol*, 291(1):177–96, Aug 1999. 53, 118

[263] S F Altschul, T L Madden, A A Schäffer, J Zhang, Z Zhang, W Miller, and D J Lipman. Gapped

BLAST and PSI-BLAST: a new generation of protein database search programs. *Nucleic Acids Res*, 25(17):3389–402, Sep 1997. 53

[264] H M Berman, J Westbrook, Z Feng, G Gilliland, T N Bhat, H Weissig, I N Shindyalov, and P E Bourne. The protein data bank. *Nucleic Acids Res*, 28(1):235–242, 2000. 53

[265] A Bairoch and R Apweiler. The SWISS-PROT protein sequence database and its supplement TrEMBL in 2000. *Nucleic Acids Res*, 28(1):45–8, Jan 2000. 53

[266] W C Barker, J S Garavelli, P B McGarvey, C R Marzec, B C Orcutt, G Y Srinivasarao, L S Yeh, R S Ledley, H W Mewes, F Pfeiffer, A Tsugita, and C Wu. The PIR-International Protein Sequence Database. *Nucleic Acids Res*, 27(1):39–43, Jan 1999. 53

[267] J M Domagala, L D Hanna, C L Heifetz, M P Hutt, T F Mich, J P Sanchez, and M Solomon. New structure-activity relationships of the quinolone antibacterials using the target enzyme. The development and application of a DNA gyrase assay. *J Med Chem*, 29(3):394–404, Mar 1986. 54, 175, 176, 177, 178, 179

[268] L M Fisher and X Pan. Methods to assay inhibitors of DNA gyrase and topoisomerase IV activities. *Methods Mol Med*, 142:11–23, 2008. 54

[269] A W Schuttelkopf and D M van Aalten. PRODRG: a tool for high-throughput crystallography of protein-ligand complexes. *Acta Crystallogr D Biol Crystallogr*, 60(Pt 8):1355–1363, 2004. 54

[270] D M van Aalten, R Bywater, J B Findlay, M Hendlich, R W Hooft, and G Vriend. PRODRG, a program for generating molecular topologies and unique molecular descriptors from coordinates of small molecules. *J Comput Aided Mol Des*, 10(3):255–262, 1996. 54

[271] M Clark, RD Cramer, and N Van Opdenbosch. Validation of the general-purpose Tripos 5.2 force-field. *Journal of Computational Chemistry*, 10(8):982–1012, December 1989. 54

[272] K Kowalski. On the Predictive Performance of Biased Regression Methods and Multiple Linear Regression. *Chemometrics and Intelligent Laboratory Systems*, 9:177–184, 1990. 55

[273] B L Bush and R B Nachbar, Jr. Sample-distance partial least squares: PLS optimized for many variables, with application to CoMFA. *J Comput Aided Mol Des*, 7(5):587–619, Oct 1993. 55

[274] S Wold, E Johannson, and M Cocchi. *PLS - Partial Least-squares Projection to Latent Structures*. Kluwer ESCOM, 1993. 55

[275] E da Cunha, W Sippl, T de Castro Ramalho, O Ceva Antunes, R de Alencastro, and M Albuquerque. 3D-QSAR CoMFA/CoMSIA models based on theoretical active conformers of HOE/BAY-793 analogs derived from HIV-1 protease inhibitor complexes. *Eur J Med Chem*, 44(11):4344–52, Nov 2009. 55

[276] S E Critchlow and A Maxwell. DNA cleavage is not required for the binding of quinolone drugs to the DNA gyrase-DNA complex. *Biochemistry*, 35(23):7387–7393, 1996. 69

[277] M Palumbo, B Gatto, G Zagotto, and G Palu. On the mechanism of action of quinolone drugs. *Trends Microbiol*, 1(6):232–235, 1993. 69, 109

[278] B Llorente, F Leclerc, and R Cedergren. Using SAR and QSAR analysis to model the activity and structure of the quinolone-DNA complex. *Bioorg Med Chem*, 4(1):61–71, 1996. 69, 126

[279] K Siegmund, S Maheshwary, S Narayanan, W Connors, M Riedrich, M Printz, and C Richert. Molecular details of quinolone-DNA interactions: solution structure of an unusually stable DNA duplex with covalently linked nalidixic acid residues and non-covalent complexes derived from it. *Nucleic Acids Res*, 33(15):4838–4848, 2005. 69

[280] C A Hunter, J Singh, and J M Thornton. Pi-pi interactions: the geometry and energetics of phenylalanine-phenylalanine interactions in proteins. *J Mol Biol*, 218(4):837–46, Apr 1991. 69

[281] E J Lee, J A Yeo, C B Cho, G J Lee, S W Han, and S K Kim. Amine group of guanine enhances the binding of norfloxacin antibiotics to DNA. *Eur J Biochem*, 267(19):6018–24, Oct 2000. 69

[282] T Skauge, I Turel, and E Sletten. Interaction between ciprofloxacin and DNA mediated by Mg2+-ions. *Inorganica Chimica Acta*, 339:239–247, 2002. 69

[283] PA Holt, JB Chaires, and JO Trent. Molecular docking of intercalators and groove-binders to nucleic acids using autodock and surflex. *J Chem Inf Model*, 2008. 69

[284] A Lauria, A Montalbano, P Barraja, G Dattolo, and A M Almerico. DNA minor groove binders: an overview on molecular modeling and QSAR approaches. *Curr Med Chem*, 14(20):2136–60, 2007. 69

[285] J E Mills and P M Dean. Three-dimensional hydrogen-bond geometry and probability information from a crystal survey. *J Comput Aided Mol Des*, 10(6):607–622, 1996. 69

[286] E Meng. personal communication. USCF Chimera Development Team. 69

[287] T A Larsen, D S Goodsell, D Cascio, K Grzeskowiak, and R E Dickerson. The structure of DAPI bound to DNA. *J Biomol Struct Dyn*, 7(3):477–91, Dec 1989. 78, 108

[288] D Goodsell and R E Dickerson. Isohelical analysis of DNA groove-binding drugs. *J Med Chem*, 29(5):727–33, May 1986. 78

[289] E Trotta and M Paci. Solution structure of DAPI selectively bound in the minor groove of a DNA T.T mismatch-containing site: NMR and molecular dynamics studies. *Nucleic Acids Res*, 26(20):4706–13, Oct 1998. 78, 108

[290] G R Clark, E J Gray, S Neidle, Y H Li, and W Leupin. Isohelicity and phasing in drug–DNA sequence recognition: crystal structure of a tris(benzimidazole)–oligonucleotide complex. *Biochemistry*, 35(43):13745–52, Oct 1996. 78

[291] A Heisig and P Heisig. personal communication. University of Hamburg, School of Pharmacy, Dept. Pharmaceutical Biology and Microbiology. 88

[292] M E Cullen, A W Wyke, R Kuroda, and L M Fisher. Cloning and characterization of a DNA gyrase A gene from Escherichia coli that confers clinical resistance to 4-quinolones. *Antimicrob Agents Chemother*, 33(6):886–94, Jun 1989. 99, 123

[293] M Oram and L M Fisher. 4-Quinolone resistance mutations in the DNA gyrase of Escherichia coli clinical isolates identified by using the polymerase chain reaction. *Antimicrob Agents Chemother*, 35(2):387–9, Feb 1991. 99, 123

[294] K Nadassy, S J Wodak, and J Janin. Structural features of protein-nucleic acid recognition sites. *Biochemistry*, 38(7):1999–2017, Feb 1999. 101

[295] D Lejeune, N Delsaux, B Charloteaux, A Thomas, and R Brasseur. Protein-nucleic acid recognition: statistical analysis of atomic interactions and influence of DNA structure. *Proteins*, 61(2):258–71, Nov 2005. 101

[296] R W Zwanzig. High-Temperature Equation of State by a Perturbation Method: I Nonpolar Gases. *J. Chem Phys.*, 22(8):1420, 1954. 104

[297] G Palu, S Valisena, G Ciarrocchi, B Gatto, and M Palumbo. Quinolone binding to DNA is mediated by magnesium ions. *Proc Natl Acad Sci U S A*, 89(20):9671–9675, 1992. 108

[298] S Madurga, J Sanchez-Cespedes, I Belda, J Vila, and E Giralt. Mechanism of Binding of Fluoroquinolones to the Quinolone Resistance-Determining Region of DNA Gyrase: Towards an Understanding of the Molecular Basis of Quinolone Resistance. *Chembiochem*, 9(13):2081–2086, 2008 Aug 1. 110

[299] J Berg, J Tymoczko, and L Stryer. *Biochemistry*. W.H. Freeman, New York, 6th ed edition, 2007. 118

[300] W S J Valdar. Scoring residue conservation. *Proteins*, 48(2):227–41, Aug 2002. 118

[301] S C Hockings and A Maxwell. Identification of four GyrA residues involved in the DNA breakage-reunion reaction of DNA gyrase. *J Mol Biol*, 318(2):351–9, Apr 2002. 118, 120

[302] R Rohs, S M West, A Sosinsky, P Liu, R S Mann, and B Honig. The role of DNA shape in protein-DNA recognition. *Nature*, 461(7268):1248–53, Oct 2009. 119

[303] I Guillemin, V Jarlier, and E Cambau. Correlation between quinolone susceptibility patterns and sequences in the A and B subunits of DNA gyrase in mycobacteria. *Antimicrob Agents Chemother*, 42(8):2084–2088, 1998. 120

[304] N Moniot-Ville, J Guibert, N Moreau, J F Acar, E Collatz, and L Gutmann. Mechanisms of quinolone resistance in a clinical isolate of Escherichia coli highly resistant to fluoroquinolones but susceptible to nalidixic acid. *Antimicrob Agents Chemother*, 35(3):519–23, Mar 1991. 120

[305] D J Sherratt and D B Wigley. Conserved themes but novel activities in recombinases and topoisomerases. *Cell*, 93(2):149–52, Apr 1998. 120

[306] B Llorente, N Rivero, R Carrasco, RS Martinez, and E Estrada. A QSAR study of quinolones based on electrotopological state index for atoms. *Quantitative Structure-Activity Relationships*, 13(4):419–425, December 1994. 126

[307] H-D Hoeltje, W Sippel, D Rognan, and G Folkers. *Molecular modeling: basic principles and applications*, volume 3. Wiley-VCH, Weinheim, 2008. 127

[308] F Lottspeich and H Zorbas. *Bioanalytik*. Spektrum Akademischer Verlag Heidelberg, 1st edition, 1998. 131

[309] A C Anderson. The process of structure-based drug design. *Chem Biol*, 10(9):787–97, Sep 2003. 133

[310] J J Irwin and B K Shoichet. ZINC–a free database of commercially available compounds for virtual screening. *J Chem Inf Model*, 45(1):177–82, 2005. 133

[311] J Barker. Antibacterial drug discovery and structure-based design. *Drug Discov Today*, 11(9-10):391–404, May 2006. 133

[312] J Schlosser and M Rarey. Beyond the virtual screening paradigm: structure-based searching for new lead compounds. *J Chem Inf Model*, 49(4):800–9, Apr 2009. 133

[313] *Protein Data Bank - Atomic coordinate and bibliography entry format description*, 1992. 167, 171

Appendix A

Example AutoDock4 docking parameter file

parameter	value	comment
Autodock_parameter_version	4.2	# used by AutoDock to validate parameter set
outlev	1	# diagnostic output level
intelec		# calculate internal electrostatics
seed	pid time	# seeds for random generator
ligand_types	A C F OA N HD	# atom types in ligand
fld	comp20_rigid.maps.fld	# grid_data_file
map	comp20_rigid.A.map	# atom-specific affinity map
map	comp20_rigid.C.map	# atom-specific affinity map
map	comp20_rigid.F.map	# atom-specific affinity map

continued on next page

parameter	value	comment
map	comp20_rigid.OA.map	# atom-specific affinity map
map	comp20_rigid.N.map	# atom-specific affinity map
map	comp20_rigid.HD.map	# atom-specific affinity map
elecmap	comp20_rigid.e.map	# electrostatics map
desolvmap	comp20_rigid.d.map	# desolvation map
move	ciprofloxacin_from_g03.pdbqt	# small molecule
flexres	comp20_flex.pdbqt	# file containing flexible residues
about	-0.3385 0.0188 0.0015	# small molecule center
tran0	random	# initial coordinates/Åor random
axisangle0	random	# initial orientation
dihe0	random	# initial dihedrals (relative) or random
tstep	2.0	# translation step/Å
qstep	50.0	# quaternion step/deg
dstep	50.0	# torsion step/deg
torsdof	3	# torsional degrees of freedom
rmstol	2.0	# cluster_tolerance/Å
extnrg	1000.0	# external grid energy
e0max	0.0 10000	# max initial energy; max number of
		# retries
ga_pop_size	300	# number of individuals in population
ga_num_evals	25000000	# maximum number of energy evaluations
ga_num_generations	27000	# maximum number of generations
ga_elitism	1	# number of top individuals to
		# survive to next generation
ga_mutation_rate	0.02	# rate of gene mutation
ga_crossover_rate	0.8	# rate of crossover
ga_window_size	10	# number of preceding generations to

continued on next page

parameter	value	comment
		# take into consideration when deciding
		# the threshold for the worst individual
		# in the current population
ga_cauchy_alpha	0.0	# Alpha parameter of Cauchy distribution
ga_cauchy_beta	1.0	# Beta parameter Cauchy distribution
set_ga		# set the above parameters for GA or LGA
sw_max_its	300	# iterations of Solis & Wets local search
sw_max_succ	4	# consecutive successes before changing rho
sw_max_fail	4	# consecutive failures before changing rho
sw_rho	1.0	# size of local search space to sample
sw_lb_rho	0.01	# lower bound on rho
ls_search_freq	0.06	# probability of performing local
		# search on individual
set_psw1		# set the above pseudo-Solis &
		# Wets parameters
unbound_model bound		# state of unbound ligand
ga_run	250	# do this many hybrid GA-LS runs
analysis		# perform a ranked cluster analysis

Table A.1: *A sample docking parameter file (dpf) as used for AutoDock4 runs*

Appendix B

Example GROMACS molecular dynamics parameter file

parameter	value	comment
title	= name_of_simulation	; name of the simulation to be run
constraints	= none or all_bonds	; fix lengths of bonds after integration of forces
integrator	= md	; leap-frog method for integrating Newtons equations of motion
dt	= 0.002	; in picoseconds (ps) (1 ns == 1000 ps == 1000·1000 fs)
nsteps	= 750000	; maximum number of steps to integrate
		; (time [ps] = dt·nsteps)
nstcomm	= 1	; [steps] frequency for center of mass motion removal

continued on next page

parameter	value	comment
nstvout	= 1000	; [steps] frequency to write velocities to trajectory
nstxout	= 1000	; [steps] frequency to write coordinates to trajectory
nstfout	= 0	; [steps] frequency to write forces to trajectory
nstlog	= 1000	; [steps] frequency to write energies topology file
nstenergy	= 1000	; [steps] frequency to write energies to energy file
nstlist	= 10	; [steps] frequency to update the neighbor list
ns_type	= grid	; make a grid in the box and only check atoms in neighboring
		; grid cells when constructing a new neighbor list
		; every nstlist steps
coulombtype	= PME	; tells GROMACS how to model electrostatics
		; PME is the Particle-Mesh-Ewald method
fourierspacing	= 0.12	;
fourier_nx	= 0	;
fourier_ny	= 0	;
fourier_nz	= 0	;
pme_order	= 4	;
ewald_rtol	= 1e-5	;
optimize_fft	= yes	;
rlist	= 0.9	; [nm] cut-off distance for the short rang neighbor list
rcoulomb	= 0.9	; [nm] distance for the coulomb cut-off
rvdw	= 1.4	; [nm] distance for the LJ cut-off
pbc	= xyz	; periodic boundary conditions
tcoupl	= berendsen	; temperature coupling with a berendsen-thermostat to a bath
		; with temperature ref_t [K] and time constant tau_t [ps]
		; several groups can be coupled separately, these are specified
		; in the tc_grps field separated by spaces
tau_t	= 0.1 0.1 1.0 0.5	; [ps] time constant for coupling

continued on next page

parameter	value	comment
		; (one for each group in tc_grps)
		; 0 means no temperature coupling
tc_grps	= Protein SOL NA+ DNA	; temperature coupling groups: DNA is DADE, DGUA, DCYT, DTHY
ref_t	= 300 300 300 300	; ref_t [K] is the reference
		; temperature for coupling
		; (one for each in tc_grps)
		; (one for each in tc_grps)
pcoupl	= berendsen	; pressure coupling is on - this means a flexible box size
tau_p	= 0.5	; [ps] time constant for coupling
compressibility	= 4.5e-5	; compressibility (NOTE: this is really in bar^{-1})
		; for water at 1 atm and 300 K the compressibility is
		; $4.5 \cdot 10^{-5}$ [bar^{-1}]
ref_p	= 1.0	; [bar] reference pressure for coupling
gen_vel	= no	; generate velocities according to Maxwells distribution
		; at temperature gen_temp [K] with random seed gen_seed
		; this is only meaningful with integrator md
gen_temp	= 300.0	; (default: 300) [K] temperature for Maxwell distribution
gen_seed	= 173529	; (173529) [integer] used to initialize random velocities

Table B.1: *Excerpt of a sample molecular dynamics parameter file (mdp) used for GROMACS*

Appendix C

Hydrogen-bonding patterns

compound	from cluster	hydrogen bonding target atom	hydrogen bonding ligand atom	hydrogen bonding distance (D–H) ··· (A) [nm]
complex 20 set A				
bay-y3118	14	nucleotide-7 H41 (D–H)	3-carboxy O1 (A)	0.21
		nucleotide-7 H41 (D–H)	3-carboxy O2 (A)	0.23
		nucleotide-8 H42 (D–H)	3-carboxy O2 (A)	0.20
		nucleotide-30 O2P (A)	piperidinium-H^+ (D–H)	0.17
moxifloxacin	25	nucleotide-7 H41 (D–H)	3-carboxy O1 (A)	0.20
		Asp^{82} OD2 (A)	piperidinium-H^+ (D–H)	0.17
moxifloxacin	26	nucleotide-7 H41 (D–H)	3-carboxy O2 (A)	0.20
		nucleotide-7 H41 (D–H)	4-keto O (A)	0.27

continued on next page

compound	from cluster	hydrogen bonding		
		target atom	ligand atom	distance (D–H) ··· (A) [nm]
		nucleotide-8 H42 (D–H)	4-keto O (A)	0.20
		nucleotide-30 O2P (A)	piperidinium-H^+ (D–H)	0.19
norfloxacin	14	nucleotide-7 H41 (D–H)	3-carboxy O1 (A)	0.22
		nucleotide-8 H42 (D–H)	3-carboxy O2 (A)	0.19
		nucleotide-8 H41 (D–H)	4-keto O (A)	0.19
		nucleotide-30 O2P (A)	piperazinium-H^+ (D–H)	0.17
pd0129603	21	nucleotide-7 H41 (D–H)	3-carboxy O1 (A)	0.19
		nucleotide-7 H41 (D–H)	3-carboxy O2 (A)	0.27
		nucleotide-8 H42 (D–H)	3-carboxy O2 (A)	0.18
		nucleotide-30 O2P (A)	piperazinium-H^+ (D–H)	0.21
pradofloxacin	9	nucleotide-7 H41 (D–H)	3-carboxy O2 (A)	0.25
		nucleotide-8 H41 (D–H)	4-keto O (A)	0.20
		Asp^{82} OD2 (A)	piperidinium-H^+ (D–H)	0.18
complex 20 set B				
ciprofloxacin	19	nucleotide-8 H42 (D–H)	3-carboxy O2 (A)	0.20
levofloxacin	10	nucleotide-7 H41 (D–H)	3-carboxy O2 (A)	0.24
		Asp^{82} OD2 (A)	piperazinium-H^+ (D–H)	0.17
		Ser^{83} HG (D–H)	morpholine O (A)	0.24
moxifloxacin	17	nucleotide-7 H41 (D–H)	3-carboxy O2 (A)	0.24
norfloxacin	22	nucleotide-7 H41 (D–H)	3-carboxy O2 (A)	0.21
		Asp^{82} OD2 (A)	piperazinium-H^+ (D–H)	0.17
pd0117962	14	nucleotide-8 H42 (D–H)	3-carboxy O2 (A)	0.20
pd0129603	15	nucleotide-7 H41 (D–H)	3-carboxy O1 (A)	0.19
		nucleotide-8 H42 (D–H)	3-carboxy O2 (A)	0.18
pd0129603	55	nucleotide-7 H41 (D–H)	3-carboxy O2 (A)	0.26
		nucleotide-8 H42 (D–H)	3-carboxy O2 (A)	0.19
pradofloxacin	14	nucleotide-8 H42 (D–H)	3-carboxy O2 (A)	0.20
		Asp^{82} OD2 (A)	piperidinium-H^+ (D–H)	0.17

continued on next page

compound	from cluster	hydrogen bonding target atom	ligand atom	distance (D–H) ··· (A) [nm]
complex 20 set C				
garenoxacin	40	Asp^{87} OD1 (A)	pyrrolidinium-H^+ (D–H)	0.26
		Asp^{87} OD2 (A)	pyrrolidinium-H^+ (D–H)	0.27
norfloxacin	49	nucleotide-30 H3T (D–H)	3-carboxy O1 (A)	0.29

Table C.1: *Hydrogens bonds between target (composed of protein and DNA) and ligand atoms. The distance between donors (D–H) and acceptors (A) is given for each pair of hydrogen bonds. Numbering of nucleotides as in fig. 5.1 and atom naming of nucleotides and amino acids as described in [313].*

compound	from cluster	hydrogen bonding target atom	ligand atom	distance (D–H) ··· (A) [nm]
complex 166 set A				
bay-y3118	2	nucleotide-31 H22 (D–H)	3-carboxy O1 (A)	0.19
		nucleotide-31 H3 (D–H)	3-carboxy O1 (A)	0.28
		Arg^{91} HH12 (D–H)	3-carboxy O2 (A)	0.22
		nucleotide-13 O3' (A)	piperidinium-H^+ (D–H)	0.20
		nucleotide-14 O1P (A)	piperidinium-H^+ (D–H)	0.17
ciprofloxacin	6	nucleotide-31 H22 (D–H)	3-carboxy O1 (A)	0.24
		nucleotide-31 H3 (D–H)	3-carboxy O1 (A)	0.18
		nucleotide-14 O1P (A)	piperazinium-H^+ (D–H)	0.23
garenoxacin	5	nucleotide-31 H22 (D–H)	3-carboxy O2 (A)	0.20
		nucleotide-31 H3 (D–H)	3-carboxy O2 (A)	0.26

continued on next page

compound	from cluster	hydrogen bonding		
		target atom	ligand atom	distance (D–H) ⋯ (A) [nm]
levofloxacin	6	nucleotide-31 H22 (D–H)	3-carboxy O2 (A)	0.21
		nucleotide-31 H3 (D–H)	3-carboxy O2 (A)	0.22
		Ser^{83} OG (A)	piperazinium-H^+ (D–H)	0.20
norfloxacin	8	nucleotide-11 H3	3-carboxy O2 (A)	0.21
		nucleotide-31 H22 (D–H)	3-carboxy O2 (A)	0.29
		nucleotide-14 O1P (A)	piperazinium-H^+ (D–H)	0.20
		Arg^{91} HE (D–H)	3-carboxy O1 (A)	0.26
		Arg^{91} HH21 (D–H)	3-carboxy O1 (A)	0.15
pd0117962	3	nucleotide-31 H22 (D–H)	3-carboxy O1 (A)	0.18
		nucleotide-31 H3 (D–H)	3-carboxy O1 (A)	0.21
		nucleotide-14 O1P (A)	piperazinium-H^+ (D–H)	0.23
pd0163449	1	nucleotide-31 H22 (D–H)	3-carboxy O2 (A)	0.17
		nucleotide-31 H3 (D–H)	3-carboxy O2 (A)	0.22
		nucleotide-13 O3' (A)	piperazinium-H^+ (D–H)	0.19
pradofloxacin	2	nucleotide-31 H22 (D–H)	3-carboxy O2 (A)	0.20
		nucleotide-31 H3 (D–H)	3-carboxy O2 (A)	0.26
		nucleotide-14 O1P (A)	piperazinium-H^+ (D–H)	0.17
		Arg^{91} HH21 (D–H)	3-carboxy O1 (A)	0.20
complex 166 set B				
bay-y3118	3	nucleotide-13 H3 (D–H)	3-carboxy O1 (A)	0.27
		nucleotide-33 H3 (D–H)	3-carboxy O1 (A)	0.22
		nucleotide-13 H3 (D–H)	3-carboxy O2 (A)	0.17
		nucleotide-33 H3 (D–H)	3-carboxy O2 (A)	0.26
enoxacin	15	nucleotide-13 H3 (D–H)	3-carboxy O1 (A)	0.17
		nucleotide-13 H22 (D–H)	3-carboxy O1 (A)	0.29
		nucleotide-13 H3 (D–H)	3-carboxy O2 (A)	0.25
		nucleotide-13 H22 (D–H)	3-carboxy O2 (A)	0.25
		nucleotide-33 H3 (D–H)	3-carboxy O2 (A)	0.19

continued on next page

compound	from cluster	hydrogen bonding		
		target atom	ligand atom	distance (D–H) $\cdots$ (A) [nm]
		His^{80} backbone O (A)	piperazinium-H^+ (D–H)	0.21
levofloxacin	4	nucleotide-13 H3 (D–H)	3-carboxy O2 (A)	0.16
		nucleotide-13 H22 (D–H)	3-carboxy O2 (A)	0.25
		nucleotide-13 H22 (D–H)	3-carboxy O1 (A)	0.26
		nucleotide-33 H3 (D–H)	3-carboxy O1 (A)	0.21
		His^{80} backbone O (A)	piperazinium-H^+ (D–H)	0.21
levofloxacin	5	nucleotide-13 H3 (D–H)	3-carboxy O1 (A)	0.18
		nucleotide-13 H22 (D–H)	3-carboxy O1 (A)	0.25
		nucleotide-33 H3 (D–H)	3-carboxy O2 (A)	0.23
		nucleotide-13 H3 (D–H)	3-carboxy O2 (A)	0.16
		Asp^{82} OD2 (A)	piperazinium-H^+ (D–H)	0.22
norfloxacin	6	nucleotide-13 H3 (D–H)	3-carboxy O2 (A)	0.18
		nucleotide-13 H22 (D–H)	3-carboxy O2 (A)	0.29
		nucleotide-13 H3 (D–H)	3-carboxy O1 (A)	0.26
		nucleotide-13 H22 (D–H)	3-carboxy O1 (A)	0.29
		nucleotide-33 H3 (D–H)	3-carboxy O1 (A)	0.18
		His^{80} backbone O (A)	piperazinium-H^+ (D–H)	0.22
pd0117962	13	nucleotide-13 H3 (D–H)	3-carboxy O2 (A)	0.23
		nucleotide-13 H22 (D–H)	3-carboxy O2 (A)	0.18
		nucleotide-33 H3 (D–H)	3-carboxy O1 (A)	0.21
pd0129603	11	nucleotide-13 H3 (D–H)	3-carboxy O1 (A)	0.17
		nucleotide-13 H22 (D–H)	3-carboxy O1 (A)	0.23
		nucleotide-13 H22 (D–H)	3-carboxy O2 (A)	0.28
		nucleotide-33 H3 (D–H)	3-carboxy O2 (A)	0.19
pd0163449	6	nucleotide-13 H3 (D–H)	3-carboxy O1 (A)	0.17
		nucleotide-13 H22 (D–H)	3-carboxy O1 (A)	0.25
		nucleotide-13 H22 (D–H)	3-carboxy O2 (A)	0.30
		nucleotide-33 H3 (D–H)	3-carboxy O2 (A)	0.20

continued on next page

compound	from cluster	hydrogen bonding		
		target atom	ligand atom	distance (D–H) ⋯ (A) [nm]
complex 166 set L				
ciprofloxacin	10	nucleotide-38 H41 (D–H)	3-carboxy O2 (A)	0.18
		Arg^{121} HH12 (D–H)	4-keto O (A)	0.25
		Asp^{87} OD1 (A)	piperazinium-H^+ (D–H)	0.23
ciprofloxacin	56	Ser^{83} OG (A)	piperazinium-H^+ (D–H)	0.19
		nucleotide-38 H41 (D–H)	3-carboxy O1 (A)	0.20
		nucleotide-39 H7 (D–H)	3-carboxy O1 (A)	0.24
		nucleotide-39 H7 (D–H)	3-carboxy O2 (A)	0.20
		nucleotide-15 H3T (D–H)	4-keto O (A)	0.23
garenoxacin	1	nucleotide-39 H7 (D–H)	3-carboxy O2 (A)	0.18
		nucleotide-15 H3T (D–H)	3-carboxy O1 (A)	0.21
		nucleotide-38 H41 (D–H)	4-keto O (A)	0.21
moxifloxacin	21	Arg^{121} HE (D-H)	3-carboxy O2 (A)	0.20
		Arg^{121} HH21 (D-H)	3-carboxy O2 (A)	0.19
		nucleotide-14 O2P (A)	piperidinium-H^+ (D–H)	0.22
		nucleotide-13 O1P (A)	piperidinium-H^+ (D–H)	0.19
moxifloxacin	37	nucleotide-15 H3T (D–H)	3-carboxy O2 (A)	0.18
pd0117962	25	nucleotide-39 H7 (D–H)	3-carboxy O2 (A)	0.21
		nucleotide-39 H7 (D–H)	3-carboxy O1 (A)	0.20
		nucleotide-15 H3T (D–H)	4-keto O (O)	0.22
pd0129603	41	nucleotide-38 H41 (D–H)	3-carboxy O1 (A)	0.17
		Ser^{83} OG (A)	piperazinium-H^+ (D–H)	0.17
pd0129603	86	nucleotide-15 H3T (D–H)	3-carboxy O1 (A)	0.22
pd0163449	47	nucleotide-15 H3T (D–H)	3-carboxy O2 (A)	0.17
		Arg^{121} HH22 (D-H)	4-keto O (O)	0.27
		nucleotide-14 O1P (A)	piperazinium-H^+ (D–H)	0.16
pradofloxacin	1	nucleotide-39 H7 (D–H)	3-carboxy O1 (A)	0.18
		nucleotide-15 H3T (D–H)	3-carboxy O2 (A)	0.20

continued on next page

compound	from cluster	hydrogen bonding		
		target atom	**ligand atom**	**distance (D–H) $\cdots$ (A) [nm]**
		nucleotide-38 H41 (D–H)	4-keto (A)	0.19
		nucleotide-14 O2P (A)	piperidinium-H^+ (D–H)	0.17
pradofloxacin	11	Ala^{119} backbone NH (D–H)	3-carboxy O2 (A)	0.21
		Arg^{121} HH22 (D-H)	4-keto O (A)	0.24
		nucleotide-14 O1P (A)	piperidinium-H^+ (D–H)	0.19
pradofloxacin	29	Met^{120} backbone NH (D–H)	3-carboxy O2 (A)	0.22

Table C.2: *Hydrogens bonds between target (composed of protein and DNA) and ligand atoms. The distance between donors (D–H) and acceptors (A) is given for each pair of hydrogen bonds. Numbering of nucleotides as in fig. 5.1 and atom naming of nucleotides and amino acids as described in [313].*

Appendix D

Homology Modelling

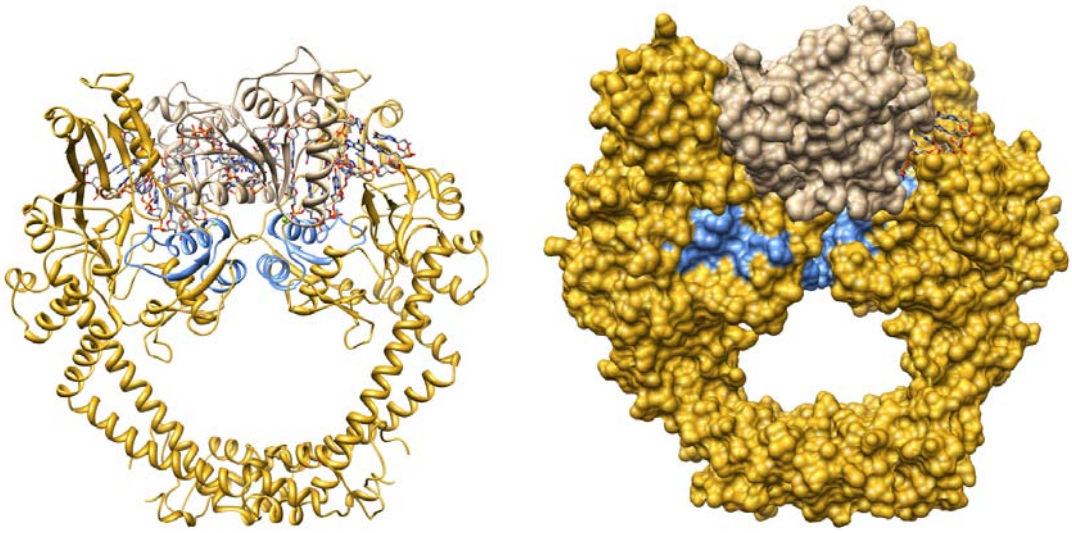

(a) (b)

Figure D.1: *Homology model of a partial E. coli DNA-gyrase structure in complex with DNA: (a) Ribbon representation of GyrA (yellow) with QRDR (blue), part of GyrB (light brown) and the DNA in capped-sticks representation. (b) Same as in (a) with surface shown.* Mg^{2+} *is shown as a green sphere.*

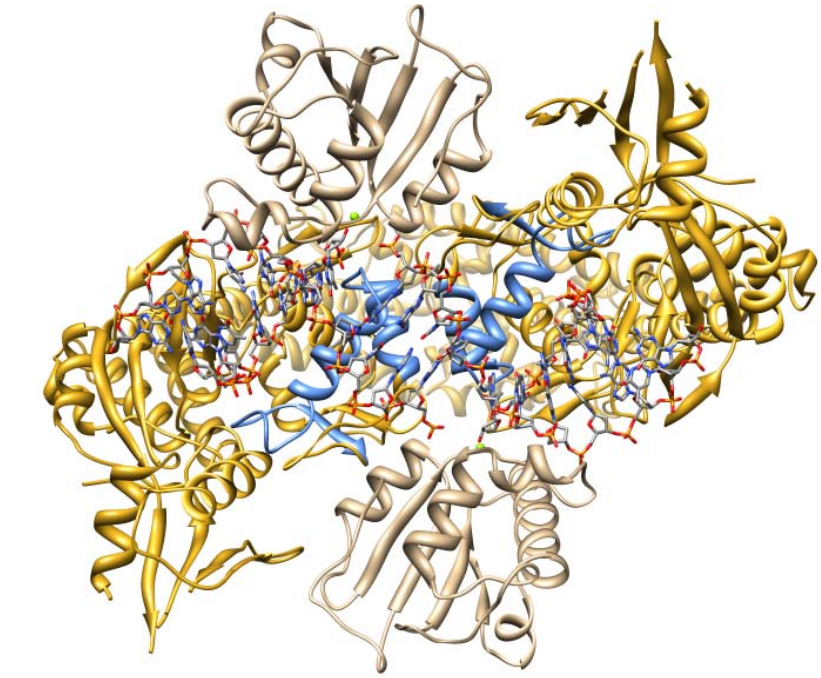

(a)

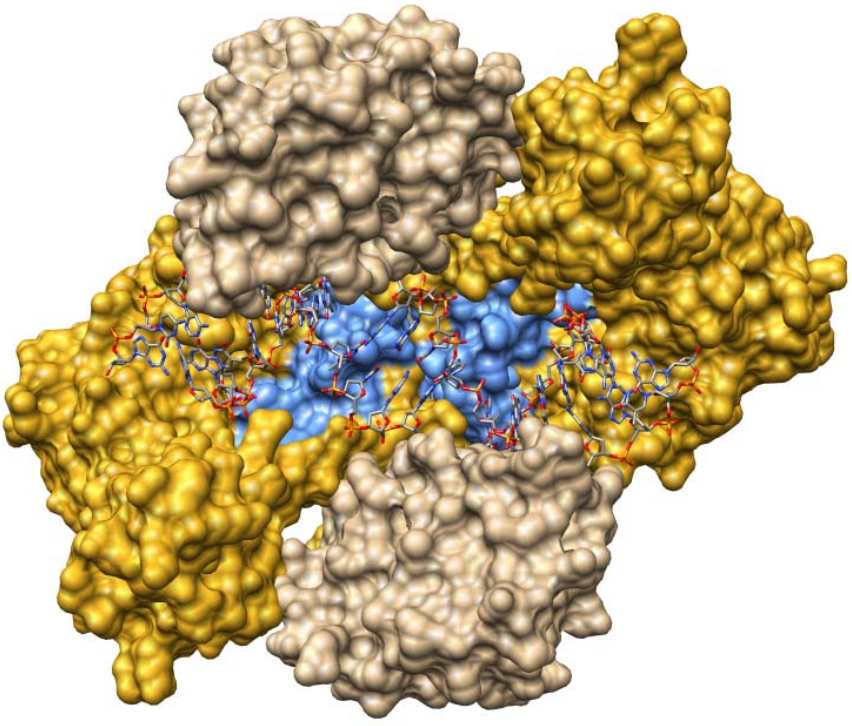

(b)

Figure D.2: *Same as in fig. D.1 rotated by 90° around the vertical axis.*

Appendix E

Compounds used for CoMSIA

E.1 Compounds of CoMSIA training set

training set				levofloxacin model		moxifloxacin model	
compound no.	compound name as in [267]	estimated net charge at pH=7.4	measured cleavage activity	predicted cleavage cleavage	residuals	predicted cleavage activity	residuals
1	1a'	0	0.92	0.96	–0.04	1.04	–0.12
2	1b'	0	1.71	1.69	0.02	1.61	0.10

continued on next page

training set				levofloxacin model		moxifloxacin model	
compound no.	**compound name as in [267]**	**estimated net charge at pH=7.4**	**measured cleavage activity**	**predicted cleavage cleavage**	**residuals**	**predicted cleavage activity**	**residuals**
3	1c'	–1	2.16	2.24	–0.08	1.86	0.29
4	1d'	–1	1.81	2.02	–0.22	1.67	0.14
5	1e'	–1	1.83	1.80	0.03	2.08	–0.26
6	1i	0	1.22	1.40	–0.17	1.86	–0.64
7	1j	–1	0.67	0.85	–0.18	1.01	–0.34
9	1m	–1	0.85	1.08	–0.23	1.14	–0.29
10	1n	–1	1.00	0.99	0	1.24	–0.24
11	1o	–1	1.78	1.84	–0.05	1.83	–0.04
13	1q	0	2.15	2.11	0.03	2.12	0.03
14	1r	–1	1.17	1.09	0.08	1.51	–0.35
15	1s	0	1.79	1.71	0.08	1.90	–0.11
16	1t	–1	2.08	2.14	–0.06	1.63	0.45
17	1u	–1	1.89	1.78	0.11	2.09	–0.20
18	1v	–1	1.68	1.61	0.07	1.81	–0.12
19	1w	0	1.56	1.62	–0.06	1.66	–0.10
20	1x	–1	1.55	1.55	0.01	1.85	–0.30
21	1y	–1	1.28	1.20	0.08	1.58	–0.30
22	1z	0	0.91	0.89	0.02	0.64	0.27
23	2c	0	0.61	0.84	–0.24	1.20	–0.59
25	2e	–1	0.77	1.07	–0.30	1.19	–0.42
26	2f	–1	0.42	0.24	0.17	0.57	–0.15

continued on next page

training set				levofloxacin model		moxifloxacin model	
compound no.	**compound name as in [267]**	**estimated net charge at pH=7.4**	**measured cleavage activity**	**predicted cleavage cleavage**	**residuals**	**predicted cleavage activity**	**residuals**
27	2g	0	0.54	0.57	–0.04	0.50	0.04
28	2h	–1	2.09	1.54	0.55	1.53	0.56
29	2i	–1	1.34	1.35	–0.02	1.48	–0.15
30	2j	–1	1.81	1.68	0.13	1.63	0.18
31	2k	0	1.76	1.81	–0.04	1.26	0.51
33	2m	–1	0.74	0.78	–0.04	0.83	–0.08
34	2o	–1	1.00	1.06	–0.06	0.76	0.24
35	2p	–1	0.74	0.74	0	0.60	0.15
37	6a	–1	0.48	0.55	–0.07	0.75	–0.27
38	6b	–1	0.50	0.38	0.13	0.68	–0.17
39	6c	–1	0.52	0.69	–0.17	0.39	0.13
40	7a	–1	0.26	0.04	0.22	–0.05	0.31
41	7b	–1	0.44	0.43	0.01	0.58	–0.14
42	7c	–1	0.44	0.37	0.06	0.28	0.15
43	AM833	–1	2.17	2.12	0.05	1.93	0.24
44	amifloxacin	–1	2.12	2.32	–0.19	2.07	0.05
45	cinoxacin	–1	0.78	0.85	–0.06	0.75	0.03
46	ciprofloxacin	0	2.82	2.64	0.19	2.54	0.28
47	enoxacin	0	1.81	2.06	–0.25	1.72	0.09

continued on next page

training set				levofloxacin model		moxifloxacin model	
compound no.	**compound name as in [267]**	**estimated net charge at pH=7.4**	**measured cleavage activity**	**predicted cleavage cleavage**	**residuals**	**predicted cleavage activity**	**residuals**
48	miloxacin	–1	1.42	1.42	0	1.12	0.30
49	nalidixic acid	–1	0.67	0.69	–0.02	0.52	0.15
50	norfloxacin	0	2.50	2.46	0.05	2.23	0.27
51	oxolinic acid	–1	1.42	1.39	0.03	1.17	0.24
52	pefloxacin	–1	2.52	2.21	0.31	2.14	0.38
53	pipemidic acid	0	0.78	0.61	0.18	0.80	–0.02
54	piromidic acid	–1	0.88	0.89	–0.01	1.02	–0.14
			SDR	0.17		0.28	

Table E.1: *Compounds of the training set: Measured and predicted cleavage activities are given in –lg(cleavage activity)[mM]. The estimated net charge is given for each compound. A residual is the differences between measured and predicted cleavage activity.*

E.2 Compounds of CoMSIA test set

training set				levofloxacin model		moxifloxacin model	
compound no.	**compound name as in [267]**	**estimated net charge at pH=7.4**	**measured cleavage activity**	**predicted cleavage cleavage**	**residuals**	**predicted cleavage activity**	**residuals**
8	1l	–1	0.85	1.03	–0.18	0.95	–0.10
12	1p	0	2.53	2.37	0.16	2.11	0.42
24	2d	–1	1.27	1.46	–0.19	1.85	–0.58
32	2l	0	1.76	2.07	–0.31	1.78	–0.02
36	2q	–1	0.56	0.85	–0.29	1.37	–0.82
55	rosoxacin	–1	2.07	1.36	0.71	1.41	0.66

Table E.2: *Compounds of the test set: Measured and predicted cleavage activities are given in –lg(cleavage activity)[mM]. The estimated net charge is given for each compound. A residual is the differences between measured and predicted cleavage activity.*

E.3 Compounds of CoMSIA external set

external set	levofloxacin model	
compound name	**estimated net charge at pH=7.4**	**predicted cleavage activity**
levofloxacin	–1	1.98
enrofloxacin	–1	1.85

Table E.3: *Compounds of the external set: The predicted cleavage activity in –lg(cleavage activity)[mM] is given with the estimated net charge for levofloxacin and enrofloxacin.*

Appendix F

Risk and safety statements of hazardous chemicals

chemical	Risk statements	Safety statements	symbol
Acetic acid 100% (glacial acetic acid)	10-35	23-26-45	
Ampicillin (sodium salt)	36/37/38-42/43	22-26-36/37	
Calcium chloride dihydrate	36	22-24	
Chloroform	22-38-40-48/20/22	2-36/37	
DMSO	36/38	26	
Ethanol 96%	11	7–16	

continued on next page

chemical	Risk statements	Safety statements	symbol
Ethidiumbromide 1% aqueous solution	22-26-36/37/38-68	26-36/37-45	
Ethylenediaminetetra-acetic acid (EDTA)	36-52/53	61	
Hydrochloric acid	34-37	26-36/37/39-45	
Isopropanol (2-propanol)	11-36-67	7-16-24/25-26	
MOPS (3-(N-morpholino)-propanesulfonic acid)	36/37/38	26-36	
Phenol	23/24/25-34-48/20/21/22-68	(1/2)-24/25-26-28-36/37/39-45	
Potassium hydroxide	22-35	26-36/37/39-45	
Sodium dodecylsulfate (SDS)	11-21/22-36/37/38	26-36/37	
Sodium hydroxide	35	26-37/39-45	
Tris(hydroxymethyl)-aminomethane TRIS	36/38		
Xylene cyanol	36	24	

Table F.1: *Risk and safety statements of hazardous chemicals*

curriculum vitæ

Persönliche Daten

geboren:	18. Februar 1978, Hamburg
Staatsangeh.:	deutsch

Wissenschaftlicher Werdegang

08/88–07/97	**Gymnasium / Abitur**
10/97–12/02	**Studium der Pharmazie**, Universität Hamburg
08/00	Erster Abschnitt der Pharmazeutischen Prüfung
11/02	Hochschulabschluss: Zweiter Abschnitt der Pharmazeutischen Prüfung
01/03–12/03	Dritter Abschnitt der Pharmazeutischen Ausbildung (Praktisches Jahr) Abschluss: Approbation als Apotheker
10/03–03/08	**Studium der Bioinformatik**, Universität Hamburg, Zentrum für Bioinformatik Abschluss: Diplom Bioinformatiker Titel der Diplomarbeit: *"Fast and Efficient Structure-based Classification of Kinases"* Betreuer: Prof. Dr. Andrew Torda (Abt. Biomolekulare Modellierung)
02/04–02/11	**Dissertation**, Universität Hamburg, Institut für Pharmazie (Abt. Pharm. Biologie und Mikrobiologie); Zentrum für Bioinformatik (Abt. Biomolekulare Modellierung) Titel: *"The ternary gyrase-DNA-quinolone complex: from molecular modelling to understanding quinolone action and resistance"* Betreuer: Prof. Dr. Peter Heisig, Prof. Dr. Andrew Torda

Berufstätigkeit

02/99–03/99	Apotheke im Ärztehaus, Hamburg-Neugraben (Famulatur)
08/99–09/99	Apotheke im Ärztehaus, Hamburg-Neugraben (Famulatur)
01/03–06/03	Apotheke im Ärztehaus, Hamburg-Neugraben (Praktisches Jahr)
07/03–12/03	Inst. für Pharmazie, Abt. Pharm. Biologie und Mikrobiologie, Universität Hamburg (Praktisches Jahr)
07/03–01/04	Teilzeitbeschäftigung, Apotheke am Mühlenkamp, Hamburg-Winterhude
02/04–02/11	Wissenschaftlicher Mitarbeiter, Inst. für Pharmazie, Abt. Pharm. Biologie und Mikrobiologie
10/08–06/10	Head of Discovery Informatics, European ScreeningPort GmbH, Hamburg
01/11–dato	Produktmanager (Onkologie), medac GmbH, Wedel

Förderungen

10/04–09/05	Stipendiat der Stiftung zur Förderung des künstlerischen und wissenschaftlichen Nachwuchses, Universität Hamburg
10/05–09/08	Stipendiat der Jürgen Manchot Stiftung, Düsseldorf

Poster

J. Lenz, T. Lemcke, P. Heisig, A. Torda; "Modelling the Gyrase-DNA-Interaction using Docking and Molecular Dynamics Simulations"; German Conference on Bioinformatics, Potsdam; 26.09.2007–28.09.2007

J. Lenz, T. Lemcke, P. Heisig, A. Torda; "Molecular Modelling and *In-Vitro* Mutagenesis: An Approach to Characterize the Quinolone-Gyrase-Interaction"; From Computational Biophysics to System Biology - Jülich; 19.05.2008–21.05.2008

J. Lenz, T. Margraf, T. Lemcke, A. Torda; "Fast, Automated Structure-Based Classification of Kinases"; From Computational Biophysics to System Biology - Jülich; 19.05.2008–21.05.2008

Publikationen

J. Lenz, T. Lemcke, P. Heisig and A. Torda; "Characterization of the quinolone-gyrase-interaction using docking, molecular-dynamics and site-directed mutagenesis; NIC Series Vol. 40: 289–292; May 2008

J. Lenz, T. Margraf, T. Lemcke and A. Torda; "Classification of kinases: A fast, automated structure-based approach"; NIC Series Vol. 40: 293–296; May 2008

M. Graettinger, J. Lenz, J.P. v.Kries, R. Kühne, J. Rademann, P. Gribbon; "Advancing Academic Drug Discovery - A Collaborative Model Involving two Germany-based Organizations"; Screening - Trends in Drug Discovery; Vol. 10: 17–19; April 2009

Mitgliedschaften

Mitgliedschaften: Deutsche Pharmazeutische Gesellschaft

Acknowledgements

Zuerst möchte ich Herrn Prof. Peter Heisig danken: Für die Bereitstellung des Themas, die Aufnahme in seine Arbeitsgruppe, die Betreuung und die Möglichkeit, parallel zu der Arbeit in seiner Arbeitsgruppe, Bioinformatik zu studieren. Ebenso möchte ich meinem zweiten Gutachter und Betreuer, Herrn Prof. Andrew Torda, danken. Beide Gutachter standen stets für Diskussionen und Anregungen zur Verfügung, die weit über die eigentliche Betreuung der Arbeit hinausgingen. Ihnen verdanke ich ebenfalls die Möglichkeit, an diversen Kongressen teilzunehmen.

Der Stiftung zur Förderung des künstlerischen und wissenschaftlichen Nachwuchses der Universität Hamburg und der Jürgen Manchot Stiftung danke ich vielmals für die finanzielle Unterstützung dieser Arbeit.

Weiterer Dank gilt Frau Dr. Anke Heisig für die anregenden Gespräche und Hinweise für meine Arbeit sowie die Bereitstellung der MHK Daten.

Frau Prof. Dr. Stahl-Biskup und Herrn Dr. Thomas Lemcke danke ich für Ihre Bereitschaft, die Gutachten meiner Disputation zu übernehmen. Thomas danke ich weiterhin für die vielen hilfreichen und anregenden Diskussionen rund um meine Arbeit und die ständige Gesprächsbereitschaft.

Meinen Kollegen aus der Pharmazie und dem Zentrum für Bioinformatik möchte ich vielmals für die großartige Arbeitsatmosphäre, die Hilfsbreitschaft, die Geduld und die gemeinsame Zeit danken. Besonderer Dank gilt Sabine Badziong und Annette Schade für Ihre andauernde Hilfe bei allen administrativen Fragen.

Meinem ZBH-Mitbewohner Thomas Margraf danke ich ebenso wie meinem ZBH-Nachbarn Stefan Bienert für die zahlreichen und absurden Diskussionen und die Unterstützung mit LaTeX , Perl und das Korrekturlesen dieser Arbeit. Meinen anderen ZBH Kollegen danke ich für die mehr als kollegiale Atmosphäre.

Meinen Skype Kollegen und Freunden Tim Wiegels, Steve Hoffmann, Thomas Margraf und Stefan Bienert sage ich nur: "Computerfreaks, Computerfreaks, Ihr lebt in Eurer

Welt ..."

Bei meinen Freunden und Kollegen Hadi, Torben, Michael, Yassin, Thomas, Daniel und Tim bedanke ich mich für die zahlreichen Gespräche. Ihr habt mir so manch schweren Tag erleichtert.

Besonderer Dank gilt meiner Familie, meinen Eltern und Schwiegereltern, meiner Großmutter Anni und meinem Bruder Sven. Sie haben mich immer unterstützt und mussten sich freiwillig und unfreiwillig meine Geschichten anhören.

Dennoch gilt mein größter Dank meiner Frau Carolin. Sie hat mir jederzeit den Rücken freigehalten, mich immer wieder aufgebaut, mich motiviert und mir gezeigt, dass es auch noch ein Leben neben der Arbeit gibt. Ohne Ihre Unterstützung und Ihren unermüdlichen Einsatz hätte ich diese Sätze hier nicht geschrieben. Danke für alles, besonders für Julius.

Erklärung

Ich versichere an Eides statt, dass ich die vorliegende Arbeit selbständig und ohne fremde Hilfe angefertigt und mich anderer als der im beigefügten Verzeichnis angegebenen Hilfsmittel nicht bedient habe. Alle Stellen, die wörtlich oder sinngemäß aus Veröffentlichungen entnommen wurden, sind als solche kenntlich gemacht.

_____

(Jörn Lenz)